

1016732 General Motors Corp.  
Indianapolis, Ind.  
@ Allison Div.

N64-16747 6

CODE-1

@ Final Report

WASA CR-53108

**Development and Testing of Electrolyte Matrix  
Combinations for Mercury-Potassium Fuel Cell**

132p.

Engineering Department Report No. 3709

→ OTS: PRICE

XEROX

MICROFILM

\$ 10.50 per  
\$ 4.16 ref.

This work is sponsored by the Space Power Technology  
Program of the NASA Headquarters. It is technically  
directed by Lewis Research Center, NASA, Cleveland, Ohio.

(Prepared under NASA Contract NASw-476)  
by Allison Division, General Motors Corporation,  
Indianapolis, Indiana

Authors: V. L. Decker, R. A. Murie, and W. S. Colwell

Jan. 1964  
1320 ref

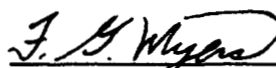
**Final Report**  
**Development and Testing of Electrolyte Matrix**  
**Combinations for Mercury-Potassium Fuel Cell**

Engineering Department Report No. 3709

January 1964



V. L. Decker  
Project Manager



F. G. Myers  
Director of Research



16747

# ABSTRACT

A

The work on this contract was performed for the National Aeronautics and Space Administration by the Research Department of Allison Division of General Motors under contract NASw-476.

A crack-free composite matrix for use in the potassium-mercury liquid metal cell has been developed utilizing MgO and employing special preparation and baking techniques. The molten salt electrolyte used in the composite is a ternary eutectic of KOH, KBr, and KI of 70-15-15 mole percents, respectively.

During development of the technique for preparation of the composite, many specimens were prepared for strength, density, flowability, electrical conductivity, and compatibility tests. Actual cell operation tests utilized  $2 \times 1/8$ -in. composites for ten small cells that were assembled and  $4 \times 1/8$ -in. composites for three large cells utilizing two different configurations. Special design features employed in the construction of the cells included screens for support of the matrix, unique serrations to effect a positive seal utilizing the plasticity of the composite, and silicon rubber O-rings to exclude atmospheric contamination.

Maximum performance data utilizing potassium as the anode metal indicate that the goal of the systems study resistivity-thickness product,  $\gamma t_e = 0.5$ , may be achieved if the electrolyte composite matrix thickness is reduced to  $1/16$  in.

RUTHOR

## TABLE OF CONTENTS

<u>Section</u>	<u>Title</u>	<u>Page</u>
I	Introduction . . . . .	1-1
II	Results, Conclusions, and Recommendations. . . . .	2-1
	Recommendations . . . . .	2-2
III	Program Results. . . . .	3-1
	Weight Analysis. . . . .	3-1
	Testing of Large Cells . . . . .	3-2
	Vertical Cell . . . . .	3-3
	Horizontal Cell. . . . .	3-16
	Final Design of Large Cells . . . . .	3-21
	Vertical Cell Design . . . . .	3-22
	Horizontal Cell Design . . . . .	3-25
IV	Development and Mechanical Property Studies of Composite Material . . .	4-1
	Composite Electrolyte Improvement and Final Fabrication	
	Methods . . . . .	4-2
	Results . . . . .	4-3
	Description of Materials. . . . .	4-3
	Modification of Preparation Procedures. . . . .	4-5
	Property Measurements . . . . .	4-11
	Fabrication and Properties of Light-Calcined, Type F, Fine	
	Grain MgO Composites . . . . .	4-13
	Composite Electrolyte Preparation . . . . .	4-14
	Processing Difficulties. . . . .	4-18
	Property Measurements . . . . .	4-19
	Results . . . . .	4-19
	Fabrication and Properties of Coarse Grain MgO Composites . . . . .	4-19
	Original Fabrication Method. . . . .	4-22
	Modification of Procedure . . . . .	4-22
	Property Measurement. . . . .	4-25

<u>Section</u>	<u>Title</u>	<u>Page</u>
V	Testing and Electrical Property Studies of Composite Material . . . . .	5-1
	Conductivity Studies. . . . .	5-1
	Small Cell Studies. . . . .	5-25
	Compatibility Studies . . . . .	5-46
	Small Differential Density Cell Resistivity Studies . . . . .	5-52
VI	Apparatus and Techniques . . . . .	6-1
	Mechanical Testing . . . . .	6-1
	Ball Penetration Test . . . . .	6-1
	Flowability Test . . . . .	6-1
	Electrical Testing. . . . .	6-2

## LIST OF ILLUSTRATIONS

<u>Figure</u>	<u>Title</u>	<u>Page</u>
3-1	Specific weight and system efficiency for minimum weight as a function of liquid metal cell merit factor. . . . .	3-1
3-2	Hydroformed sections for a lightweight cell design. . . . .	3-3
3-3	The assembly of a lightweight cell from hydroformed sections . . . . .	3-4
3-4	Vertical cell configuration in a preassembly layout . . . . .	3-5
3-5	Vertical cell configuration in the test stand. . . . .	3-6
3-6	The vertical cell after assembly . . . . .	3-7
3-7	Results of a maximum power investigation, showing the effect of diffusion. . . . .	3-14
3-8	The anode side of a 4- × 1/8-in. matrix after test in cell XIII . . . . .	3-19
3-9	Composite matrix after test in cell XI showing breaks and region of short . . . . .	3-20
3-10	Microphotos for matrix analysis . . . . .	3-20
3-11	Detailed sketch showing vertical cell design . . . . .	3-23
3-12	Schematic of the horizontal cell. . . . .	3-25
4-1	Composite electrolyte shapes produced during the program . . . . .	4-1
4-2	Gas-tight specimen holder. . . . .	4-6
4-3	Reverse image X-ray photograph (4X) of 1-in. dia × 1/8-in. baked specimen from contaminated Batch IX—MgO coarse type C . . . . .	4-7
4-4	Reverse image X-ray photograph (4X) of 1-in. dia × 1/8-in. baked specimen from Batch IX after removing metal particle contamination—MgO coarse type C . . . . .	4-8
4-5	Two-inch dia specimen from Batch 110, No. 23 electronic grade fine MgO type FF . . . . .	4-10
4-6	Two-inch dia specimen from Batch 107, No. 15 light calcined fine MgO type F . . . . .	4-10
4-7	Cross section of electrolyte showing gas pockets . . . . .	4-24
5-1	Conductivity of 31/69 unconsolidated electrolyte matrices (type C MgO) . . . . .	5-15
5-2	Conductivity of 33/67 unconsolidated electrolyte matrices (type C MgO) . . . . .	5-15

<u>Figure</u>	<u>Title</u>	<u>Page</u>
5-3	Conductivity of 35/65 unconsolidated electrolyte matrices (type C MgO) . . . . .	5-17
5-4	Conductivity of 33/67 and 31/69 unconsolidated electrolyte matrices to show density effect (type C MgO) . . . . .	5-17
5-5	Conductivity of 31/69, 33/67, and 34/66 unconsolidated electrolyte matrices with 86.2% theoretical density (type C MgO) . . . . .	5-18
5-6	Conductivity of 34/66 unconsolidated electrolyte matrices (type C MgO) . . . . .	5-18
5-7	Conductivity of 34/66 unconsolidated electrolyte matrices (type C MgO) . . . . .	5-19
5-8	Conductivity of thin unconsolidated electrolyte matrices (type C MgO) . . . . .	5-19
5-9	Conductivity of fine grain unconsolidated electrolyte matrices (type F MgO) . . . . .	5-20
5-10	Conductivity of 63/37 unconsolidated electrolyte matrices (type F MgO) . . . . .	5-20
5-11	Conductivity of 33/67 (nominal 34/66) unconsolidated electrolyte matrices (type C MgO) . . . . .	5-22
5-12	Conductivity of 33/67 unconsolidated electrolyte matrices (type C MgO) . . . . .	5-22
5-13	Conductivity of 50/50 unconsolidated electrolyte matrices (type F MgO) . . . . .	5-23
5-14	Conductivity of 60/40 unconsolidated electrolyte matrices (type F MgO) . . . . .	5-23
5-15	Conductivity of 65/35 unconsolidated electrolyte matrices (type FF MgO). . . . .	5-24
5-16	Test equipment for first small unit . . . . .	5-25
5-17	Results of test teardown on silicon rubber O-ring . . . . .	5-27
5-18	Small cell test setup . . . . .	5-28
5-19	Small cell assembly . . . . .	5-29
5-20	Cell after matrix removal. . . . .	5-37
5-21	Sections of matrix from the seal region. . . . .	5-38

<u>Figure</u>	<u>Title</u>	<u>Page</u>
5-22	Sections of matrix from second cell seal region . . . . .	5-40
5-23	Cross section of electrolyte matrix showing failure due to K-metal penetration . . . . .	5-44
5-24	A series of photos showing serration marks near the top of the anode side, which indicate improper sealing. . . . .	5-47
5-25	Test rig for compatibility studies . . . . .	5-48
5-26	Electrolyte matrix after test number 6 . . . . .	5-50
5-27	Broken edges of sixth test matrix. . . . .	5-50
5-28	Cross section of matrix showing holes . . . . .	5-51
5-29	Liquid metal cell performance characteristics. . . . .	5-52
5-30	Schematic diagram of differential density cell used in resistivity studies. . . . .	5-53
5-51	Plot of data obtained from cell resistivity studies for the pure electrolyte. . . . .	5-54
6-1	Compressive strength test apparatus . . . . .	6-2
6-2	Low-stress compressive creep machine . . . . .	6-3
6-3	Flowability test apparatus. . . . .	6-4
6-4	Flowability specimens after compression . . . . .	6-4
6-5	Electrolyte matrices conductivity apparatus . . . . .	6-6
6-6	Modified Kelvin bridge. . . . .	6-6

# LIST OF TABLES

<u>Table</u>	<u>Title</u>	<u>Page</u>
3-I	Data on composite electrolyte matrix cells . . . . .	3-8ff.
3-II	Correlation of cell performance and test configuration factors . . . . .	3-17
4-I	Typical analysis of type FF MgO powder . . . . .	4-4
4-II	Fisher Scientific Company certified analyses of materials for composite electrolyte powder. . . . .	4-14
4-III	Composition of electrolyte/MgO composites (type F MgO). . . . .	4-17
4-IV	Summary of ball penetration strength tests of fine grain type F MgO composites. . . . .	4-20
4-V	Summary of flowability tests of fine grain type F MgO composites . . . . .	4-21
4-VI	Composite electrolyte material composition (type C MgO). . . . .	4-23
4-VII	Ball penetration test results on coarse type C MgO composite electrolyte at 350°C . . . . .	4-25
4-VIII	Flow test results on coarse type C MgO composite electrolyte at 350°C . . . . .	4-26
4-IX	Composite electrolyte specimen fabrication data . . . . .	4-27ff.
5-I	Conductivity specimen identification . . . . .	5-2f.
5-II	Conductivity specimen data . . . . .	5-4ff.
5-III	Data on composite electrolyte matrix cells . . . . .	5-30ff.

## I. INTRODUCTION

This is the final report on the development and testing of electrolyte matrix combinations for mercury-potassium fuel cells. This work was conducted by the Research Department of Allison Division of General Motors under NASA Contract NASw-476.

Systems studies<sup>1</sup> of the liquid metal cell direct conversion unit have shown that cell performance must be improved to provide system weights lower than those of dynamic systems. Specifically, the resistivity-thickness products,  $\gamma t_e$ , must approach 0.5 ohm-cm<sup>2</sup>. Tests of cells using a porous ceramic matrix of 1.5 mm thickness had shown this performance parameter to be approximately 2 ohm-cm<sup>2</sup>. Improvement of cell performance was expected by increasing the matrix porosity and decreasing the matrix thickness to the limit of engineering development.

The approach under study in this contract was to use an unconsolidated ceramic-electrolyte composite matrix. This work was initiated previously in the Allison Materials Research Laboratory with the successful development of a technique for the preparation of a 5-micron average MgO particle size composite. It had been shown<sup>2</sup> theoretically that the use of smaller particle sizes would bring about a considerable improvement in  $\gamma t_e$ . Therefore, it was proposed to devise techniques for employing smaller particle size composite matrices and testing these in actual advanced cell designs.

The statement of work under the contract called for research on advanced electrolyte matrix combinations for mercury-potassium liquid metal fuel cells. The study was to include the following fields of investigation.

- A study of paste electrolyte preparation techniques, employing variations in the pressures, temperatures and ceramic particle size. Tests for mechanical strength, density, and electrical conductivity were to be made for evaluation of the various samples attained.
- Cell designs were to be completed for the more promising paste electrolytes. These designs were to be based on measured parameters and to incorporate such features as screens for the support of the paste electrolyte and seals employing the plasticity of the paste electrolyte.

---

<sup>1</sup>Systems Analysis of Nuclear (SNAP II) Liquid Metal Cell Space Power System, Allison Division, General Motors Corporation, Indianapolis, Indiana, EDR 3113 (5 December 1962), pp 19-23.

<sup>2</sup>Op. cit., Appendix G.



- At least two different types of cells were to be fabricated of sizes of no less than 3 in. in diameter. These cells were to be thoroughly tested for static and dynamic electrochemical characteristics and operating endurance. The resulting data were to be used to provide estimates of advanced space powerplant system weights.

This final report is a statement of accomplishment of the statement of work. The report is organized in a reverse chronology to first report the final accomplishments and to then review the evolution of the program work.

## II. RESULTS, CONCLUSIONS, AND RECOMMENDATIONS

The significant results and conclusions derived from this program follow.

1. Three large cells utilizing two different configurations were assembled to test 4- × 1/8-in. matrices prepared from the final composite (65% electrolyte-35% type FF MgO). Electrochemical data were collected from the best of these cells for 82 hr before the cell was disassembled for examination. These test results now establish the feasibility of a paste matrix liquid metal cell.
2. A new composite electrolyte was developed using fused, fine-grain, type FF MgO powder. Crack-free matrices were prepared by utilizing the new composite and employing special vacuum baking techniques. This is a new development and establishes a much-refined state of the art, since no previous matrix has been satisfactory.
3. Ten small cells were assembled to evaluate the 2- × 1/8-in. matrices prepared from both coarse and fine grain MgO during the composite development program. A resistivity-thickness product of 1.0 ohm-cm<sup>2</sup> was the best performance obtained in the evaluations of these cells. These tests have proved the value of actual cell testing of the matrix on a reduced scale.
4. Specimens prepared from 65% electrolyte and 35% type FF MgO do not show permeability to argon gas when tested at pressures as high as 32 in. of water and temperatures of 300°C. This shows that liquid electrolyte cannot be displaced by the pressure differentials expected to exist within the cell.
5. The maximum electrolyte content for the preparation of satisfactory matrices was 65% for fine grain type FF MgO and 33% for coarse grain type C MgO. Matrices of greater electrolyte content are extremely fluid at 300°C.
6. Electrical conductivities reached a maximum value of  $K = 0.37$  mho/cm, in the 65% electrolyte-35% type FF MgO composites. The conductivity of 100% electrolyte was measured to be 0.74 mho/cm. Therefore, the program achieved 50% of pure electrolyte conductivity as compared to 20% at the beginning of the program.

7. Serrations machined into the anode and cathode sides of the cells provided positive seals with the matrix. In no case was cell failure found to be due to seal design. This work has now confirmed earlier predictions that paste matrices are easily sealed.
8. Screens of 12 wires per inch were found to be satisfactory for the support of the 1/8-in. thick 65% composite matrix within the cell. Posttest analysis showed that the cathode side screen was unnecessary and that larger mesh size screens could be used on the anode side. The 1/8-in. thick matrix was an improvement over the 1/2-in. matrix used previously. It should be possible to reduce this thickness even further.
9. Silicon rubber O-rings were found to be adequate in the prevention of atmospheric contamination whether in contact with the matrix (a most extreme condition) or exterior to it. This was an important development in use of materials since it makes lightweight designs possible.

## RECOMMENDATIONS

1. Further study of electronic and ionic conductivities of the pure electrolyte eutectic in the presence of mercury and potassium should be carried out as an aid to defining cell limitations.
2. Resistivity studies to show the effect of trace contaminants should be performed.
3. Further development of the method used to fabricate matrices should be pursued to attain consistent matrix quality for future multicell designs. These development programs should include investigations of the production of various shapes and sizes of matrices.

### III. PROGRAM RESULTS

This section has been divided into three parts to report those major items listed in the Statement of Work as the contract goals: weight analysis, testing of two types of 3-in. diameter cells, and the final design of cells.

#### WEIGHT ANALYSIS

One goal was to estimate the weight of an advanced space powerplant system from performance test data obtained. Early work in systems analysis was based on the SNAP II LMC (Liquid Metal Cell) System.<sup>3</sup> Since weight estimates must be made on the basis of applications, the data reported in the SNAP II LMC report are used as a standard and are summarized in Figure 3-1. Figure 3-1 reflects the minimum specific weight of a system as a function of a LMC Merit Factor,  $M = (\gamma t_e) \rho$ .

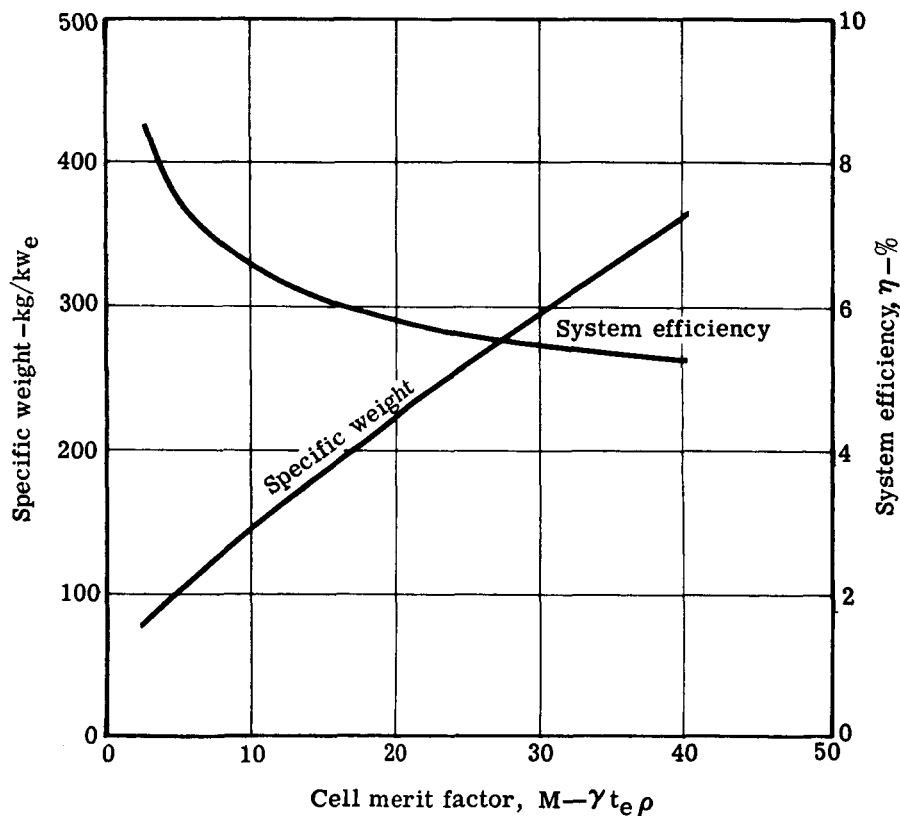


Figure 3-1. Specific weight and system efficiency for minimum weight as a function of liquid metal cell merit factor.

<sup>3</sup>Op. cit.

The merit factor as developed in this work is a measure of both the electrochemical performance and the engineering excellence in design and fabrication of a LMC. Therefore, data for a weight estimate are, by necessity, derived from two sources. First, the parameter of electrochemical performance, the resistivity thickness product ( $\gamma t_e$ ), is obtained from cell performance data. Results from large cell work using amalgam anode, reported subsequently in this section, show this parameter to be  $2.7 \text{ ohm-cm}^2$  ( $\gamma = 8 \text{ ohm-cm}$ ). Early work with small cells reported in Section IV of this report shows this parameter to be  $2 \text{ ohm-cm}^2$  ( $\gamma = 6 \text{ ohm-cm}$ ) for amalgam anode cells, and as low as  $1.0 \text{ ohm-cm}^2$  ( $\gamma = 3 \text{ ohm-cm}$ ) for potassium anode cells. The matrix thickness was nominally  $1/8 \text{ in.}$  or  $1/3 \text{ cm}$  for all cells tested in this program.

The second part of the weight analysis is the cell weight-to-area ratio,  $\rho$ . This parameter is a measure of weight per unit active cell area. A very low value reflects the engineering excellence associated with the development of advanced designed hardware. It is natural for all electrochemical research devices to be designed at very large values of  $\rho$ . For instance, the weight of the vertical cell is so great that the merit factor,  $M$ , is greater than the scale value of Figure 3-1; that is, the weight of 6755 gives  $\rho = 150 \text{ gm/cm}^2$ . Therefore, the merit factor,  $M$ , is limited to  $75 \text{ ohm-gm}$  for even the best performance parameter  $\gamma t_e = 0.5 \text{ ohm-cm}^2$ . For comparison, a lightweight design was investigated relative to fabrication processing. The basic hydroformed cell half is shown in Figure 3-2 and one design concept is shown in Figure 3-3. The weight of the design shown in Figure 3-3, when fully loaded with Hg and amalgam, is  $471 \text{ gm}$ . This gives a weight ratio  $\rho = 10.5 \text{ gm/cm}^2$  for the  $45 \text{ cm}^2$  area. The electrode metals in this configuration weigh  $320 \text{ grams}$  and the matrix  $70 \text{ grams}$ . Therefore, when these are cut in half, the weight is reduced to  $276 \text{ gm}$  and  $\rho = 6.1 \text{ gm/cm}^2$ . Now change of electrolyte thickness gives an electrochemical performance improvement from  $\gamma t_e = 2.0 \text{ ohm-cm}^2$  to a performance parameter of  $\gamma t_e = 1 \text{ ohm-cm}^2$  and, therefore, a resultant merit factor of near  $6 \text{ ohm-gm}$ . This corresponds to a system weight of  $110 \text{ kg/kw}_e$  from the curve of Figure 3-1. The conclusion to be drawn is that improved lightweight designs, together with the expected improvements in the composite, will give a competitive system.

## TESTING OF LARGE CELLS

This part of the program was fully dependent on the success of fabricating large 4-in. dia composite electrolyte disks. Fabrication of these disks is reported in Section IV. Success of the program was ultimately measured by testing these matrices in the last month of the performance period. Design of the two cell configurations which is reported later in this section was essentially completed on the basis of the small cell work reported in Section V. Through

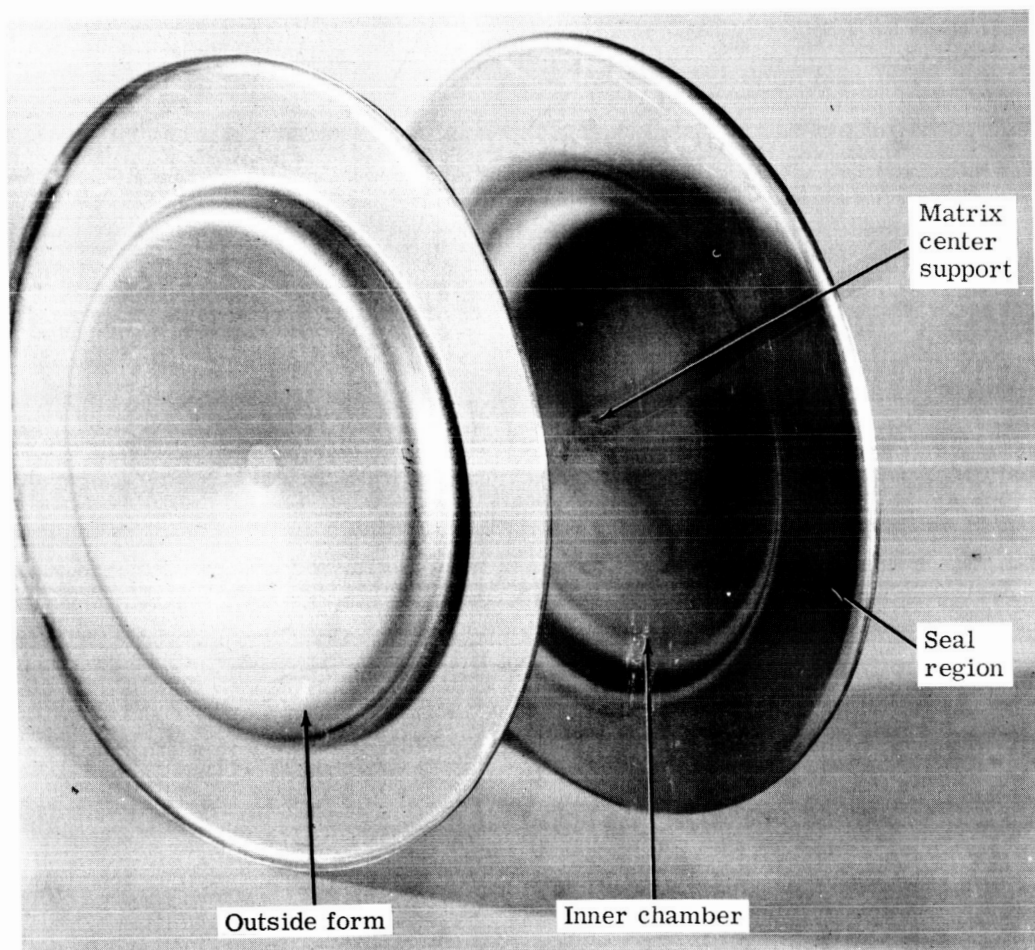


Figure 3-2. Hydroformed sections for a lightweight cell design.

the use of small cells for composite evaluation, maximum time was gained for work in the area of composite electrolyte development, prior to the time for large cell design decisions.

#### Vertical Cell

The two special features which account for the difference in the two large cell configurations are the sealing surface design and the orientation of the matrix plane. This vertical cell design utilizes concentric serrated seals, as shown in Figure 3-4, to withstand the high Hg head pressure when tested in the vertical position. The vertical plane was chosen so that the cell is subjected to the maximum failure conditions. This cell is shown in the test position in Figures 3-5 and 3-6. Design details are given in the portion of this section dealing with the final design of large cells.

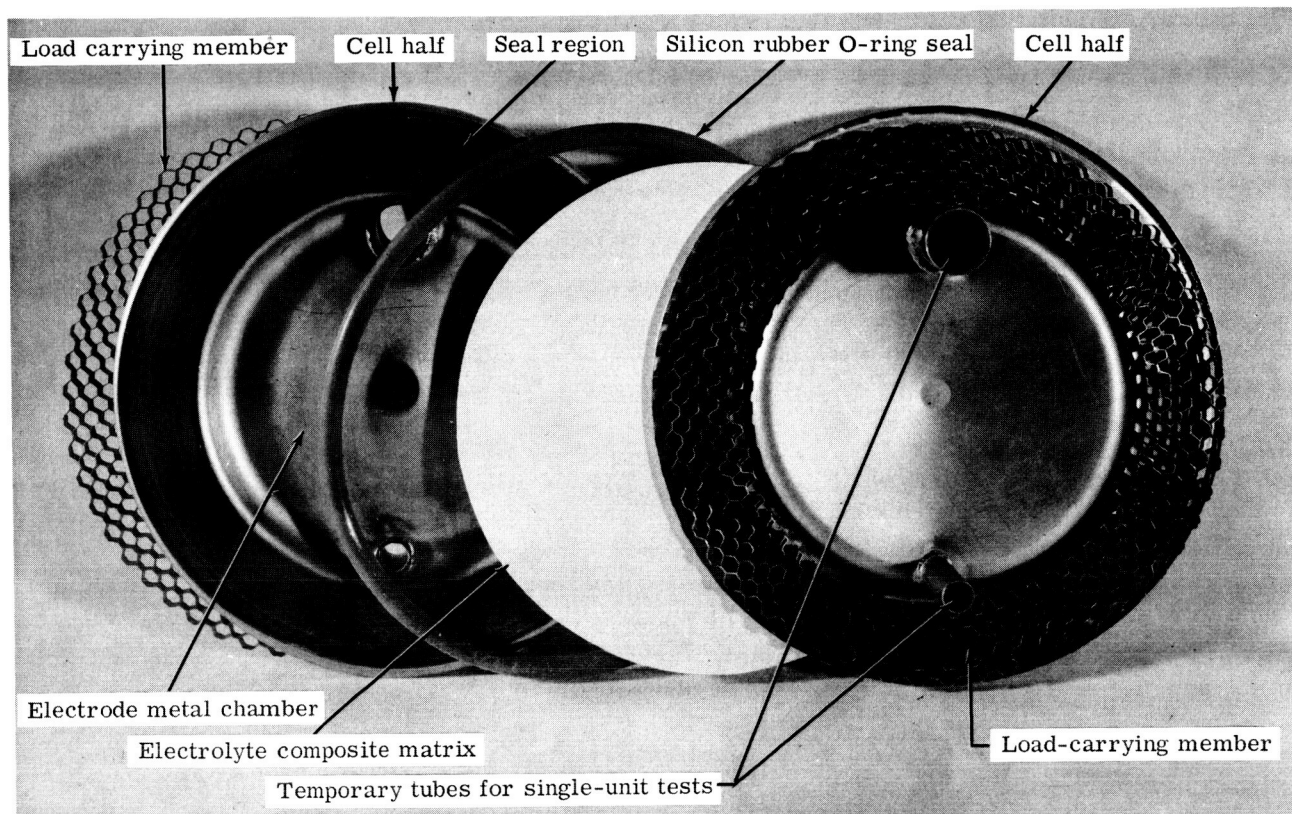


Figure 3-3. The assembly of a lightweight cell from hydroformed sections.

Features of the test stand and cell assembly are indicated in Figures 3-5 and 3-6. These photographs were taken after the test had been accomplished and the front of the furnace removed. The cell assembly and all auxiliary components are made an integral part of the furnace. The procedure for loading the electrolyte matrix was as follows:

1. The cell halves (see Figure 3-4) were placed in an inert gas glove box, with the matrix, ceramic stops, and silicon rubber seal.
2. The unit was assembled in the horizontal position with the 3/16-in. rubber O-ring taking the top-half load and thereby protecting the matrix.
3. The assembly was removed from the dry box, with all lines sealed, and placed into the furnace. The furnace was positioned on the left side at that time.

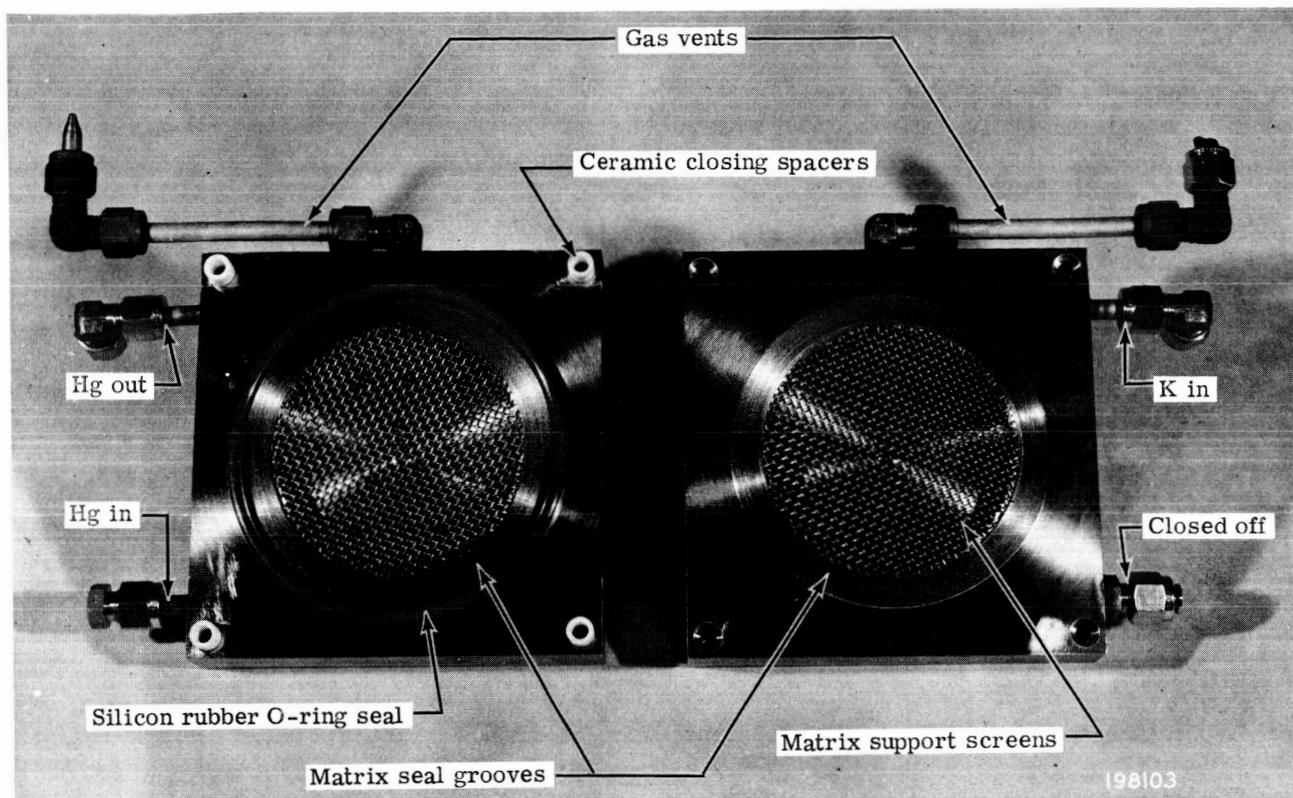


Figure 3-4. Vertical cell configuration in a preassembly layout.

4. After the clamp was applied and all line connections were made, the furnace was brought up to temperature while the cell was slowly closed. This ensured that the matrix was not damaged prior to becoming a paste.
5. Then the entire test rig was rotated to the position shown in Figures 3-5 and 3-6.

This vertical cell design was operated twice during the final testing period. The second test, cell XII, was considered to be entirely successful and is reported first. Table 3-I is a chronologic listing of data from three cell tests; the last cell, cell XII, is dated 7 November 1963.

The test period for the second test was from prior to 10:00 a.m., 7 November 1963, to 8:19 p.m., 11 November 1963. This is a total activity of 106 hr. The period of actual operation as a cell started at 10:19 a.m. on 8 November 1963 and therefore endurance is stated as 82 hr.



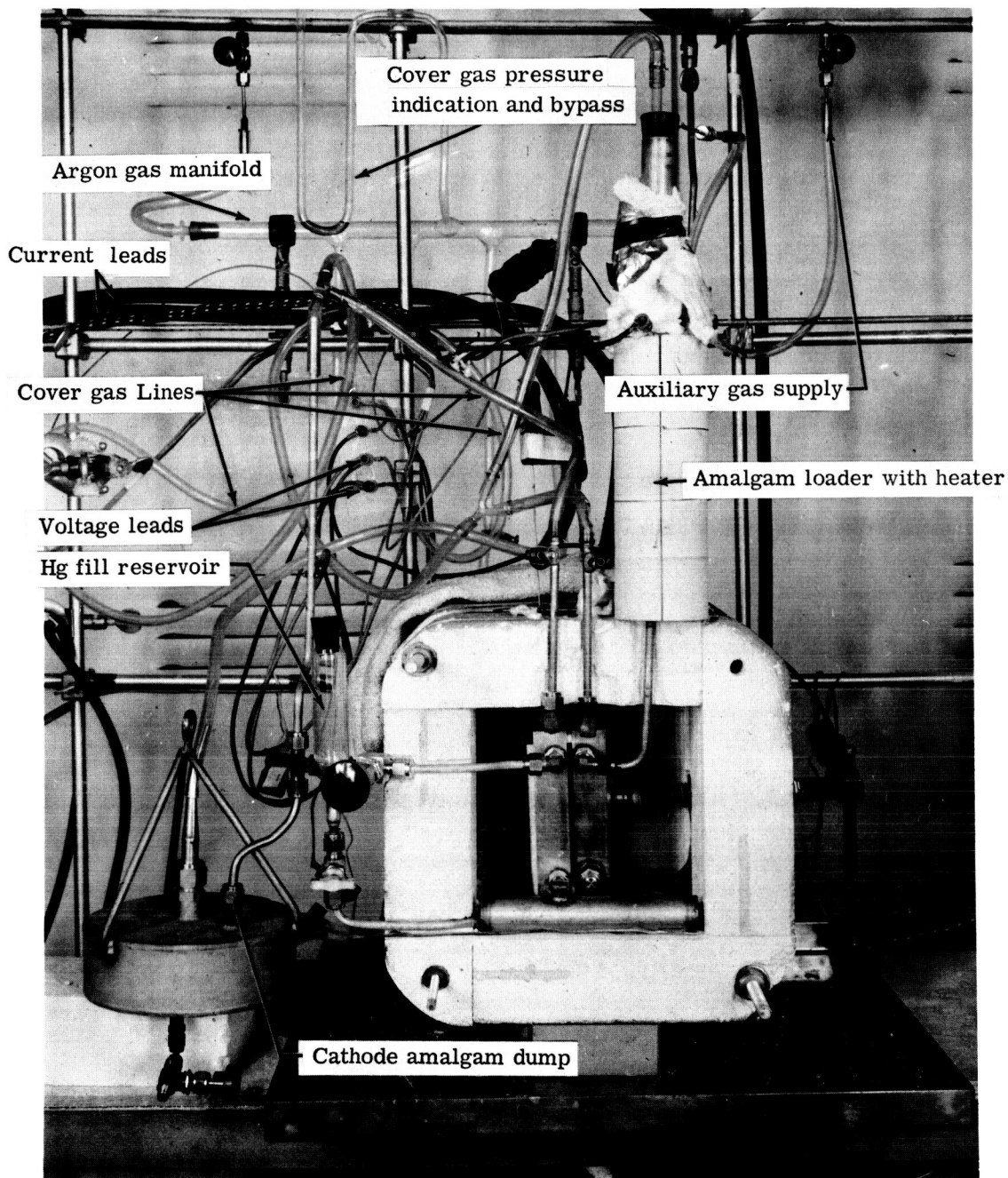


Figure 3-5. Vertical cell configuration in the test stand.

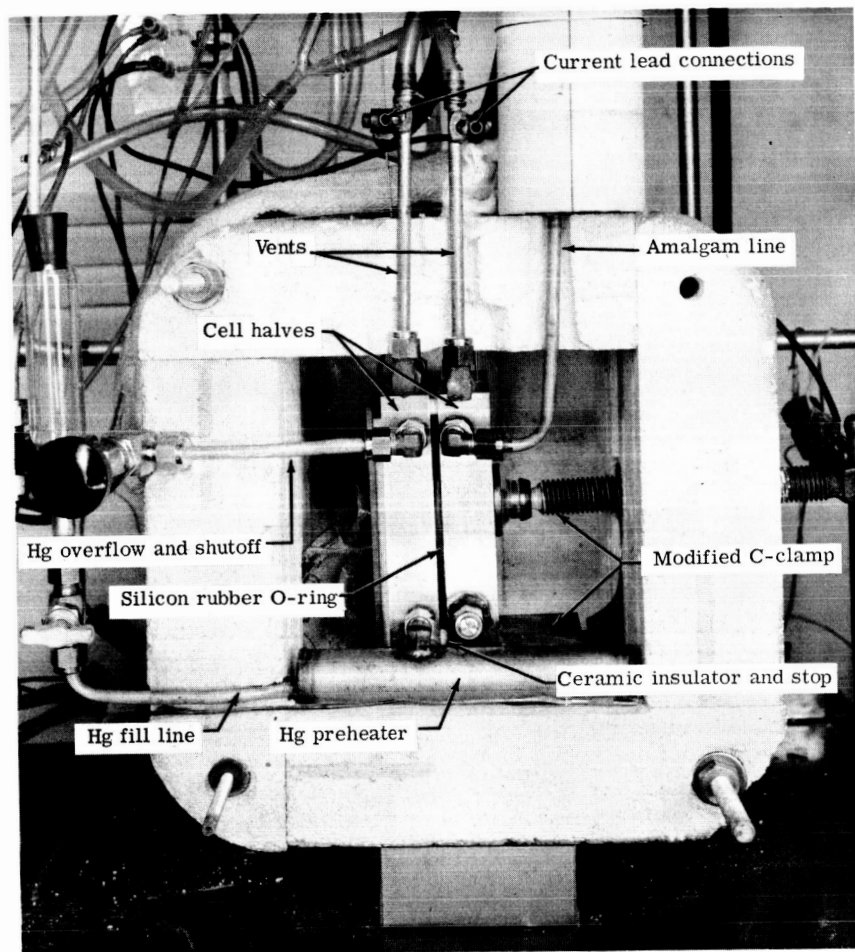


Figure 3-6. The vertical cell after assembly.

A more careful review of the data reveals that uninterrupted performance existed until 8:11 p.m. on 9 November 1963, or for 33 hr. At that time a continuous recharge brought the cell back for another series of charge-discharge cycling. A steady decrease in the apparent cell potential until the 450th cycle at 7:55 a.m. on 10 November 1963 indicated that the anode was becoming deficient in K-metal. However, the cell was not dead and was placed on open circuit at 9:02 a.m. Total operating time was 47 hr.

Table 3-I.  
Data on composite electrolyte matrix cells.

Cell electrolyte percentage, and date	Time of day	Open circuit potential $V_0$	Operating potential $V_0^*$	Operating voltage $V_c$	Load current, I (amp)	Computed cell resistance R (ohms) <sup>1</sup>	Resistivity $\gamma$ (ohm-cm)		
Cell XIII 65% 10-24-63 Type FF MgO	Cycle No. 1 (1:25 PM)	0.93	0.86	0.42 d	1.0 (regulated)	0.44	59		
		1.08	1.112	1.37 c		0.25			
		0.975	0.91	0.61		0.30			
		2	1.10	1.13		1.40	0.27	40	
			0.97	0.90		0.59	0.31		
			1.095	1.12		1.395	0.275		
		3	0.98	0.92		0.62	0.30	40	
			1.09	1.12		1.385	0.265		
			0.98	0.92		0.63	0.29		
		5	1.09	1.12		1.36	0.24	39	
			0.985	0.93		0.64	0.29		
			1.075	1.12		1.36	0.24		
		(Began unstable operation with intermittent shorts.)							
		7	0.985	0.935		0.67	0.265	36	
			1.06	1.11		1.34	0.23		
	0.98		0.935	0.655		0.28			
	8	1.06	1.10	1.33		0.23	38		
		0.98	0.94	0.675		0.265			
		1.05	1.09	1.30		0.21			
	10	0.98	0.94	0.695		0.245	33		
		1.02	1.07	1.28		0.21			
		0.975	0.93	0.67		0.26			
	11	0.98	1.015	1.23		0.215	35		
		0.965	0.92	0.685		0.235			
		1.01	1.035	1.26		0.225			
	13	0.91	0.86	0.605		0.255	34		
		0.97	1.02	1.24		0.22			
		0.94	0.86	0.62		0.24			
	14	0.95	1.01	1.225		0.215	32		
		(Highly unstable—readings average)							
		(5:36 PM) 15	0.89	?		0.62		--	
	0.89		0.96	1.17		0.21			
	(Major breakdown—cell dead)								
Cell XI	1:30 PM	(Cell fabricated—start heat-up)							
65%	8:00	(Cell at 300°C—tighten clamp)							
10-28-63	7:50 AM								
10-29-63									
Type FF									
MgO	8:45	(Hg loaded to preheater)							
	9:15	0.0	—	0.35	0.1	3.5 (resistance test)			
	9:28	(Start Hg loading)							
	10:05	(Hg full)							
	10:15	(Start amalgam heat-up)							
	10:21	0.50	(amalgam loading)						
	10:21:12	0.75							
	10:21:24	0.85							
	10:22	0.93							
	10:23	0.98							
	10:24	1.00							
	10:41			0.51	2.6				
	10:45		0.79	0.51	2.6	<u>0.108</u> 0.059	8.1		

Table 3-I. (cont)

Cell electrolyte percentage, and date	Time of day	Open circuit potential $V_0$	Operating potential $V_0^*$	Operating voltage $V_c$	Load current, I (amp)	Computed cell resistance R (ohms) <sup>1</sup>	Resistivity $\gamma$ (ohm-cm)
Cell XII 65% 11-7-63 11-8-63 Type FF MgO	10:46	0.88					
	10:58	(Start charge-discharge cycling)					
	Cycle No. 1			0.985 c	1.0		
		0.84		0.485 d	2.6		
	5			0.975	1.0		
		0.83		0.48	2.6		
	10			0.965	1.0		
		0.82		0.48	2.6		
	11:33		0.76	0.475	2.6	$\frac{0.11}{0.061}$	8.4
	14			0.955	1.0		
		0.81		0.47	2.6		
		(Slight internal short indicated)					
	11:41		0.73	0.41	3.0	$\frac{0.107}{0.058}$	8.0
	15			0.935	0.95		
		0.805		0.46	2.55		
	20			0.915	1.0		
		0.78		0.44	2.6		
	25			0.895	1.05		
		0.76		0.40	2.6		
	30			0.885	1.05		
		0.75	0.67	0.40	2.6	$\frac{0.104}{0.055}$	7.6
	1:26 PM	(Frequent shorting—cyclor turned off)					
	1:29			0.50	1.7		
	1:32			0.15	0.5		
	1:33			0.06	0.3		
	1:42		0.05	0.17	2.2	$\frac{0.055}{0.006}$	0.8
	1:53	(Unexplained recovery)					
	1:56			0.76	1.25		
	1:57	0.15	(Internal shorting)				
	1:58		0.105	0.25	2.05	$\frac{0.071}{0.022}$	3.0
	2:22		0.07	0.22	2.1	$\frac{0.071}{0.022}$	3.0
	2:32		0.07	0.49	6.1	$\frac{0.069}{0.020}$	2.8
	3:32		0.02				
		(Shutdown)					
		Posttest lead resistance study					
		0.0		0.49	10.0	0.049	
		0.0		0.05	1.0	0.05	
	10:00 AM	(Cell fabricated—start heat-up)					
	4:45 PM	(Cell at 300°C—tighten clamp)					
	8:45 AM	(Cell rotated to vertical position)					
	9:17	(Add Hg to preheater)					
	9:56	(Start amalgam heat-up)					
	10:02	(Start Hg fill)					
	10:14	(Hg filled)					
	10:19	0.50	(Amalgam loading)				

Table 3-I. (cont)

Cell electrolyte percentage, and date	Time of day	Open circuit potential $V_0$	Operating potential $V_0^*$	Operating voltage $V_c$	Load current, I (amp)	Computed cell resistance R (ohms) <sup>1</sup>	Resistivity $\gamma$ (ohm-cm)
	10:19:12	0.67					
	10:19:24	0.70					
	10:20	0.70					
	10:21	0.85					
	10:22	0.91					
	10:24	0.95					
	10:30	1.04					
	10:34	(Start cycling)					
	10:38		0.80	0.53	3.35	0.081	11.2
	10:43		0.80	0.58	3.00	0.073	10.1
	11:26		0.68	0.17	6.8	0.075	10.4
	1:21 PM		0.75	0.52	2.33	0.099	13.7
	Cycle No. 40			0.59 d	1.95		
		0.83		1.15 c	1.95		
	2:26		0.77	0.60	1.95	0.087	12.0
	3:11 50			0.60	1.95		
		0.83		1.18	1.95		
	4:04 60		0.76	0.59	1.95	0.087	12.0
		0.825		1.225	1.95		
	4:30		0.67	0.27	3.60	0.111	15.3
	5:07	Maximum power investigation				P watts (1)	
				1 min 2 min		1 min 2 min	
	Cycle No. 63	0.81		0.74 0.74	0.60	0.445 0.445	
	68			0.73 0.725	0.65	0.474 0.471	
	70			0.725 0.72	0.70	0.506 0.504	
	72			0.71 0.695	0.825	0.585 0.573	
	73			0.67 0.65	1.10	0.736 0.715	
	76			0.66 0.64	1.20	0.790 0.768	
	77			0.65 0.625	1.30	0.846 0.812	
	79			0.635 0.60	1.42	0.90 0.852	
	80			0.63 0.60	1.52	0.945 0.900	
	81			0.62 0.58	1.60	0.99 0.928	
	82			0.56 1.60	2.0	1.12 1.00	
	84			0.455 0.385	2.8	1.27 1.08	
	8:37		0.67	0.26	3.8	0.108	14.9
	10:07		0.75	0.66	1.0	0.090	12.4
	Cycle No. 150			0.66	1.0		
		0.805		0.965	1.0		
	200			0.645	1.0		
		0.80		0.965	1.0		
	213			0.62	1.0		
		0.775		0.775	1.0		
	7:08AM 215	(indication of internal short $\Delta V = 0.02$ volts)					
	10:08 249	(indication of internal short $\Delta V = 0.04$ volts)					
	250			0.58	1.0		
		0.75		0.895	1.0		
	264			0.58	1.0		
		0.74		0.875	1.0		
	11:31		0.68	0.58	1.0	0.10	13.8
	11:38		0.51	0.285	2.63	0.086	11.7
	11:56	(on charge)		0.90	0.55		
	1:10 PM	0.73					

(1) Figures in this column, between the lines above and below, record power values. Balance of the column are resistance figures.

Table 3-I. (cont)

Cell electrolyte percentage, and date	Time of day	Open circuit potential $V_0$	Operating potential $V_0^*$	Operating voltage $V_c$	Load current, I (amp)	Computed cell resistance R (ohms) <sup>1</sup>	Resistivity $\gamma$ (ohm-cm)
	1:14	(on charge)		1.06	1.05		
	1:28	0.82					
	Cycle No. 267 (Change cycle ratio for longer charge time 150 sec charge—30 sec open circuit—115 sec discharge—30 sec open circuit)						
	No. 273			0.59	0.6		
		0.725		0.85	0.6		
	2:26	(on charge)		1.05	1.0		
	2:49	(off charge—on cycling)					
	3:18 No. 280			0.59	0.7		
		0.815		1.07	0.7		
	4:18 No. 289			0.56	0.75		
		0.805		1.05	0.75		
	No. 300			0.50	0.75		
		0.73		0.97	0.75		
	(Frequent internal shorting—stop cycling on No. 331)						
		0.61					
	8:11	(on charge)		0.765	0.70		
	8:46			1.25	2.68		
	9:06	0.80					
	9:16	(Start cycling)					
	No. 333			0.50	0.55		
		0.56		0.64	0.55		
	No. 339			0.195	0.55		
		0.26		0.335	0.55		
	No. 370			0.11	0.58		
		0.195		0.27	0.58		
	No. 401			0.04	0.58		
		0.15		0.26	0.58		
	No. 425			0.00	0.55		
		0.11		0.22	0.55		
	Power supply driving cell neg from No. 425 to No. 450						
11-10-63	7:55 AM No. 450			Neg	0.55		
		0.12		0.245	0.55		
	8:15		0.185	0.245	0.55	0.109	15.0
	8:15		0.11	0.16	0.55	0.091	12.6
	9:02	0.08	(Left on open circuit overnight)				
11-11-63	8:05 AM	0.032					
	9:07	0.035					
	9:46	(on charge)		0.13	0.55		
	10:17		0.10	0.165	0.55	0.118	16.3
	10:30	0.05					
		(Indicates anode is K-metal deficient)					
		(Placed total of 10 grams K-metal in loader)					
	11:18	0.10					
	11:19	0.20					
	11:20	0.20					
	11:21	0.25					
	11:26		0.160	0.105	0.80	0.069	9.5
	11:27	0.23					
	11:29	(on charge)		0.35	1.10		
	11:57	0.24					
	12:05 PM	0.26					
	12:06	0.08					

Table 3-I. (cont)

Cell electrolyte percentage, and date	Time of day	Open circuit potential $V_0$	Operating potential $V_0^*$	Operating voltage $V_c$	Load current, I (amp)	Computed cell resistance R (ohms) <sup>1</sup>	Resistivity $\gamma$ (ohm-cm)
	12:11	(on charge)		0.14	1.10		
	12:14	(Flushed cathode with 30 cc Hg)					
	12:15		0.075	0.12	1.10	0.041	5.7
	1:36		0.085	0.13	0.85	0.053	7.3
	1:50	0.06	(5 gram K-metal loaded)				
	1:55	0.08					
		(On open circuit to make ac bridge measurements)					
	2:28	Frequency 10 <sup>4</sup> cps—R = 0.088 - 0.041 = 0.047 ohm					
		Frequency 10 <sup>3</sup> cps—R = 0.088 - 0.041 = 0.047 ohm					
	2:36	0.07					
	2:49	(on charge)		0.165	1.0		
		(Start cell heat-up from 300°C)					
	3:27		0.11	0.16	1.0	0.05	6.9
	3:45			0.46	1.0	(Temperature at 320°C)	
	3:49	(Start cycling with No. 452)					
	Cycle No. 455			0.25	1.35		
		0.375		0.48	1.35		
			0.29	0.25	1.35	0.03	4.1
	4:19 No. 457	Stop cycling		0.46	1.35		
	4:24	(Flushed cathode with 30 cc Hg)					
	4:33		0.07	0.085	1.35	~0.011	1.5
	4:38	0.045					
	5:00	0.03	(Place on charge)		1.35		
	5:57	(charge)		0.085	2.0		
	6:30	(charge)		0.125	3.05		
	6:53		0.10	0.17	3.05	0.023	3.2
	7:00			0.185	3.1		
	7:03			0.23	3.1		
	7:04			0.42	3.1		
	7:05			0.46	3.1		
	7:06			0.465	3.1		
	7:07			0.36	1.0		
	7:09	(Start cycling with No. 458)					
	No. 459			0.232	1.0		
		0.29		0.345	1.0		
			$\Delta V \approx 0.02$		1.0	>0.02	~2.8
	8:18 No. 470			0.242	1.0		
		0.295		0.35	1.0		
		Indicates a low resistance cell					
11-11-63	8:19 PM	Shutdown operation					

Note: c indicates charge  
d indicates discharge

<sup>1</sup>Cell resistance is computed from an instantaneous cell potential to eliminate the effect of electrode concentration gradients. This technique is described in Figure 5-29 of this report and is given as

$$R_c = \frac{V_0^* - V_c}{I}$$

After another 13 hr on open circuit (until 10:17 a.m. on 11 November 1963), a test of cell internal resistance indicated that the cell was not tending toward a low-resistance short. Subsequent charging indicated a deficiency in K-metal on the anode side. Total test time was 72 hr.

Table 3-I shows that attempts to regenerate by adding K-metal to the anode and flushing the cathode with fresh Hg were partially successful. An unexplained reduction in cell internal resistance began and became increasingly troublesome as additional attempts were made to regenerate the cell. It is interesting to note that the cell was never in a state of absolute shorting and was on charge-discharge cycle No. 470 with an open circuit potential of approximately 0.30 volt and an internal resistance of approximately 0.02 ohm when the testing program was shut down at 8:19 p.m. on 11 November 1963. Total test time was 82 hr.

Another highlight of this test is seen at 2:28 p.m. on 11 November 1963. The a-c bridge measurement was taken by equipment described in Section V. Since the four leads method described in Section VI was not used, the lead resistance ( $\Delta R = 0.041$  ohm) was applied from a measurement made earlier. It is of primary importance to note that the a-c bridge technique and the instantaneous voltage  $V_O^*$  technique agree favorably on this cell. Cell measurements taken one hour before and after the a-c bridge measurement agree favorably.

During operation of the vertical cell, an investigation of maximum power point was made. During regulated current operation, the cell potential drops with an attendant decrease in power. The maximum power investigation is shown in Table 3-I at 5:07 p.m. on 8 November 1963. Two sets of data were taken—the first at one minute after the initial load was applied and the second at two minutes. Corresponding power has been tabulated. This work was accomplished during cycling operation so that the average cell potential remained at  $V_O = 0.81$  volt. The data have been plotted for analysis in Figure 3-7.

First, cell resistance was measured at the time of the investigation by the slope of the line through  $V_O^* = 0.67$  and  $V_C = 0.26$  at  $I = 3.8$  amp. The resistance,  $R$ , is the slope of the line and is 0.108 ohm. Second, this same slope has been drawn through the average open circuit voltage of 0.81 volt, which becomes the ideal voltage-current line. The ideal power curve is developed from the  $V$ - $I$  product of this line and is seen to become a maximum at  $V_C = \frac{V_O}{2} = 0.405$  volt. This same curve can be thought of as the power at the instant the current load is applied. When the two curves (for 1 min and 2 min) which are developed from the data are compared, it is seen that the maximum power point shifts to the left with time.



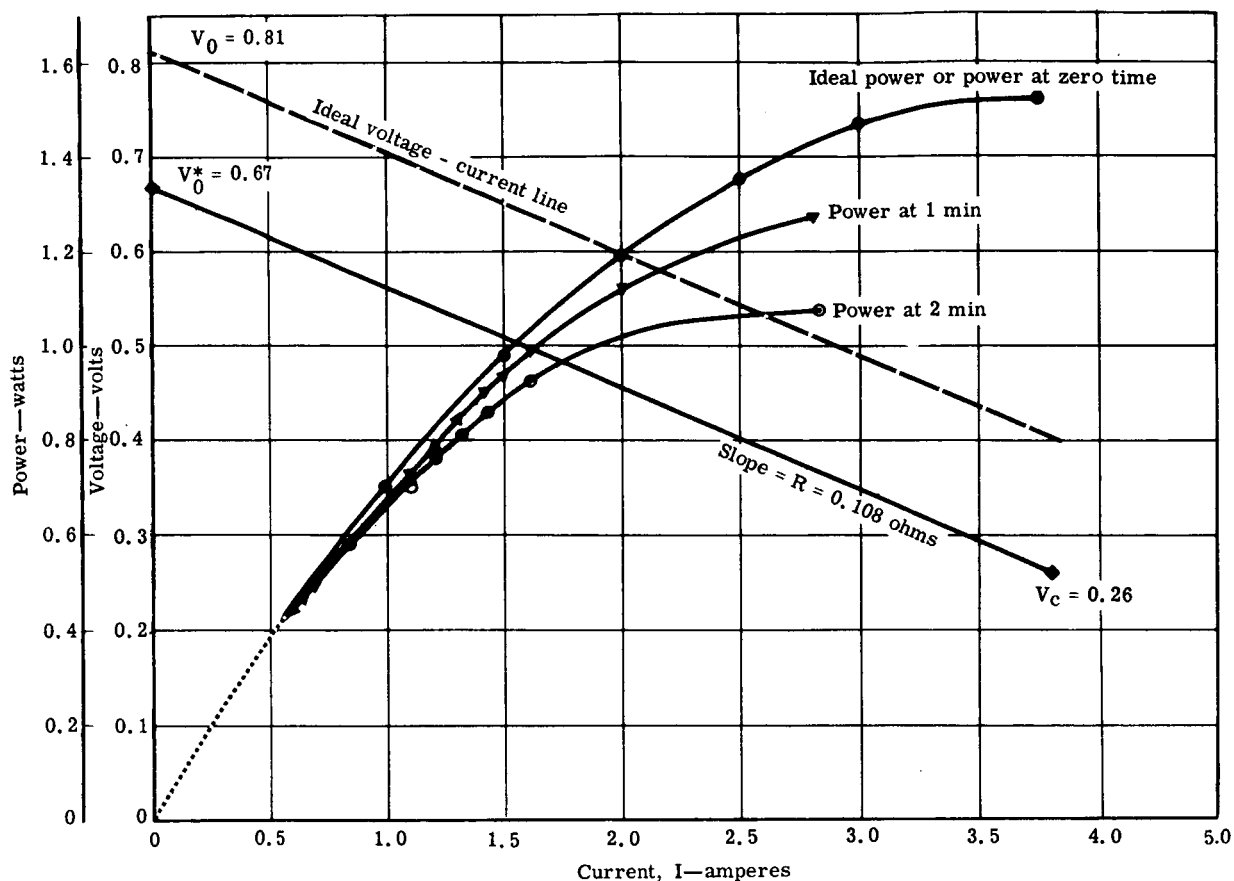


Figure 3-7. Results of a maximum power investigation, showing the effect of diffusion.

Since the open circuit potential was maintained at 0.81 volt by electrochemical regeneration using cycling equipment, the time variation in power is seen to be caused by poor diffusion. The most likely source of poor diffusion is stagnation within the pockets formed by the supporting screens. The projected area of the screen has been determined to be approximately 50% of the total area. Posttest analysis by use of the microscope has shown that the screen makes point contact with the matrix on the anode side and no contact on the cathode side. Therefore, the resistance effect on the cell active area is negligible. Two modifications are proposed with reference to diffusion. First, the cathode screen should be removed. Second, the screen used on the anode side should be of larger mesh to provide better diffusion within the amalgam.

The preceding paragraphs discuss the evaluation of cell performance. Cell performance is directly dependent on matrix characteristics (dimensional and chemical stability and electrical resistivity). After a stable matrix has been developed, the resistivity is the true matrix performance factor. The resistivity of cell XII was 10 to 15 ohm-cm, which is inconsistent with performance of other fine grain composites with 6 ohm-cm (Section V). This may be due to processing, since the matrices were not all prepared at the same time.

Results from the other vertical cell run, designated cell XI, are also shown in Table 3-I. This cell performed for 3.2 hr before serious shorting caused a lower resistance and lower cell potential. The total electrical performance existed for 5.2 hr.

The voltage measurements obtained during this cell run were made by attaching the voltage leads to the current-carrying terminals. Therefore, a correction factor was applied as determined by a posttest investigation. This investigation, which used a brass plate in place of the matrix, showed the correction factor ( $\Delta R$ ) to be 0.049 ohm. The resistivity values shown in Table 3-I are corrected for this constant.

The resistivity values of cell XI (near 8 ohm-cm) compare favorably with those of other fine grain composites but do fall short of values obtained on the small cell work reported in Section V. These values are shown as near 6 ohm-cm for cells IX and X which were fabricated from early batches of 65% composite. It is noted that conductivity specimens 63, 64, and 65 show an increase in resistivity between the early 65% electrolyte composites and the last batch of 65% electrolyte composite. Specifically, the resistivities at cell operating temperature are 2.7, 2.8, and 4.0 ohm-cm, respectively. This is the same trend as found in cell performance.

It should be noted that a discrepancy also exists between values of resistivity obtained from cell performance and those from conductivity measurements. Some insight into the problem can be derived from the organization of data shown in Table 3-II. All cell tests, including the small cells reported in Section V, are listed. Four of the eleven were so short-lived or unstable that a resistance measurement was not obtained. Failures were, in general, due to cracking of the matrix.

From the seven cells with known performance a good range of test and design configuration variables was available for comparison studies. The variables selected for evaluation are shown in Table 3-II. The resistivity ratio is approximately 1.0 for cells I and VIII and is approximately 2.0 for cells IX, X, and XI. The other cells in the table show higher ratios.

Note that in each case of a unity ratio, pure potassium was used for the anode. In all cases when the 32 mole percent amalgam was used, the ratio is 2.0 or greater. An extra resistance at the electrolyte-liquid metal interfaces is indicated by these results. Further work will be required in this area to gain greater understanding and possible corrective measures.

## Horizontal Cell

The remaining large cell work to be reported is that of the horizontal cell XIII. This cell was operated on 24 October 1963. This configuration allowed a control over the level (and, therefore, the pressure) of the Hg cathode on the bottom and could be operated much like a differential density cell. Data are recorded in Table 3-I. From the beginning, the cell was operated in a cycling charge-discharge mode. The open-circuit potentials ( $V_o$  shown in Table 3-I) are those potentials recorded at the instant cycling was reversed. The actual open-circuit potential will be between these values.

The high resistance of this cell is apparently caused by factors associated with the configuration. Differential density cell configurations can be expected to trap minute quantities of gas or vapor under the matrix. In the case of a pure electrolyte, this gas may bubble through to the anode with only a momentary performance discontinuity.

The cell failed very abruptly after a steady lowering of resistance during the four hours of operation. The resistance change was about 20% and was due to the development of a crack in the matrix. Figure 3-8 shows the matrix after it was separated from the anode side of the cell. The sharp breaks were caused during removal. The ragged break at the top is along the ridge of an erupted region caused by a force from the underside, thereby resulting in cell failure.

Cell XI also failed from a break in the matrix; however, in this case it appeared that the break was caused by stresses during assembly or heat-up prior to the time of plasticity. Figure 3-9 shows the cathode side of the matrix. A semicircular break near the bottom of the cell in the seal region is typical of a fracture pattern caused from edge stresses. The shorted region that caused the failure is not evident in this picture but was located at the point shown by the arrow. The microphotos in Figure 3-10 show the region of the intersecting cracks and the hairline short through the matrix. Although the other cracks were etched near the surface, all were closed and had not shorted.

Cell XII was analyzed for shorts after the test had been discontinued. Since no cracks were apparent, there was no clue to which region might contain the intermittent short.

Table 3-II.  
Correlation of cell performance and test configuration factors.

Cell data						Conductivity specimen data				Resistivity ratio (cell specimen)	
Cell No.	Percent electrolyte	Percent density	Cell resistivity ( $\gamma$ ) (ohm-cm)	Anode material	Supporting screens	Conductivity specimen No.	Percent electrolyte	Percent density	Conductivity (K) (mho/cm)		Specimen resistivity ( $\gamma$ )(ohm-cm)
I	33	86.2	10	K	No	14	33	86	0.097	10.3	1.0
II	Bad seal—no performance			K	N						
III	No resistance measurements			K	No						
IV	No resistance measurements			K	No						
V	No performance—matrix break			Not filled	No						
VI	No resistance measurements			K	Yes						
VII	No resistance measurements			K	No						
VIII	65	93	3.0 to 3.3	K	Yes	63, 64	65	65.8	0.37	2.7	1.0
									0.357	2.8	
IX	65	94.2	6.0 to 11.0	K (32 m/o*)-Hg	Yes	63, 64	65	65.8	0.37	2.7	2.0
									0.357	2.8	
X	65	93.1	5.0 to 6.0	K (32 m/o*)-Hg	Yes	63, 64	65	65.8	0.37	2.7	2.0
									0.357	2.8	
XI	65.8	85.8	8.0	K (32 m/o*)-Hg	Yes	65	65	85.1	0.251	4.0	2.0
XII	65.8	82.5	10 to 15	K (32 m/o*)-Hg	Yes	65	65	85.1	0.251	4.0	2.5
XIII	65.8	82.2	31 to 40	K	No	65	65	85.1	0.251	4.0	>10.0

Note: All cell matrices were 1/8 in. thick.  
\*m/o indicates mole percent



Figure 3-8. The anode side of a 4- x 1/8-in. matrix after test in cell XIII.

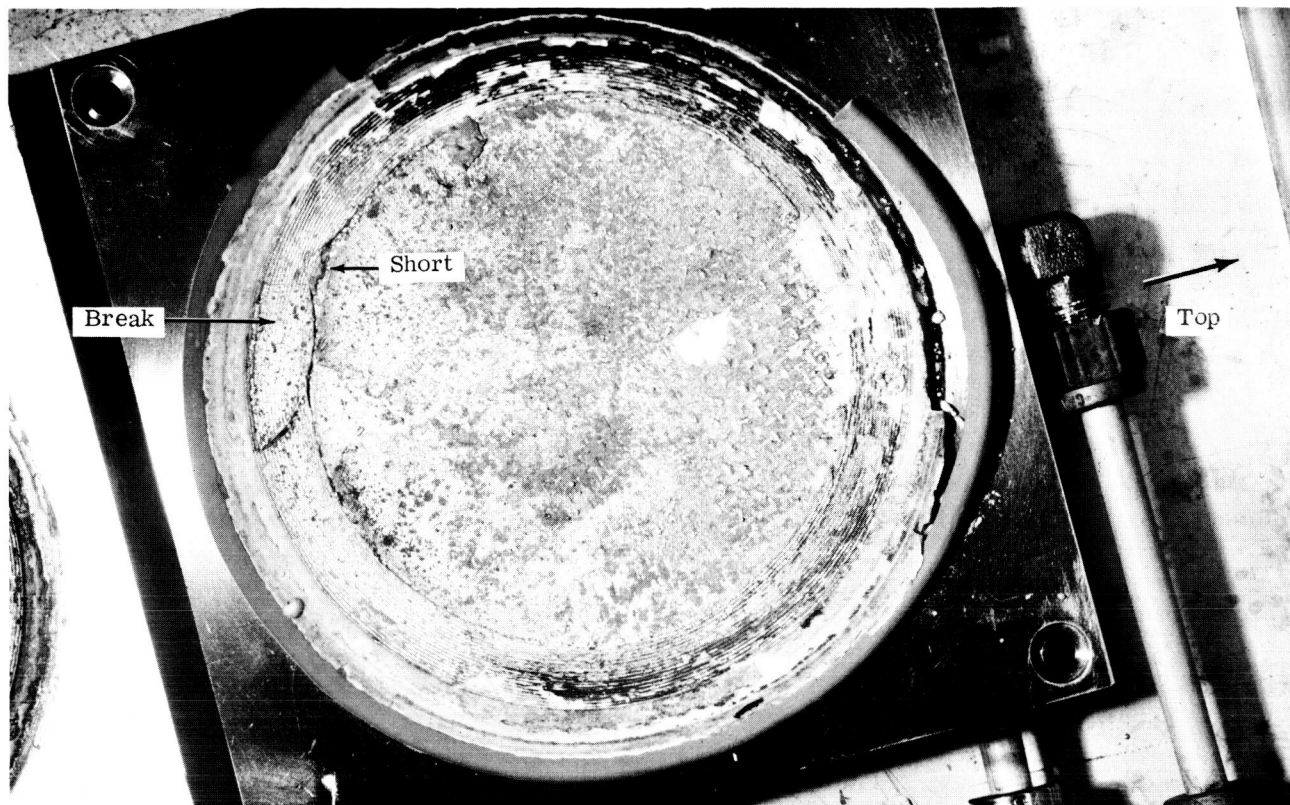
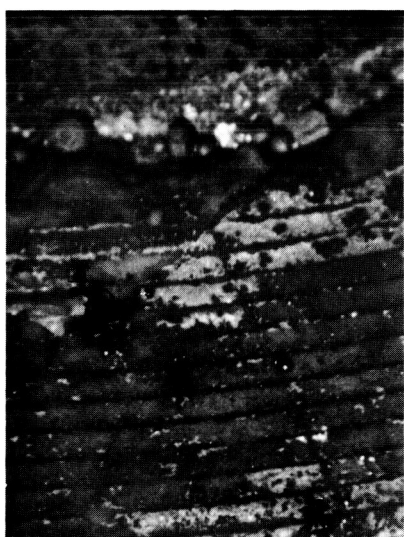
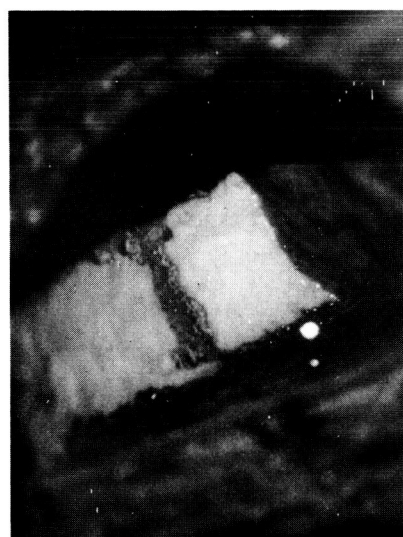


Figure 3-9. Composite matrix after test in cell XI showing breaks and region of short.



Region of short.



Thin line of metal penetration suspected as the short path.

Figure 3-10. Microphotos for matrix analysis.

## FINAL DESIGN OF LARGE CELLS

The final design of cells for this program was primarily dictated by the successes with the small cell design. This small cell design is described in Section V along with the ten small cell tests. The primary considerations in the design are the properties of the electrolyte matrix material to be used. The significant properties are: conductivity, strength, surface sealing, and material compatibility.

The conductivity of the matrix must be high to ensure high cell performance. The electrochemical requirements dictate the use of a thin matrix with large area. The mechanical needs prescribe thicker materials and short unrestrained spans (low area) for strength. Therefore, the electrochemical and mechanical problems are interrelated and must be solved together in an intricate optimization.

Strength of the matrix is a hard-to-define parameter. Various tests have shown the material to be brittle at storage temperatures, and ranging in weakness from crumbling to plastic flow at operating temperature depending on its composition. Therefore, strength is an elusive parameter and may be gained through the use of supporting structures—supporting structures which may play a degrading role in the electrochemical performance. Consequently, a tie-in is again seen to exist between the electrochemical and mechanical properties to be optimized.

The third property of the material is that of sealing characteristics and compatibility of the matrix to the mating surfaces at the seal regions. The one greatest mechanical advantage of a paste matrix over that of a rigid impregnated matrix is the ease of sealing. The paste exhibits a pliable, moist surface which will conform to the mating material under a light pressure. Selection of a good seal form, such as serrations on the surface, is all that is required to attain a seal.

Compatibility of the matrix material is another important design consideration in the choice of materials for cell construction. A simple seal may be formed by use of a basic cell material—for example, stainless steel. Chemical reaction with the mating metal surfaces which form the seal should be held to a minimum. Also, the possibility that direct contact of the electrolyte with the two cell halves may cause an electronic short through the electrolyte in the seal regions poses a problem and must be considered. In the case of the K-Hg cell system using the KOH-KBr-KI eutectic, this problem is minimal. Conductivity studies show that the ionic conductance is many times that of the electronic conductance of the pure electrolyte. The use

of the serrated seal design in early small cells, as reported in Section V of this report, also bears this out. These studies were carried out with the seal area three times that of the active cell area, and there was no degrading effect. Any electronic conductance through the seal region would have appeared as an external electrical load and would have reduced the cell potential. This did not appear to be a problem.

Another consideration in the design of the cell is that the system is reactive with moisture and other components of the atmosphere. Precautionary measures taken in the laboratory to exclude atmospheric contamination do not necessarily produce lightweight, refined designs. Completely enveloping the cell is the most basic technique but produces heavy designs. The simple, lightweight approach is to sandwich the matrix between two cell halves with independently sealed electrode metal supply systems. The problem of atmosphere contamination is then narrowed to the protection of the matrix periphery. Since the edge of the thin matrix presents minimal area, a small O-ring made of silicon rubber may be used.

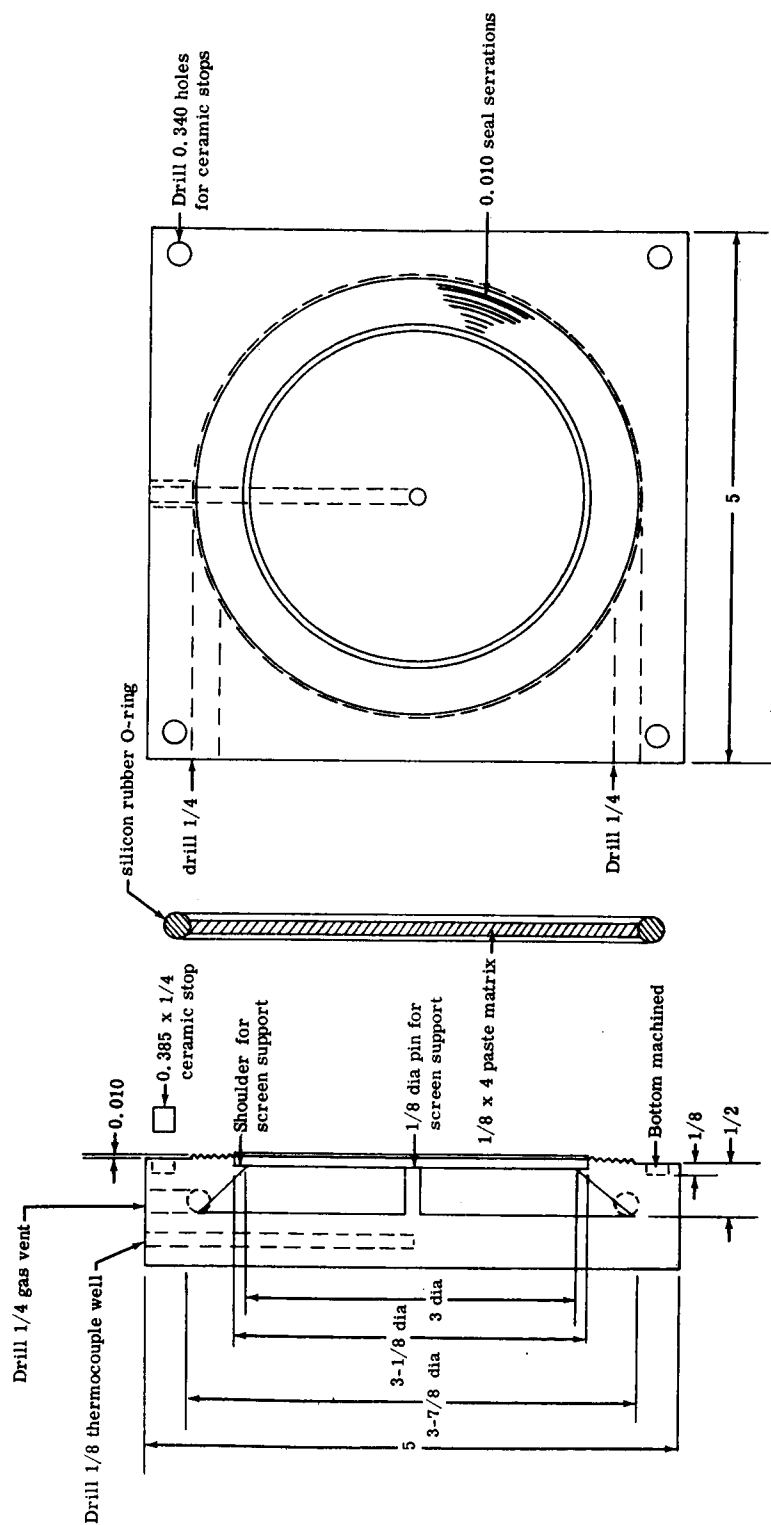
## Vertical Cell Design

The design used in testing composite matrix performance and durability is shown in the design sketch, Figure 3-11. The laboratory device shown in Figure 3-11 does not represent the ultimate in lightweight compact cells for systems work.

Two reference dimensions are used as a basis for the design. First, the contractual requirements call for an active electrochemical region of not less than 3 in. in diameter. Second, the nominal matrix dimension of 4 in. diameter was chosen early in the program and fixed arbitrarily so that a fabrication die could be constructed. The difference between these two dimensions allows sufficient area for sealing.

The center drawing of Figure 3-11 shows a cross section of a matrix with the silicon-rubber O-ring in place. This O-ring was molded of a high temperature silicon rubber to exact specifications. The inside diameter was fixed at 3-7/8 in. to permit a firm grip when mounted on a cold composite matrix disk prior to cell assembly. The O-ring cross section diameter was chosen as 3/16 in. (nominal) to allow as much as 1/16 in. compression of the material with the use of a 1/8-in. matrix.





Note: All dimensions are shown in inches.

Figure 3-11. Detailed sketch showing vertical cell design.

The cell halves (only one is shown) were machined from a  $5 \times 5 \times 1$  in. stainless steel block. The concentric serrations were formed by  $90^\circ$  vee grooves with radial indexing to form the points. The serration height was 0.010 in. above the block surface and was therefore 0.020 in. peak-to-peak. This gives approximately 18 serrations in the  $3/8$  in. region. The design was fixed so that a 0.005-in. serration penetration is made into the paste matrix when the cell halves are closed. Since two cell halves close onto the  $1/8$ -in. matrix, this leaves a gap of 0.135 in. at the outside edge. Four ceramic spacers are located at the corners to hold this critical dimension. The measured diameter of the ceramic spacers was 0.336 in. Therefore, the bottom machined holes were opened to 0.340 in. diameter and bottomed at  $1/8$  in. (0.125 in.). The spacer length (0.385 in.) is fixed at the sum of the two bottom depths plus the desired gap of 0.135 in.

Each cell half was machined to accept a matrix supporting screen. The supporting shoulders and center pins were machined after the selection of the particular stainless steel wire mesh. The mesh used in this design was made with 0.020-in. dia wire, woven at 12 strands/in. The shoulder and pin were machined to a depth of 0.050 in., corresponding to the measured screen thickness. These screens were spot resistance-welded into place at the pin and around the circumference. The design allows for only point contact of the wire to the composite matrix. If the support is found to be unnecessary, then one or both may be omitted without further modification of the design.

The electrode metal chambers were machined with a conical cavity as was done in the early small cell design. The vent lines and fill lines were drilled into the chambers near the largest radius so that they were located at the highest or lowest points, respectively, when the cell was assembled in the vertical plane. This minimizes the chance of mechanical erosion of the matrix during filling. Short sections of stainless steel tubing were welded into place (not shown) so that appropriate fittings could be used to complete the plumbing during assembly.

The resulting heavy section served two functions. First, it gave absolute rigidity to the design in transmitting the clamping force to the O-ring, matrix, and ceramic spacers. Second, it served as thermal damping to the on-off control of the kiln (shown in Figures 3-5 and 3-6). A thermocouple well was drilled into the heavy section in both cell halves. The thermocouples were used to monitor the electrode temperatures during operation. The assembly, used to clamp the cell within a furnace, and the subassemblies which were incidental to the operation are best shown by Figures 3-5 and 3-6.

### Horizontal Cell Design

The horizontal cell was designed and fabricated as a backup to the testing program. In this design, shown in Figure 3-12, the matrix was positioned in the horizontal plane. This configuration permitted control of the Hg level and, therefore, the pressure across the matrix. This resembles the differential density cells where 100% electrolyte levels (no MgO present) are maintained by Hg-level control.

The cell was fabricated from welded cylindrical stainless steel sections and plates. The bottom section (cathode side) consisted of a 3-in. ID cylinder with a bottom and a ring flange welded into position. The ring flange had a radius greater than 4 in. diameter so that the composite electrolyte matrix made a flat contact seal in this region.

The top section (anode side) was constructed of two cylinders and two flat ring sections. The large ring flange was attached to the large cylinder to act as the seal region much as that on the cathode side. The upper cylinder was formed as an access to the anode chamber for filling. The shoulder formed by the reduced radius was used to apply a load for seal pressure. This load was formed by a dead weight placed in position during assembly.

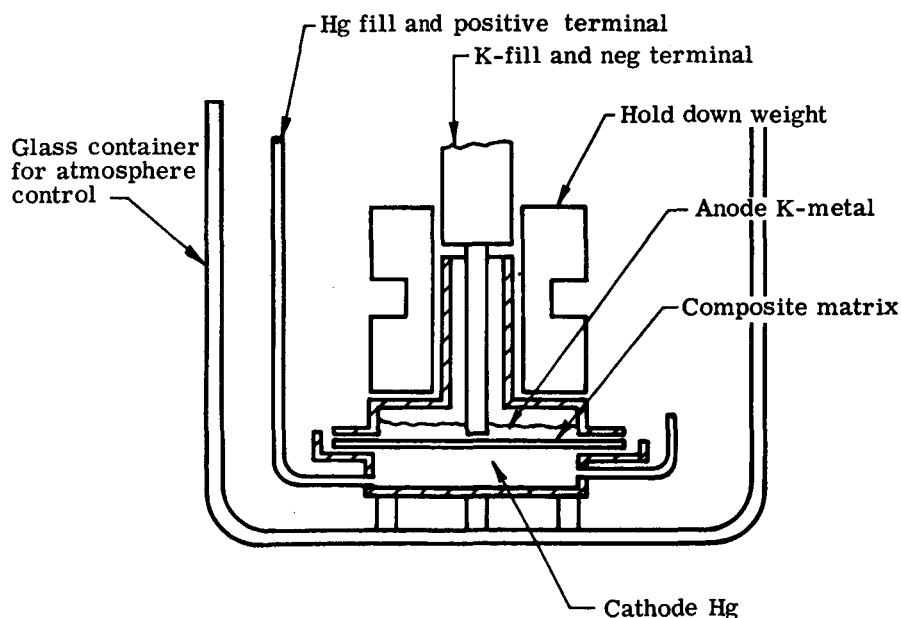


Figure 3-12. Schematic of the horizontal cell.

Supporting screens for the electrolyte matrix were not used. The matrix floats on the Hg during assembly and loading procedure. Mercury was added through a tube and level control was obtained by means of an overflow tube. All gases and vapors must escape from under the matrix through the seal path prior to application of seal pressure and after the cell is at temperature. Therefore, an inherent problem with the design is seen to be the chance of trapped gases or vapor accumulating under the matrix during operation.

The environment for this cell was controlled through the use of a glass envelope sealed at the top around the Hg-fill and K-fill tubes. For this design an internal seal was needed to protect the anode chamber from the Hg vapor atmosphere within the glass envelope to prevent carry-over of Hg to the anode chamber.

#### IV. DEVELOPMENT AND MECHANICAL PROPERTY STUDIES OF COMPOSITE MATERIAL

The development of techniques for fabrication of composite electrolyte-ceramic materials was the major activity in the program. Although the contract work statement called for the ultimate operation within cell configurations, the matrix is classified as the heart of the program, just as the electrolyte and its electrochemical performance must be classified in the overall LMC systems program. Initial electrolyte-ceramic fabrication techniques led to the composites shown in Figure 4-1. This then gave impetus to the present program, and only in retrospect is it now seen that solidified shapes at room temperature were only the beginning of a rigorous testing program.

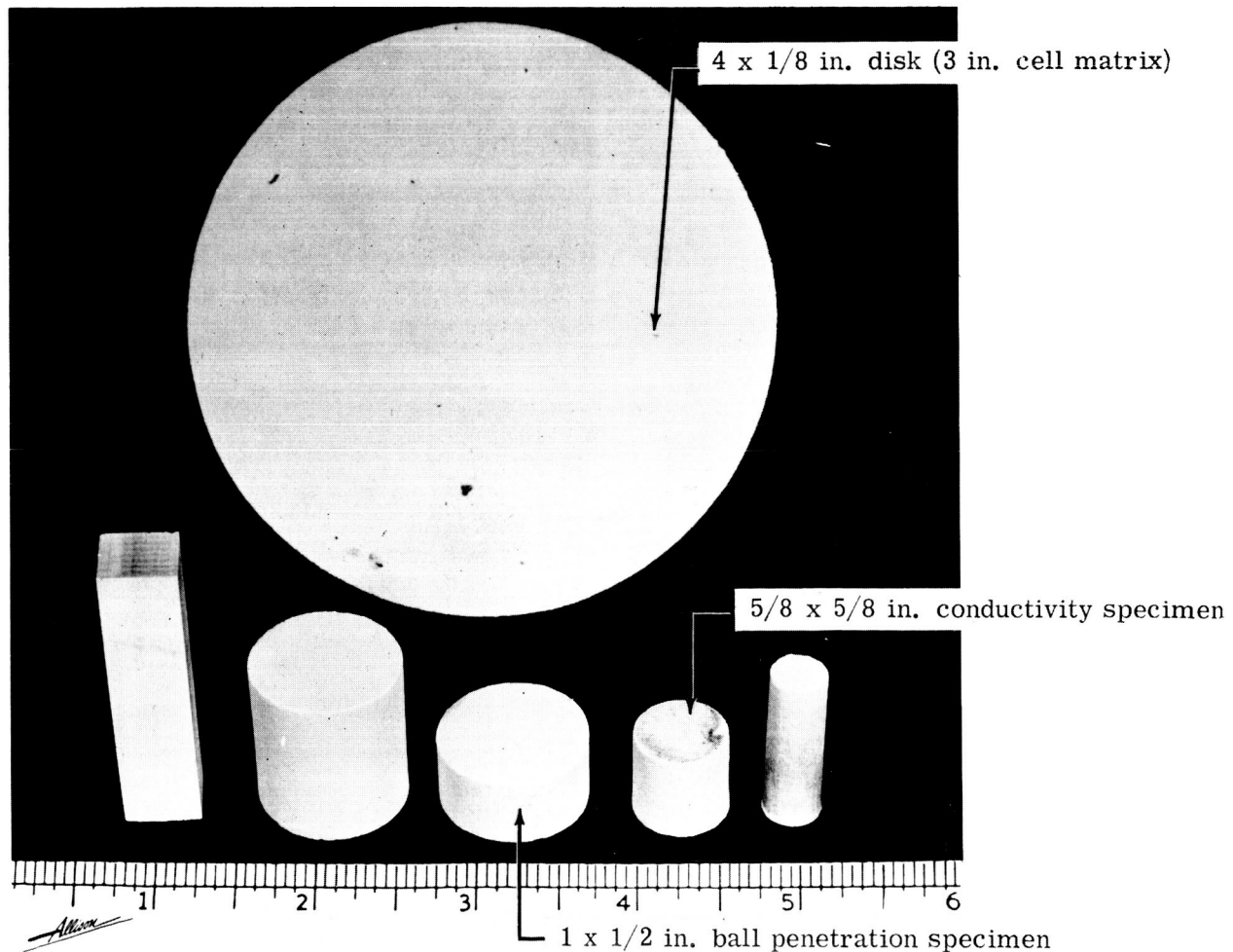


Figure 4-1. Composite electrolyte shapes produced during the program.

This section is made up of three parts:

- A presentation of the final steps leading to the successful fabrication of test specimens from a new ceramic material and new fabrication procedures
- A discussion of the various fabrication methods used
- A discussion of the important procedures related to coarse grain ceramic composites

## COMPOSITE ELECTROLYTE IMPROVEMENT AND FINAL FABRICATION METHODS

A study was made to optimize the materials and procedures used in the preparation of composite electrolyte matrices. The composites consisted of three different types of MgO particles in combination with the ternary salt eutectic mixture of 70-KOH, 15-KBr, and 15-KI mole percentages. A new baking method, called the vacuum pack technique, was developed. Crack-free and blister-free material was produced consistently using a fused, 0.08-micron grain MgO, provided the vacuum pack bake method was used and the material was kept free of impurities.

This MgO was shown to retain 65 weight percent electrolyte when formed into a composite. It is recommended over all other composite electrolyte materials for liquid metal cell studies. Crack-free or blister-free material could not be produced by any method using a 0.05-micron grain, light-calcined MgO.

Nearly all of the composite electrolyte specimens fabricated prior to July 1963 exhibited irregularities in final specimen quality. Blistering of specimens during the bake cycle was the major difficulty encountered when using 5-micron grain MgO in the composite material. Some specimens were of good quality, while others exhibited varying degrees of blistering and surface irregularities after the bake cycle. The exact causes of this condition were not thoroughly understood, although the presence of water vapor was known to be one source of blistering. When fine-particle, 0.05-micron, light-calcined MgO was used in the composite, the blistering problem was even further aggravated. In addition, severe cracking of the fine MgO specimens occurred during the bake cycle.

To materially improve the quality of these composites, a study was made to determine the effect of different baking cycles, baking environment, and other steps in the fabrication process which might contribute to the undesirable quality. During the investigation, a third type of MgO, a fused grade having an average particle diameter of 0.08 micron, was tried.

## Results

A new type of composite electrolyte was developed using fused fine (type FF) 0.08-micron MgO powder. Crack-free composite specimens up to 4 in. in diameter have been made using 65% electrolyte. This material exhibited an effective strength of 4 psi and an effective ductility of 20%.

Crack-free, unblistered specimens using type FF MgO were obtained by maintaining the composite free of metallic and moisture contamination and baking the pressed specimens in a pack of dry MgO powder with a cooling rate of 10°F/hr after baking.

Neither crack-free nor blister-free specimens can be fabricated using light-calcined, fine, 0.05-micron MgO (type F) powder when following the procedure described in the preceding paragraph.

Crack-free, unblistered specimens have been fabricated using coarse, 5-micron MgO powder (type C) when care was taken to reduce metallic and moisture contamination and the postbake cooling rate was less than 100°F/hr.

Reprocessing the composite materials increases the probability of contamination and shows no improvement.

The presence of metallic particles in a composite produces specimens which contain cracks and are blistered.

Rapid cooling of baked specimens promotes stress cracking.

Composite specimens using type FF MgO powder and containing 65% electrolyte at low densities have been shown to be gas impermeable at 300°C.

## Description of Materials

Composite electrolyte materials were prepared using the following three types of MgO powder:

- Coarse, 5-micron, fused MgO—coded type C
- Fine, 0.05-micron, light-calcined MgO—coded type F
- Fine, 0.08-micron, fused MgO—coded type FF

The type C MgO is a product of General Electric and is identified as G. E. 12780A MgO. Type F MgO is obtainable through the Fisher Scientific Company as Light Calcined MgO U. S. P. Grade—Catalog No. M-49. Type FF MgO is also obtainable through Fisher Scientific Company as Electronic Grade MgO—low activity—Catalog No. M-300, and is a product of Morton Chemical Company. Table 4-I shows a typical analysis of the Morton product.

Table 4-I.  
Typical analysis of type FF MgO powder.

Magnesium oxide assay (weight percent)	97.5
Ignition loss (weight percent)	2.0
Insoluble in concentrated HCl (weight percent)	0.09
Water soluble (weight percent)	0.55
NH <sub>4</sub> OH precipitate (weight percent)	0.005
SiO <sub>2</sub> (weight percent)	0.10
Sulfur (weight percent)	0.013
Calcium (weight percent)	0.14
Iron (weight percent)	0.03
Chloride	Trace
Copper	Trace
Silver	Trace
Vanadium	Trace
Boron	Trace
Sodium	None
Titanium	None
Zinc	None
Manganese	None
Aluminum	None
Barium	None
Nitrate	None

The electrolyte used with all three types of MgO was a ternary eutectic mixture having a mole percent composition of 70-KOH, 15-KBr, and 15-KI. The individual purity analysis of each constituent is shown later in this section.



The composite electrolytes studied were as follows:

<u>Batch No.</u>	<u>Weight percent electrolyte</u>	<u>MgO type</u>
IX	34.5	C
X	33.0	C
107	56.5	F
110	54.0	FF
111	50.0	F
112	65.0	FF

#### Modification of Preparation Procedures

##### Coarse MgO (Type C)

##### Minimization of Moisture in Transfer Operations

The first step taken to reduce the moisture level in the finished composite was to flood all working areas with a flow of dry argon gas where materials transfer operations were performed. Weight data taken on a composite electrolyte specimen placed in such an argon-flooded area showed no change in weight for a period of 20 minutes. All process steps in a fabrication procedure require less than five minutes in such an area.

Final specimen containers were constructed of heavy Plexiglas sheet separated by O-rings. These were found to be gas tight and were convenient for holding the specimens during micro-examination, X-ray analysis, and storage prior to tests. The effectiveness of this type of container was evaluated by observing weight changes over a three-week period. No change in weight was noted. A photograph of this container is shown in Figure 4-2.

##### Comminution Study

It was thought that material improvement could be achieved by reprocessing the coarse composite powder through a second grinding, baking, and screening operation. Batch IX, a composite of 34% electrolyte/66% coarse type C MgO, was reprocessed through burr grinding, re-baking, etc, to evaluate the effect of such reprocessing on the quality of the specimens.

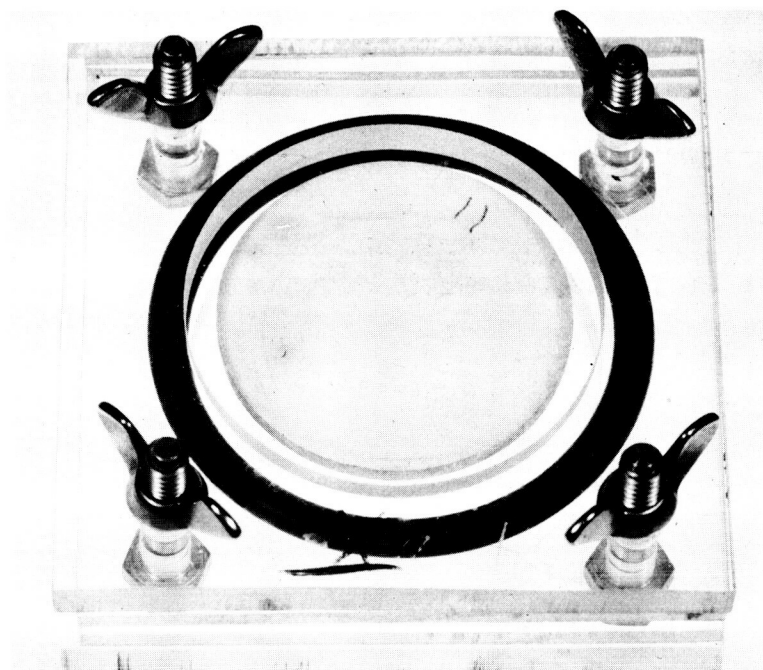


Figure 4-2. Gas-tight specimen holder.

Batch IX became contaminated during the reprocessing with fine metal particles from the burr grinder and produced a composite which blistered severely upon baking. An X-ray photograph of a contaminated specimen from Batch IX is shown in Figure 4-3.

The next step was to try to remove these metal particles with a magnet to verify the cause of the severe blistering. Figure 4-4 shows the much improved quality of a specimen after removal of fine metal particles from Batch IX powder.

#### Baking Procedure Modification

A new batch of coarse type C MgO composite powder, Batch X, was made by the modified procedure. This material which had the composition 33% electrolyte/67% coarse type C MgO, was prepared by argon flooding all transfer steps in the process, and further, all grinding was done by ceramic-to-ceramic (alumina) contact to eliminate metal contamination.

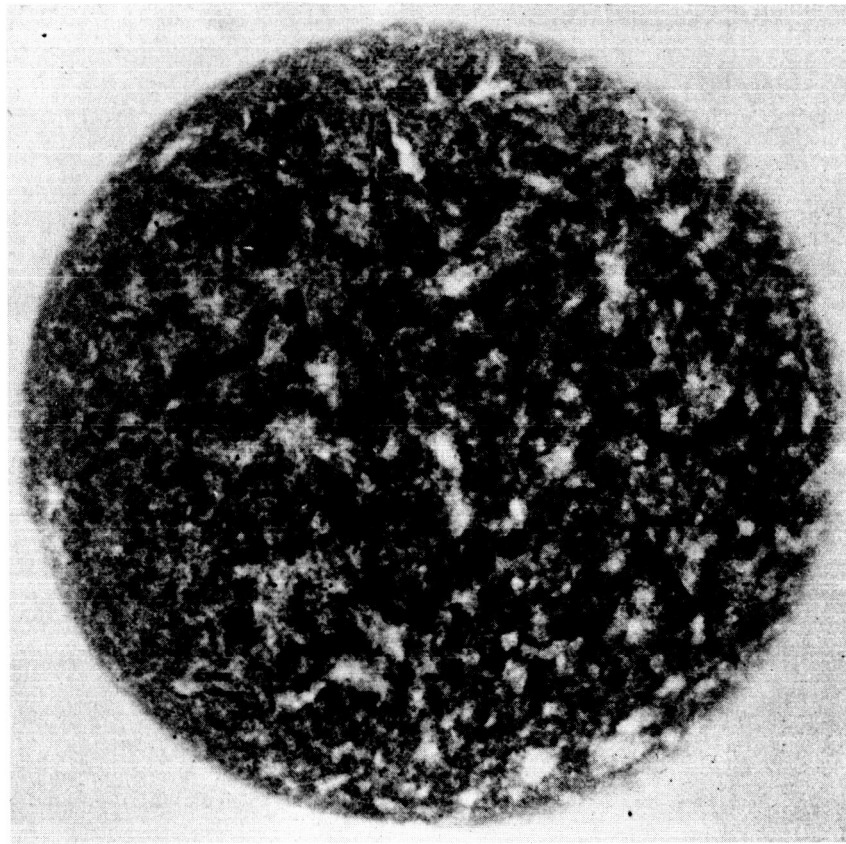


Figure 4-3. Reverse image X-ray photograph (4X) of 1-in. dia x 1/8-in. baked specimen from contaminated Batch IX—MgO coarse type C.

A series of specimens 1 in. in diameter  $\times$  1/8 in. thick was prepared to evaluate quality as a function of baking procedure as follows:

- Vacuum bake versus argon bake
- Rapid postbake cooling (from 650°F) versus slow cooling
- Nickel support versus gold support during bake

Specimens baked under vacuum were more sensitive to blistering than those baked under argon. Specimens baked under argon were largely free of blisters on the surface.

No difference in quality was noted between samples baked on nickel or gold sheet.

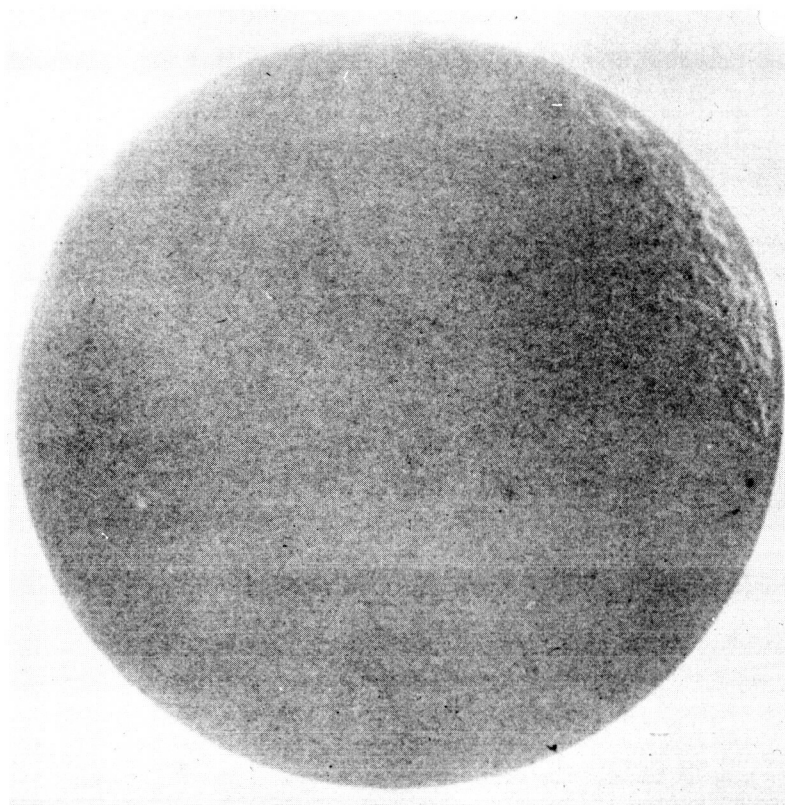


Figure 4-4. Reverse image X-ray photograph (4X) of 1-in. dia x 1/8-in. baked specimen from Batch IX after removing metal particle contamination—MgO coarse type C.

Rapid cooling (water quench) of the furnace holding the specimens at 650°F caused stress or solidification shrinkage cracks. Normal cooling of the furnace at a rate of less than 100°F/hr produced crack-free and warpage-free material.

For coarse type C MgO composites, the best overall quality was achieved by baking under argon atmosphere and postbake cooling at less than 100°F/hr.

#### Fine MgO (Type F)

Exercising all of the precautions previously described for coarse type C MgO failed to produce satisfactory specimens using fine, light-calcined type F MgO. All specimens were subject to cracking, blistering, and warpage. Slow cooling (10°F/hr) eliminated most of the cracking, but failed to eliminate warping.

A different approach was evaluated on subsequent samples by packing the cold-pressed specimens on all sides with clean, dry, 5-micron particle, fused type C MgO. Samples were baked under vacuum for 1 hr at 650°F and then allowed to cool very slowly under vacuum to 375°F, and then at an increased rate to room temperature. Slow cooling occurred from 650°F to 375°F over a 20-hr period, at a nearly constant rate. This technique is now known as the vacuum pack method.

Type F MgO composite electrolyte specimens made by the vacuum pack process were somewhat improved; blistering was eliminated, but small cracks were still evident upon X-ray examination.

#### Fine MgO (Type FF)

Use of the vacuum pack method with electronic grade type FF MgO material produced specimens which were free of cracks, blisters, and warpage. The use of this material, when properly prepared to eliminate moisture and contaminants and when baked by the vacuum pack process, has resulted in the best quality specimens attainable to date. X-ray studies reveal the greatly improved quality of type FF MgO composite electrolyte. Some specimens still show a variable density as evidenced by shadow areas on the X-rayed composite (see Figure 4-5).

Composites made from type FF MgO powder are much more stable and reproducible than composites made from the more active type F MgO. Figures 4-5 and 4-6 show reverse X-ray photographs of 2- × 1/8-in. specimens from Batch 110 (type FF) and Batch 107 (type F), respectively. Note the cracks or fissures in Figure 4-6.

To prove the effectiveness of the vacuum pack baking procedure, one specimen from a group of four specimens (prepared using type FF MgO powder) was baked on 5-micron MgO but not packed in the material as were the remaining three specimens. The three packed specimens were of good quality while the nonpacked specimen exhibited severe blistering on the top surface. Properly packed fine electronic grade type FF MgO composite electrolyte specimens have been shown to retain their original, green, cold-pressed configuration after baking and proper cooling.

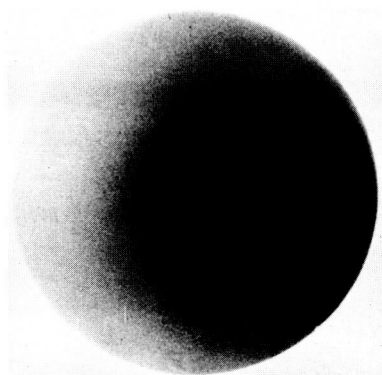


Figure 4-5. Two-inch dia specimen from Batch 110, No. 23 electronic grade fine MgO type FF.

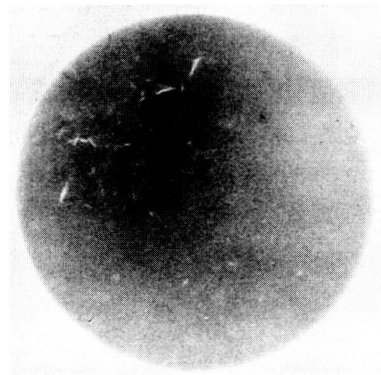


Figure 4-6. Two-inch dia specimen from Batch 107, No. 15 light calcined fine MgO type F. Cracks are evident in the X-ray.

Specimens improperly packed for the baking process show a marked tendency to produce replica surfaces of the contacting MgO surfaces during the pasty (semifluid) stage of the baking. For example, loosely packed MgO will produce irregular surfaces on the final specimen, while firmly packed MgO produces a smooth surface. The pack process, when properly carried out, closely approximates an isostatic retaining medium during the complete baking process, and allows complete freedom for expansion and contraction of the packed specimen.

### Optimum Procedure

Both type F and type FF MgO composites must be prepared by the vacuum pack procedure to ensure maximum quality. The detailed procedure for fabrication of composite specimens from these powders incorporates all recent modifications, and can be used for type C MgO composites although it was specifically developed for type FF MgO composites.

The detailed optimum procedure is as follows:

1. Place the required weight of previously prepared composite electrolyte powder into a hardened steel die cavity, level the powders by tapping and vibrating the die assembly, and cold press the desired preform at 30,000 psi. Keep all working area flooded with dry argon gas.
2. Carefully remove the green specimen from the die and place on a firmly pressed, clean, dry, 5-micron MgO surface previously prepared in a stainless steel tray.

3. Pour additional 5-micron MgO powder over the specimens and cover to a depth of at least 1 in. Press MgO firmly over the entire top surface of the filled tray. All packing operations are performed in a dry argon atmosphere.
4. Place the packed tray in a vacuum furnace. Heat to approximately 450°F and hold that temperature until an absolute pressure of 2 microns of mercury pressure is reached.
5. Increase the temperature to full baking temperature (650°F) and hold for at least 1 hr at 2 microns of mercury pressure.
6. Cool the tray of specimens while still in furnace under vacuum at the rate of about 10°F/hr, from 650°F to 375°F.
7. Remove the tray from the furnace and allow it to cool to room temperature under a cover of dry argon.
8. When samples are at room temperature, remove them from the packing medium and place them in an argon-filled plastic bag and transfer to an argon dry box for weight and dimensional measurements.
9. From the weight and volume measurements, calculate the density of the specimens. Compute the percentage of theoretical density based on the 100% density of the composite materials.
10. Store all specimens in dry, gas-tight containers. All specimens requiring quality inspection by X-ray methods are sealed in the specially constructed Plexiglas holders, allowing the specimens to be X-ray analyzed while still sealed in the holder.

## Property Measurements

### Mechanical Properties

The physical properties of two typical composites made with type FF fine MgO powders are compared in the following tabulation to similar composites made with light-calcined, fine grain type F MgO powders. The vacuum pack baking method was used on all specimens. The properties at 300°C are as follows:

Batch No.	Type MgO	Original powder	Percent electrolyte		Strength (psi)	Flowability (% deformation)
			Specimen baked	Percent density		
110	FF	55.0	54.0	92.0	5.6	16.8
112	FF	65.2	65.0	93.0	4.0	22.2
111	F	56.5	50.0	91.0	10.0	12.0
107	F	61.7	56.4	97.0	3.3	8.3

Test specimens prepared by the vacuum pack method show some loss of electrolyte to the packing medium, particularly when light-calcined type F MgO powders are used to fabricate the composite. Analysis of final baked specimens show the ability of type FF MgO to retain higher levels of electrolyte during the bake cycle than those composites made from type F MgO. This useful property allows the use of the improved vacuum pack baking method with a higher level of confidence. High-level electrolyte composites may be processed with a minimum of electrolyte loss.

## Gas Permeability

One specimen from Batch 110, which is highly porous, and specimens of three different percentage density levels, using Batch 116 composite electrolyte, were evaluated for gas permeability at 300°C. The results are as follows:

Batch No.	Percent electrolyte	Percent density	Argon pressure (in. H <sub>2</sub> O)	Permeable
110	54.0	78.0	32	No
116	65.8	84.0	32	No
116	65.8	86.5	32	No
116	65.8	89.8	32	No

These results show that highly porous material exhibited by low percent density is not gas permeable at the normal operating pressures to be experienced in the liquid metal cell.



### Creep Rate at 300°C

Creep rates were determined for 65% electrolyte, type FF MgO composites at 300°C (572°F), at two stress levels—4 psi and 1.2 psi. These lower load values were chosen because of the low apparent strength (5 psi) of this particular composite ratio. The creep rates were as follows:

<u>Percent electrolyte</u>	<u>Load (psi)</u>	<u>Accumulated time (hr)</u>	<u>Percent total creep</u>	<u>Average creep rate (%/hr)</u>
65.8	4	1	5.0	5.0
65.8	4	2	33.8	16.9
65.8	4	3	37.5	12.5
65.8	1.2	3	3.6	1.2
65.8	1.2	6	7.2	1.2
65.8	1.2	100	11.0	0.11

It is apparent from the creep data that this material exhibits very high creep characteristics when loaded to 80% of hot strength value; however, at a load of 25% of hot strength value, the material does not undergo excessive creep. In both cases, the majority of the creep takes place during the first few hours.

### FABRICATION AND PROPERTIES OF LIGHT-CALCINED, TYPE F, FINE GRAIN MgO COMPOSITES

A dry processing technique was developed for the fabrication of the composite electrolyte. Effective strength and flowability were determined as functions of electrolyte/MgO ratio at maximum density over the range 52.5% to 69.3% electrolyte.

The aqueous composite electrolyte fabrication technique that was found to be satisfactory using coarse (5-micron) type C MgO, was found to be unsatisfactory with this material due to blistering during the bake cycle. Blistering was attributed to the release of moisture and/or carbon dioxide from the surface of the MgO which, due to its light calcination, undoubtedly had a high specific surface and an associated high surface reactivity and absorptivity. Consequently, a dry processing technique was developed.

## Composite Electrolyte Preparation

The preparation of composite electrolyte specimens by the dry process involves three general steps, as discussed in the following paragraphs.

### Preparation of Electrolyte

The electrolyte portion of the composite is prepared separately as a fused, dry, finely divided (60 mesh) ternary eutectic salt mixture having a mole percent composition of 70-KOH, 15-KBr, and 15-KI. These materials are Fisher Certified Reagent A. C. S. or U. S. P. grade chemicals. Purity analyses are shown in Table 4-II.

Table 4-II.  
Fisher Scientific Company certified analyses of  
materials for composite electrolyte powder.\*

	Percent KBr	Percent KI	Percent KOH	Percent MgO
Fe	0.00005	0.0000	0.0002	0.03
Ba	0.000	Trace		None
Na	0.020	0.005	0.02	None
Ca				0.14
R <sub>2</sub> O <sub>3</sub>	0.004	0.000	0.01	0.005
Heavy metals (Pb)	0.0000	0.0000	0.0002	None
PO <sub>4</sub>		0.000	0.0001	
N	0.0005	0.0010	0.0002	None
IO <sub>3</sub>		Trace		
SO <sub>4</sub>	0.001	0.000	0.001	0.013
Cl	0.10	0.01	0.002	Trace
BrO <sub>3</sub>	0.001			
SiO <sub>2</sub>				0.10
Insoluble	0.001	0.000	0.002	
K <sub>2</sub> CO <sub>3</sub>			0.8	
Purity (min)	99.85	99.95	86.5	99.5
Grade	A. C. S. reagent	A. C. S. reagent	A. C. S. reagent	U. S. P.

\*Blank spaces in columns indicate that no analysis was made for these items. The balance of percent KOH is H<sub>2</sub>O.

---

Since the eutectic mixture of fused salt depends on a specific composition of the ternary phase, an accurate analysis must be made of the effective KOH content of the normal 87% purity KOH. This is accomplished by titrating a weighed sample of KOH pellets (dissolved in distilled water) with standardized HCl solution to the methyl orange end point. The exact purity of the KOH is then calculated and accounted for in the formulation of the electrolyte.

The detailed procedure for preparing the electrolyte is as follows:

1. For 1000 gm of electrolyte, weigh exactly 480 gm of 100% KOH, 300 gm KI, and 220 gm KBr into a dry glass bottle and mix thoroughly.
2. Transfer the mixture to a pure nickel can and fuse under vacuum at an absolute pressure of 2 microns of mercury for 2 hr at 650°F.
3. Remove the molten electrolyte salt mixture from the furnace and solidify quickly under an argon gas atmosphere. Pour molten salt onto a stainless steel or nickel sheet to facilitate initial reduction of solid salt to a coarse particle size.
4. The solidified salt mixture is then ball milled in a ceramic ball mill until all material passes through a 60-mesh screen. (All screening should be done in an argon-filled dry box.)
5. Take two 5-gm samples for analysis, and store remaining electrolyte powder in a clean, dry, glass jar fitted with a gas-tight seal.
6. Titrate the electrolyte samples with standard 1.0 normal HCl to the methyl orange end point as before. Calculate the KOH content of the electrolyte to determine the exact KOH percentage in the final electrolyte powder. (The percentage should be 48%  $\pm$  0.5% by weight to meet acceptance.)

#### Preparation of Composite Powder

Composites are prepared by mixing a predetermined amount of light-calcined, fine particle MgO powder with the electrolyte powder. The detailed procedure for preparing the composite powder is as follows:

1. The MgO is first dried at 1600°F in air for 2 hr. Calculated amounts of previously prepared electrolyte and MgO are weighed into a dry, gas-tight container and mixed thoroughly by tumbling.
2. Compress this powder mixture in a steel die into 4-in. diameter briquettes at approximately 10,000 psi. One hundred grams of composite powder at this pressure produces a briquette approximately 1/2-in. thick. Store the briquettes in an argon atmosphere.
3. Place the composite briquettes on a pure nickel sheet, and bake at 650°F under 2 microns of mercury for 2 hr. Remove the briquettes from the furnace while still hot (paste range of 450°F to 650°F) and stir the paste composite with a Teflon spatula until the material cools into coarse granules. All cooling is done in an argon atmosphere.
4. Place the coarse material into a clean, dry, ceramic ball mill jar. Mill and screen material until all powder passes a 60-mesh screen. Remove two 10-gm samples for analysis and keep the remainder of the composite powder stored in a dry, gas-tight glass jar.
5. Analyze the two samples for electrolyte content and MgO content. The electrolyte component of the composite is completely soluble in cold distilled water, while the MgO is almost entirely insoluble. A careful solution and filtration of these samples ensures a good method for separation and ultimate analysis of electrolyte by acid titration of the filtrate, and igniting the retained MgO to constant weight for the MgO content.
6. The electrolyte content of the composite is calculated by using the exact KOH analysis of the previously analyzed powdered electrolyte.

Table 4-III shows compositions determined in this manner.

## Preparation of Composite Specimens

Composite specimens are prepared in the following manner.

1. Place the required weight of composite electrolyte powder into a hardened steel die cavity and cold press the desired preform at 30,000 psi. Keep the working area flooded with dry argon gas.

Table 4-III.  
Composition of electrolyte/MgO composites (type F MgO).

<u>Batch No.</u>	<u>Nominal electrolyte content</u>	<u>Percent electrolyte</u>	<u>Percent MgO</u>	<u>Percent total</u>
101	55%	54.90	44.70	99.60
		<u>55.12</u>	<u>44.78</u>	<u>99.90</u>
		55.01	44.74	99.75
102	57%	56.40	42.80	99.20
		<u>56.40</u>	<u>42.40</u>	<u>98.80</u>
		56.40	42.60	99.00
103	61%	61.05	38.60	99.65
		<u>61.30</u>	<u>38.65</u>	<u>99.95</u>
		61.17	38.63	99.80
104	63%	63.22	36.55	99.77
		<u>62.84</u>	<u>36.56</u>	<u>99.40</u>
		63.03	36.56	99.59
105	70%	69.32	28.33	97.65
		<u>69.34</u>	<u>28.38</u>	<u>97.72</u>
		69.33	28.36	97.69
106	52.5%	52.53	47.06	99.59
		<u>52.35</u>	<u>46.85</u>	<u>99.20</u>
		52.44	46.95	99.39
107	62%	61.28	37.64	98.92
		<u>62.12</u>	<u>37.52</u>	<u>99.64</u>
		61.70	37.60	99.30
108	55%	55.0	45.0	
109	58%	58.0	42.0	
111	56.5%	56.57	43.30	99.87
		<u>56.78</u>	<u>43.10</u>	<u>99.88</u>
		56.68	43.20	99.88

2. Remove the preformed specimen from the die, place it on a pure nickel sheet, and bake under a vacuum or argon atmosphere for at least 1 hr at 650°F.
3. Allow the specimens to cool slowly (30°F/hr) from 650°F down to 375°F. Remove the specimens from the furnace when the specimens are at room temperature.
4. Transfer the specimens to previously tared weighing bottles to determine the exact weight of baked specimens.
5. Transfer the specimens to a dry glove box for dimensional measurements to calculate the volume of specimens.
6. Calculate the density (gm/cc) of each specimen and then calculate the percent theoretical density based on the 100% density calculated from the composition and the density of the four pure components.
7. All specimens should be stored in dried and sealed glass containers.

## Processing Difficulties

The major difficulties encountered with the use of light-calcined, fine particle MgO composites were blistering, cracking, and warping of specimens during the bake cycle.

Blistering of specimens during the bake cycle, whether accomplished under vacuum or argon flow, has in the past been attributed largely to the incomplete removal of moisture during the first baking of the composite briquettes. It is now known that the presence of contaminants, such as small particles of metal, can produce extreme cases of blistering in these specimens.

Cracking seems to occur in all specimens of this material to a varying degree. Cracks have been observed in specimens associated with and without the presence of metal particle contaminants. Cracking is also more severe when the cooling rate is not controlled.

All specimens from Batches 101 through 103 (Table 4-III) were final baked on nickel sheet. This is the same baking procedure as is used on coarse type C MgO composites. All fine particle, light-calcined type F MgO composites exhibited staining on contact with nickel. This staining becomes more pronounced as the electrolyte content increases. Sticking to the baking surface is also very pronounced.

All subsequent composites of this material were baked on gold- or rhodium-plated surfaces. The gold-plated surface offers a rather inert surface on which specimens may be baked without staining. Rhodium-plated surfaces are destroyed by the action of the molten electrolyte.

All specimens made from composites using light-calcined type F MgO were troublesome in that cracking consistently occurred during the bake cycle. Low level electrolyte content composites gave the least amount of trouble, but with high level electrolyte composites blistering, cracks, or warping were quite common.

#### Property Measurements

The detailed results of the ball penetration strength tests are shown in Table 4-IV. All tests were performed on 1-in. diameter  $\times$  1/8-in. thick specimens using the apparatus and procedure described in Section VI.

The results of the flowability tests are shown in Table 4-V. All tests were performed on 1-in. diameter  $\times$  1/2-in. thick specimens as described in Section VI.

#### Results

The following results are based on data taken from the electrolyte range 52.5% to 69.3% by weight, with a density range of 80% to 90% of theoretical.

- Strength values decrease with increasing electrolyte content.
- Flowability increases with the electrolyte content.
- The fabrication characteristics of this material are unsatisfactory in view of the poor quality of composite specimens produced. X-ray photography indicated the material to be subject to stress or solidification shrinkage or cracking during cooldown from the bake temperature (300°C) to room temperature.
- Light-calcined type F MgO appears to be more chemically active than fused or crystalline grades of MgO of the same particle size.

#### FABRICATION AND PROPERTIES OF COARSE GRAIN MgO COMPOSITES

Because blistering and cracking were prevalent, it was necessary to improve upon early work with composite fabrication using coarse type C MgO. Therefore, the earlier fabrication procedure was somewhat modified. This new work represents a continuation of the earlier work with better definition of quality control and property data as a function of process variables.

Table 4-IV.  
Summary of ball penetration strength tests  
of fine grain type F MgO composites

Sample size: 1 in. diameter  $\times$  1/8 in. thick (cold pressed at 30,000 psi)

<u>Batch No.</u>	<u>Sample No.</u>	<u>Density (percent of theoretical)</u>	<u>Strength at 300°C (psi)</u>	<u>Strength at 350°C (psi)</u>	<u>Percent electrolyte content</u>
101	3	87.2	2.35		55
	4	86.7	2.52		
	5	86.7		12.3	
	6	88.1		10.1	
102	25	77.8	3.6		57
	26	74.6	3.6		
			1.9		
	17	80.2		8.67	
	18	81.3		8.67	
	19	81.6		7.99	
103	4	90.0		2.9	61
	5	90.0		2.9	
	6	90.0		3.0	
	10	89.7	1.85		
	11	90.4	1.84		
104	4	90.3	2.52		63
	5	90.7	2.52		
105	Too soft to test at 300°C				70
106	1	87.1	22.0		52.5
	2	84.7	22.0		
107	1	90.2	2.6		62
	2	89.5	2.6		
108	1	84.5	15.1		55
	2	83.5	15.3		
109	1	85.0	1.5*		58
	2	84.5	1.5*		
111	11	91.9	10.0		56.5
	12	90.5	10.0		

\*These figures are considered low because of questionable specimen quality due to blister formation during the bake cycle.



Table 4-V.

Summary of flowability tests of fine grain type F MgO composites.All specimens were of 1-in. diameter  $\times$  1/2 in. thick (cold pressed at 30,000 psi)

Batch No.	Sample No.	Density (percent of theoretical)	Percent flow at 300°C	Percent flow at 350°C	Percent electrolyte content
101	11	85.4	10.4		55
	12	86.3	9.1		
	8	85.7		4.3	
	9	87.8		4.2	
102	22	84.8	12.7		57
	23	87.0	16.8		
	24	86.3	17.6		
	21	84.5		3.9	
	20	82.7		4.0	
103	7	91.1		9.9	61
	8	90.4		9.0	
	9	89.7		9.8	
	10	90.2	12.3		
104	1	88.9	24.4		63
	2	90.7	13.2		
	3	89.2	20.6		
105	No tests—material too weak				70
106	3	88.5	3.1		52.5
	5	89.5	4.0		
107	3	92.4	4.1		62
	4	91.0	18.3		
	5	84.8	17.5		
108	3	86.6	8.9		55
	4	87.0	9.8		
109	3	87.0	11.0		58
	4	88.0	11.0		
111	7	89.4	15.4		56.5
	8	90.5	9.1		
	13	91.2	14.2		
	14	90.8	9.3		

## Original Fabrication Method

The following procedure was used for coarse grain work:

1. The MgO powder is weighed into a Teflon-coated pan. The KBr and KI are each dissolved in a minimum of hot distilled water and stirred into the MgO. The mixture is evaporated to dryness at 250°F in air, with periodic stirring.
2. KOH of known chemical content is dissolved in a minimum of hot distilled water and stirred into the mixture. The material is again evaporated to dryness at 250°F with frequent stirring and subsequent breaking into fine granules. It is further dried in air at 500°F.
3. The mixture is then transferred to a stainless steel pan and dried in a vacuum furnace at 650°F until a pressure of 2 microns of mercury is reached. The material is removed, while still hot, and broken into fine granules while cooling.
4. The material is then loaded into an oven-dried ceramic ball mill, milled for 1 hr, and passed through a 60-mesh screen.
5. The powder is stored in a dry container and kept in a desiccated glove box.
6. The powder is pressed at 10,000 to 30,000 psi.
7. Bake the pressed shapes in argon or vacuum.

## Modification of Procedure

The specific changes which were made in the original method are described in detail as follows.

### Drying

A larger vacuum furnace with a large pumping capacity is now being used for drying the bulk batch prior to grinding. The material is spread out as much as possible in a stainless steel pan and dried at 650°F. The process is continued until the pressure has been reduced to at least 2 microns of mercury.

### Pressing

To obtain high density specimens, pressing is done at 30,000 psi; previously, 20,000 psi was used. Low density specimens are obtained using a 10,000-psi pressing pressure.

### Baking

The high density composite electrolyte specimens are baked in an argon atmosphere. It was found that vacuum baking caused blistering after pressing at high pressures. The argon eliminated this problem. The low density specimens are still baked under vacuum.

### Electrolyte Composition Determination

The KOH and MgO contents are determined by wet chemical analyses. The MgO content is determined by solution of electrolyte in water. The solution is filtered, and the residue is weighed after firing at 1800°F in air. The KOH content of the aqueous filtrate is determined by an acid titration. Table 4-VI gives the data obtained on the material used.

Table 4-VI.  
Composite electrolyte material composition (type C MgO).

<u>Batch No.</u>	<u>Nominal ratio</u>	<u>Percent MgO</u>	<u>Percent KOH</u>	<u>Percent electrolyte*</u>	<u>Total</u>	<u>Measured ratio</u>
I	35/65 = 0.539	64.3	16.8	35.0	99.3	0.545
II	35/65 = 0.539	64.5	16.7	34.8	99.3	0.539
III	35/65 = 0.539	64.5	16.7	34.8	99.3	0.539
IV	33/67 = 0.493	66.2	15.5	32.3	98.5	0.488
V	31/69 = 0.449	68.9	14.8	30.8	99.7	0.447
VII	34/66 = 0.515	65.1		33.0	98.1	0.507
VIII	34/66 = 0.515	65.4		32.9	98.3	0.503

\*Calculated from the KOH content—assuming the KOH-KBr-KI electrolyte contains 48 weight percent KOH.

A review of these procedures shows the importance of a dry process for the fabrication of the composite. The complete elimination of moisture is difficult. Handling in air also adds to the  $\text{CO}_2$  pickup. The problem with baking shows the need to keep an atmosphere pressure on the material to eliminate the residual gas or vapor explosion when baked under vacuum. Low density, high porosity specimens relieve this gas without apparent damage to the material. However, it is likely that these materials develop gas pockets as shown in Figure 4-7.

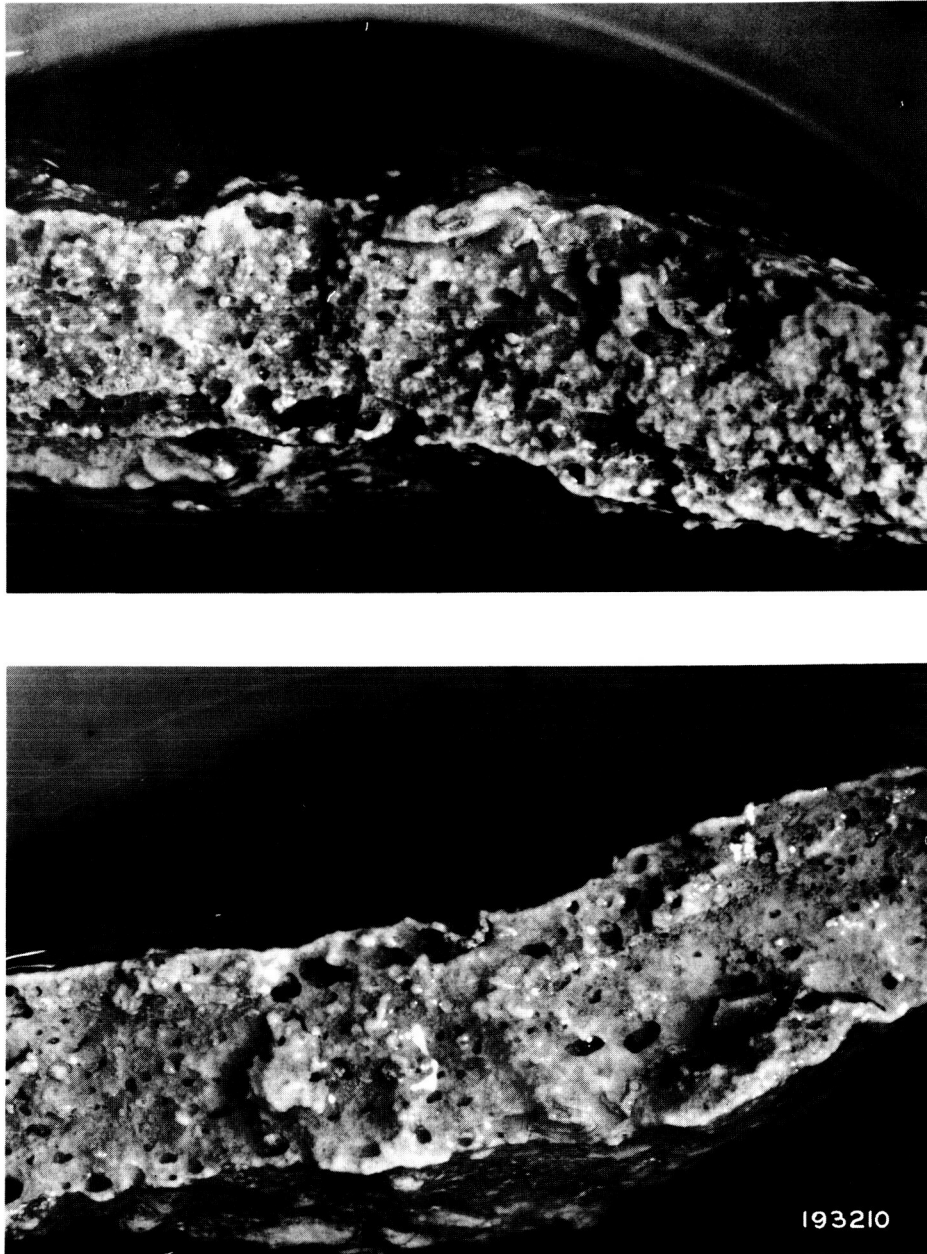


Figure 4-7. Cross section of electrolyte showing gas pockets.

## Property Measurement

The detailed results of the ball penetration strength test are shown in Table 4-VII. The results of the flowability test are shown in Table 4-VIII. These tables are included to reflect the total scope of work accomplished in the development program. A record of all specimen production for this program has been tabulated in Table 4-IX.

Table 4-VII.

Ball penetration test results on coarse type C MgO composite electrolyte at 350°C.

Nominal ratio	Batch No.	Specimen size* (in.)	Density (percent of theoretical)	Pressing pressure (psi)	Strength** (psi)
35/65	I	1 × 1/2	71.8	10,000	6.2
35/65	I	1 × 1/2	73.7	10,000	6.5
35/65	I	1 × 1/2	76.0	10,000	5.8
35/65	II	1 × 1/2	86.5	30,000	1.0
35/65	II	1 × 1/2	87.5	30,000	1.0
35/65	II	1 × 1/2	88.5	30,000	0.97
35/65	III	1 × 1/2	74.7	500	5.6
35/65	III	1 × 1/2	87.2	30,000	1.5
35/65	III	1 × 1/2	87.5	30,000	1.4
35/65	III	1 × 1/2	88.1	30,000	1.3
35/65	III	1 × 1/8	83.7	30,000	1.1†
35/65	III	1 × 1/8	83.7	30,000	1.3†
35/65	III	1 × 1/8	85.6	30,000	1.2†
33/67	IV	1 × 1/2	75.3	10,000	10.1
33/67	IV	1 × 1/2	75.3	10,000	12.3
33/67	IV	1 × 1/2	75.6	10,000	10.1
33/67	IV	1 × 1/2	84.6	30,000	20.2
33/67	IV	1 × 1/2	84.9	30,000	18.5
33/67	IV	1 × 1/2	85.9	30,000	20.2
33/67	IV	1 × 1/8	82.1	30,000	11.1
33/67	IV	1 × 1/8	85.3	30,000	15.8
33/67	IV	1 × 1/8	89.7	30,000	12.3
33/67	IV	1 × 1/8	84.3	30,000	9.2†
33/67	IV	1 × 1/8	86.2	30,000	11.0†
33/67	IV	1 × 1/8	86.2	30,000	7.9†
33/67	IV	1 × 1/8	84.3	30,000	11.0†
33/67	IV	1 × 1/8	88.8	30,000	11.0†
33/67	IV	1 × 1/8	90.1	30,000	10.0†
31/69	V	1 × 1/2	84.9	30,000	22.2
31/69	V	1 × 1/2	85.9	30,000	22.2
31/69	V	1 × 1/2	86.9	30,000	22.2
34/66	VIII	1 × 1/8	86.2	30,000	3.36
34/66	VIII	1 × 1/8	87.5	30,000	3.36
34/66	VIII	1 × 1/8	88.1	30,000	3.26
34/66	VIII	1 × 1/8	85.3	30,000	22.2†
34/66	VIII	1 × 1/8	85.3	30,000	22.2†
34/66	VIII	1 × 1/8	73.1	10,000	11.1
34/66	VIII	1 × 1/8	74.7	10,000	12.3
34/66	VIII	1 × 1/8	77.2	10,000	15.9

\*Specimen size = diameter × thickness.

\*\*Strength =  $\frac{\text{load}}{\text{impression area}}$ ; Load = 0.111 lb; Ball diameter = 0.499 in.

†Load = 0.055 lb.

‡300°C.

Table 4-VIII.

Flow test results on coarse type C MgO composite electrolyte at 350°C.

<u>Nominal ratio</u>	<u>Batch No.</u>	<u>Specimen size* (in. )</u>	<u>Density (percent of theoretical)</u>	<u>Percent deformation</u>
35/65	I	1 × 1/2	73.7	20
35/65	I	1 × 1/2	73.7	20
35/65	I	1 × 1/2	74.4	20
35/65	I	1 × 1/2	72.4	30
35/65	I	1 × 1/2	74.7	30
35/65	I	1 × 1/2	74.0	30
35/65	I	1 × 1/2	73.4	40
35/65	I	1 × 1/2	73.4	40
35/65	I	1 × 1/2	74.4	50
35/65	II	1 × 1/2	88.5	50
33/67	IV	1 × 1/2	75.6	40
33/67	IV	1 × 1/2	75.6	30
33/67	IV	1 × 1/2	74.7	20
33/67	IV	1 × 1/2	85.3	30
31/69	V	1 × 1/2	85.9	30
31/69	V	1 × 1/2	86.2	20
34/66	VIII	1 × 1/2	85.9	24.9
34/66	VIII	1 × 1/2	86.9	28.1
34/66	VIII	1 × 1/2	86.9	16.9
34/66	VIII	1 × 1/2	90.0	27.0†
34/66	VIII	1 × 1/2	90.0	32.0†
34/66	VIII	1 × 1/2	74.7	19.0
34/66	VIII	1 × 1/2	76.0	18.7
34/66	VIII	1 × 1/2	76.9	7.4

\*Specimen size = diameter × thickness.

†300°C.

Table 4-IX.  
Composite electrolyte specimen fabrication data.

Cell number	Batch number	MgO type	Percent electrolyte	Specimen number	Specimen size (in.)	Pressing pressure (psi)	Percent density	Type test specimen	Disposition
I	IV	C	32.3	--	2 x 1/8	30,000	86.2	Cell test	tested - analyzed - discarded
—	VIII		32.9	--	2 x 1/8	30,000	84.0		discarded
III	IXb		34.5	3	2 x 1/8	30,000	85.3		tested - analyzed - discarded
—	X		33.0	11	2 x 1/8	30,000	81.9		blisters on surface - discarded
IV	X		33.0	12	2 x 1/8	30,000	81.9		tested - analyzed - discarded
—	X		33.0	1	2 x 1/8	20,000	78.7		stored
II	101	F	55.0	--	2 x 1/8	30,000	86.4		tested - analyzed - discarded
—	106		52.4	9	2 x 1/8	--	87.0		stored
—	107		61.7	10	2 x 1/8	--	90.9		stored
—	110	FF	55.0	12	2 x 1/8	15,000	82.0		broken during cell assembly
—				13	2 x 1/8	30,000	92.6		fissures detected in X-ray - re-processed
—				13r	2 x 1/8	--	95.4		found to be cracked - discarded
VI				14	2 x 1/8	20,000	86.2		tested - analyzed - discarded
—				15	2 x 1/8	20,000	85.5		found to be cracked - discarded
VII				23	2 x 1/8	20,000	85.5		tested - analyzed - discarded
V	111	F	56.5	10	2 x 1/8	20,000	83.7		tested - analyzed - discarded
VIII	112	FF	65.2	10	2 x 1/8	20,000	93.0		tested - analyzed - discarded
IX	114		65.7	1	2 x 1/8	20,000	94.2		tested - analyzed - discarded
X				15	2 x 1/8		93.1		tested - analyzed - discarded
—				16	2 x 1/8		90.2		stored
—				17	2 x 1/8		98.2		stored
—	115		50.0	--	4 x 1/8	--	--		unbaked - discarded
XI	116		65.8	27	4 x 1/8	10,000	85.8		tested - analyzed - discarded
XIII	116		65.8	28	4 x 1/8	10,000	82.2		tested - analyzed - discarded
—				7	4 x 1/8	13,000	81.5		stored
—				8	4 x 1/8	13,000	80.4		stored
—				1	2 x 1/8	20,000	86.2		nonuniform density - discarded
—				2	2 x 1/8		87.3		nonuniform density - discarded
—				3	2 x 1/8		85.8		stored
—				4	2 x 1/8		85.5		nonuniform density - discarded
—				5	2 x 1/8		82.9		nonuniform density - discarded
—				6	2 x 1/8		84.4		stored
XII				30	4 x 1/8	13,000	82.5		tested - analyzed - discarded

Table 4-IX. (cont)

NASA specimen No.	Batch number	MgO type	Percent electrolyte	Specimen number	Specimen size (in.)	Pressing pressure (psi)	Percent density	Type test specimen	Disposition
I	C	35.0	1c	1 × 1/2	10,000	73.7	ball penetration	tested - discarded	
			2c			70.0	flowability	discard	
			3c			71.8	ball penetration	tested - discarded	
			4c			72.1	flowability	discarded	
			5c			76.0	ball penetration	tested - discarded	
			6c			78.5	flowability	discarded	
			F1c			73.7		tested - discarded	
			F2c			73.7			
			F3c			74.4			
			F4c			72.4			
			F5c			74.7			
			F6c			74.0			
			F7c			73.4			
			F8c			73.4			
			F9c			74.4			
			7c			79.8			ball penetration
			8c			80.1			
			9c			81.1	density improvement	program to study density versus pressing pressure	
			10c			80.8			
			11c			81.1			
			12c			80.8			
			--			30,000	density improvement	measured and discarded	
			--			40,000			
			7c1			87.5			
			8c1			84.5			
			9c1			94.6			
10c1	94.6								
11c1	93.3								
12c1	95.2								
13c1	--								
14c1	--								
15c1	30,000	flowability	some surface blistering						
7c2	93.3								
8c2	93.6	ball penetration	some surface blistering						
9c2	93.2								
10c2	92.6	density improvement	measured - discarded						
11c2	91.3								
12c2	---								
II	C	34.8	1c	1 × 1/2	40,000	87.2	density improvement	tested - discarded	
			2c	1 × 1/2	30,000	86.5	ball penetration	tested - discarded	
			3c	87.8					
			4c	86.2					
			7c3	88.5	flowability	discarded			
			8c3	87.5					
			9c3	86.5					
			10c3	88.5	conductivity	tested - discarded			
			11c3	87.2					
			12c3	86.2					
			13c	5/8 × 5/8	88.5	trial 1/8 in. configuration			
			14c		90.5				
			15c		89.5				
			16c	1 × 1/8	85.6				
17c	1 × 1/8		88.5						



Table 4-IX. (cont)

NASA specimen No.	Batch number	MgO type	Percent electrolyte	Specimen number	Specimen size (in.)	Pressing pressure (psi)	Percent density	Type test specimen	Disposition
22 23 24	III	C	34.8	18c	1 × 1/8	30,000	83.7	conductivity	trial 1/8 in. configuration
				19c	↓		83.7	ball penetration	tested - discarded
				20c	↓		85.6	↓	↓
				21c	↓		83.7	↓	↓
				22c	5/8 × 1/8		92.9	conductivity	↓
				23c	↓		95.8	↓	↓
				24c	↓		98.1	↓	↓
				1c	1 × 1/2		88.1	ball penetration	tested - discarded
				2c	↓		87.5	↓	↓
				3c	↓		87.2	↓	↓
18 16 17 15 13 14	IV	C	32.3	4c	↓	10,000	74.7	↓	↓
				22a	1 × 1/2		75.6	flowability	tested - discarded
				23a	↓		75.6	↓	↓
				24a	↓		75.3	ball penetration	↓
				25a	↓		75.6	↓	↓
				26a	↓		75.3	↓	↓
				27a	↓		74.7	flowability	↓
				28a	↓	30,000	84.9	ball penetration	↓
				29a	↓		85.3	flowability	↓
				30a	↓		85.9	ball penetration	discarded
				31a	↓		84.9	flowability	tested - discarded -
				32a	↓		84.6	ball penetration	discarded
				33a	↓		84.9	flowability	↓
				34a	1 × 1/8		90.1	ball penetration	tested - discarded
				35a	↓		88.8	↓	↓
				36a	↓		84.3	↓	↓
				37a	↓		88.1	--	discarded
				38a	↓		90.1	--	↓
				39a	↓		88.1	--	↓
				40a	5/8 × 5/8	30,000	78.2	conductivity	tested - discarded
				41a	↓		74.7	↓	↓
				42a	↓		74.7	↓	↓
				43a2	↓		86.8	↓	↓
				44a2	↓		87.8	↓	↓
				45a2	↓		86.2	↓	↓
				--	1 × 1/8		85.3	ball penetration	↓
				--	↓		82.1	↓	↓
				--	↓		84.3	↓	↓
				--	↓		86.2	↓	↓
21 20 19	V	C	30.8	--	↓		86.2	↓	↓
				--	↓		89.7	↓	↓
				49b	1 × 1/2	30,000	84.9	↓	tested - discarded
				50b	↓		85.9	↓	↓
				51b	↓		86.9	↓	↓
				52b	↓		85.9	flowability	↓
				53b	↓		86.2	↓	discarded
				54b	↓		84.9	↓	tested - discarded
				55b	5/8 × 5/8		86.2	conductivity	↓
				56b	↓		87.2	↓	↓
				57b	↓		87.8	↓	↓
28 29 30	VI	C	nominal 34	1	5/8 × 5/8	20,000	86.9	conductivity	tested - discarded
				2	5/8 × 5/8		86.2	↓	↓
				3	↓		86.5	↓	↓

Table 4-IX. (cont)

NASA specimen No.	Batch number	MgO type	Percent electrolyte	Specimen number	Specimen size (in.)	Pressing pressure (psi)	Percent density	Type test specimen	Disposition		
31	VI	C	nominal 34	4	5/8 × 5/8	20,000	89.4	conductivity	tested - discarded		
32				5			85.6				
33				6			85.6				
34				7			86.5				
35				8			85.0				
				9			85.9				
				10			85.9				
				--				strength			
				--						discarded	
				--						discarded	
				--						undetermined number	
				--						discarded after tests	
				--						showed disagreement	
				--						with 33% and 35% data	
48	VIII	C	32.9 nominal 34	20k	5/8 × 5/8	20,000	82.4	conductivity	tested - discarded		
49				21k			82.1				
50				22k			81.4				
51				23k		30,000	84.6				
52				24k			83.6				
53				25k			84.6				
				26k	1 × 1/8		87.5	ball penetration			
				27k			86.2				
				28k			88.1				
				29k	1 × 1/2		85.9	flowability		Further strength tests were not made since the planned composite of 34% was not obtained. specimen were discarded	
				30k			86.9				
				31k			86.9				
				35k	90.0						
				36k	90.0						
				37k	88.5						
				38k	1 × 1/8	10,000	85.3	ball penetration			
				39k			85.3				
				40k			74.7				
				41k			77.2				
				42k			73.1				
				43k			76.0				
				44k	76.9						
				45k	74.7						
	IX	C	34.5						Reprocessed to IXa		
	IXa	C	34.5	1	1 × 1/8	30,000	--	quality	Severe blistering as a result of metal particle contamination. repro- cessed to IXb		
				2	2 × 1/8		--				
									observed to be fair - discarded		
	IXb	C	34.5	3	2 × 1/8	30,000	85.3	quality	strength checked - discarded		
				4	1 × 1/8		--	ball penetration	tested - discarded		
	X	C	33.0	1	1 × 1/8	30,000	83.3	ball penetration	stored stored tested - discarded tested - discarded		
				2			85.3				
				3			85.0				
				4			85.0				
				5			85.3				
				6	1 × 1/2		85.3	flowability			
				7			84.3				
				8			84.0				
54				9	5/8 × 5/8		84.6	conductivity			
55				10			81.1				
56				13	1 × 1/8		82.7	ball penetration		cracked during baking - discarded	
				14			83.3				
				15			84.0				

Table 4-IX. (cont)

NASA specimen No.	Batch number	MgO type	Percent electrolyte	Specimen number	Specimen size (in.)	Pressing pressure (psi)	Percent density	Type test specimen	Disposition
	X	C	33.0	16	1 × 1/8	30,000	84.3	ball penetration	cracked during baking - discarded
				17			84.9		↓
				5 specimens			--		blistered during baking - discarded
				18			84.5		tested - discarded - not reported
				19			84.8		↓
				20			83.9		
				21			83.9		
				22			85.5		
				23			73.5		surface blisters - discarded
				24			79.7		↓
	101	F	55.0	1d	1 × 1/8	30,000	97.2	ball penetration	discarded
				2d			94.4		↓
				4 specimens					unsatisfactory after processing
				3d			87.2		tested - discarded
				4d			86.7		↓
				5d			86.7		
				6d			88.1		
				7d			87.1		discarded
				8d	1 × 1/2		85.7	flowability	tested - discarded
				9d			87.8		↓
				10d			87.4		discarded
36				11d	5/8 × 5/8	20,000	90.9	conductivity	tested - discarded
37				12d			88.2		↓
38				13d			90.9		
				11	1 × 1/2		85.4	flowability	↓
				12			86.3		
39	102	F	56.4	14E	5/8 × 5/8	20,000	82.7	conductivity	↓
40				15E			82.7		
41				16E			81.3		
				17E	1 × 1/8	30,000	80.2	ball penetration	↓
				18E			81.3		
				19E			81.6		
				20E	1 × 1/2		82.7	flowability	surface blistering on
				21E			84.5		all specimens -
				22E			84.8		discarded
				23E			87.0		↓
				24E			86.3		
				25E	1 × 1/8		77.8	ball penetration	tested - discarded
				26E	1 × 1/8		74.6	ball penetration	↓
42	103	F	60.6	1F	5/8 × 5/8	20,000	88.9	conductivity	
43				2F			88.2		↓
44				3F			87.2		
				4F	1 × 1/8	30,000	90.0	ball penetration	↓
				5F			90.0		
				6F			90.0		
				7F	1 × 1/2		91.1	flowability	discarded
				8F			90.4		tested - discarded
				9F			89.7		↓
				10			90.2		
				10			89.7	ball penetration	
				11			90.4		↓

Table 4-IX. (cont)

NASA specimen No.	Batch number	MgO type	Percent electrolyte	Specimen number	Specimen size (in.)	Pressing pressure (psi)	Percent density	Type test specimen	Disposition
45 46 47	104	F	63.0	1H	1 × 1/2	30,000	88.8	flowability	surface stains - discarded
				2H	↓	↓	90.6	↓	↓
				3H	↓	↓	89.2	↓	↓
				4H	1 × 1/8	↓	90.3	ball penetration	tested - discarded
				5H	↓	↓	90.7	↓	↓
				6H	↓	↓	87.5	↓	discarded
				7H	5/8 × 5/8	20,000	89.2	conductivity	tested - discarded
				8H	↓	↓	88.1	↓	↓
				9H	↓	↓	88.4	↓	↓
57 58 59	105	F	69.3	1	1 × 1/8	30,000	73.0	ball penetration	↓
				2	↓	↓	73.0	↓	↓
				3	↓	↓	73.0	↓	↓
	106	F	52.4	1	1 × 1/8	30,000	87.1	↓	↓
				2	↓	↓	84.7	↓	↓
				3	1 × 1/2	↓	88.5	flowability	discarded
				4	↓	↓	92.7	↓	↓
				5	↓	↓	89.5	↓	tested - discarded
				6	5/8 × 5/8	20,000	87.5	conductivity	↓
60 61 62				7	↓	↓	87.5	↓	↓
				8	↓	↓	87.8	↓	↓
	107	F	61.7	1	1 × 1/8	30,000	90.2	ball penetration	↓
				2	↓	↓	89.5	↓	↓
				3	1 × 1/2	↓	92.4	flowability	↓
				4	↓	↓	91.0	↓	↓
				5	↓	↓	84.8	↓	↓
				6	5/8 × 5/8	20,000	89.9	conductivity	↓
				7	↓	↓	90.2	↓	↓
				8	↓	↓	89.2	↓	↓
				11	1 × 1/8	30,000	99.3	ball penetration	cracked during baking - discarded
				12	↓	↓	99.3	↓	↓
				13	1 × 1/2	↓	98.9	flowability	↓
				14	↓	↓	96.0	↓	↓
	108	F	55.0	1	1 × 1/8	30,000	84.5	ball penetration	discarded
				2	↓	↓	83.5	↓	↓
				3	1 × 1/2	↓	86.6	flowability	↓
				4	↓	↓	87.0	↓	↓
	109	F	58.0	1	1 × 1/8	30,000	87-88	ball penetration	small visible cracks - discarded
				2	1 × 1/2	↓	87-88	flowability	small visible cracks - discarded
	110	FF	55.0	1	1 × 1/8	30,000	88.0	ball penetration	tested - discarded
				2	↓	↓	90.1	↓	↓
				5	1 × 1/2	↓	90.1	flowability	↓
				6	↓	↓	91.5	↓	↓
				3	1 × 1/8	↓	94.7	ball penetration	↓
				4	↓	↓	92.6	↓	↓
				7	1 × 1/2	↓	92.2	flowability	↓
				8	↓	↓	91.2	↓	↓
				9	5/8 × 5/8	20,000	90.8	conductivity	stored
				10	↓	↓	91.5	↓	↓
				11	↓	↓	90.5	↓	↓
				16	1 × 1/8	10,000	78.0	gas permeability	tested - discarded
				17	↓	20,000	84.8	↓	↓
				18	↓	30,000	89.0	↓	↓

Table 4-IX. (cont)

NASA specimen No.	Batch number	MgO type	Percent electrolyte	Specimen number	Specimen size (in.)	Pressing pressure (psi)	Percent density	Test type specimen	Disposition
	110	FF	55.0	19	1 × 1/8	30,000	96.8	ball penetration	blistering - discarded
				20	↓		97.9	↓	↓
				21	1 × 1/2		97.9	flowability	↓
				22	1 × 1/2		97.9	↓	↓
	111	F	56.5	1	5/8 × 5/8	20,000	86.2	conductivity	practice test runs - discarded
				2	↓		91.2	↓	↓
				3			90.8	↓	↓
				4	1 × 1/8	30,000	86.6	ball penetration	(all specimens of No. 111 cracked and warped upon cooling)
				5	↓		91.2	↓	↓
				6			91.2	↓	↓
				7	1 × 1/2		89.4	flowability	tested - discarded
				8	↓		90.5	↓	↓
				11	1 × 1/8		91.9	ball penetration	↓
				12	↓		90.5	↓	↓
				13	1 × 1/2		91.2	flowability	↓
				14	↓		90.8	↓	↓
	112	FF	65.0	1	1 × 1/8	20,000	88.0	ball penetration	↓
				2	↓		92.3	↓	↓
				3			87.6	↓	↓
				4			96.0	↓	↓
				5	1 × 1/2		82.5	flowability	↓
				6	↓		85.4	↓	↓
				7	5/8 × 5/8		84.7	conductivity	↓
				8	↓		85.0	↓	↓
63				3	1 × 1/2	20,000	95.3	flowability	discarded
64		FF	65.7	4	↓		90.5	↓	↓
				5	1 × 1/8		95.3	ball penetration	↓
				6	↓		90.1	↓	↓
	115	FF	50.0	4	1 × 1/8	30,000	65.7	↓	↓
				5	↓		68.5	↓	↓
	116	FF	65.8	9	1 × 1/2	20,000	85.8	flowability	tested - discarded
				10	↓		85.8	↓	↓
65				11	5/8 × 5/8		85.1	conductivity	stored
				12	↓		84.7	↓	↓
				13			83.3	↓	↓
				14	1 × 1/8		87.6	ball penetration	tested - discarded
				15	↓		89.5	↓	↓
				16			89.5	↓	↓
				17		10,000	84.0	gas permeability	stored
				18	↓		84.0	↓	↓
				19		20,000	86.5	↓	tested - discarded
				20	↓		84.9	↓	stored
				21		30,000	89.8	↓	tested - discarded
				22	↓		88.4	↓	stored

## V. TESTING AND ELECTRICAL PROPERTY STUDIES OF COMPOSITE MATERIAL

### CONDUCTIVITY STUDIES

Conductivity studies were initiated to gather data for predicting the performance of a specific electrolyte matrix configuration in a cell, and to compare one configuration to another. Early data<sup>4</sup> were presented in graphical form on plots of conductivity (K) versus temperature in degrees centigrade. The limited data taken for each specimen, as few as three data points, gave the impression of a linear curve over the range of investigation. However, when these data were plotted with conductivity on a logarithmic scale versus the reciprocal absolute temperature on a linear scale, it was shown that a break in the data occurred at the lower temperatures. That is, in the relation

$$\log K = A - B/T$$

the values of the constants A and B changed in the lower temperature range. Therefore, all data gathered in this program have been plotted on semilog scales. Critical studies of this phenomenon were not made, other than to notice that this break consistently occurred near or above  $1.745 (10)^{-3} (^\circ K)^{-1}$ , which corresponds to the temperature range 300°C and below.

In general, the quality of data attained from testing of specimens in this program has been adequate for property correlations, but not for the more critical study of phase or chemical change with temperature. The major interest has been near 300°C, which is fixed as the operating temperature of the potassium-mercury cell.

The data have been compiled in a chronological order of tests and tabulated in Tables 5-I and 5-II. These data have been plotted and are discussed in the following paragraphs.

Figures 5-1, 5-2, and 5-3 are plots of conductivity data for the 31/69, 33/67, and 35/65 weight ratio, coarse grain type CMgO composite specimens. The data of the 31/69 material are tightly grouped since the densities of the three specimens are nearly identical. A spread in the conductivity values of the 33/67 material (Figure 5-2) is seen to exist as a function of density. Although specimens 16 and 17 have identical properties, the data do not reproduce. Further, it is noticed that the slopes of all plots are irregular. The single specimen in Figure 5-3 plotted

---

<sup>4</sup>Design and Development of a Liquid Metal Fuel Cell, USAF, ASD-TDR-62-1045, December 1962, pp 72-74. (Prepared by Allison Division of General Motors Corporation under contract AF33(657)-7847—Allison EDR 3100.)

Table 5-I.  
Conductivity specimen identification.

Specimen No.	Nominal weight ratio	MgO type	Percent of theoretical density	Diameter (in.)	Height (in.)	Test height (in.)
12	35/65	C	90.40	0.595	0.740	0.600
13	33/67	C	87.80	0.606	0.667	0.600
14	33/67	C	86.20	0.608	0.669	0.600
15	33/67	C	86.80	0.606	0.658	0.600
16	33/67	C	74.70	0.616	0.688	0.600
17	33/67	C	74.70	0.618	0.689	0.600
18	33/67	C	78.20	0.606	0.690	0.600
19	31/69	C	87.80	0.613	0.648	0.600
20	31/69	C	87.20	0.612	0.660	0.600
21	31/69	C	86.20	0.613	0.654	0.600
22	35/65	C	92.90	0.603	0.136	0.132†
23	35/65	C	95.80	0.604	0.146	0.085†
24	35/65	C	98.10	0.604	0.132	0.127†
25	33/67	C	86.20	0.621	0.145	0.138†
26	33/67	C	84.60	0.621	0.143	--
27	33/67	C	85.90	0.621	0.119	0.117†
28	34/66	C	86.90	0.603	0.660	0.600
29	34/66	C	86.20	0.604	0.614	0.600
30	34/66	C	86.50	0.602	0.633	0.600
31	34/66	C	89.40	0.601	0.631	0.600
32	34/66	C	85.60	0.605	0.636	0.600
33	34/66	C	85.60	0.606	0.643	0.600
34	34/66	C	86.50	0.604	0.640	0.600
35	34/66	C	85.00	0.603	0.727	0.600
36	55/45	F	90.9	0.598	0.687	0.603†
37	55/45	F	88.2	0.601	0.685	--
38	55/45	F	90.9	0.598	0.689	0.613†

†Measured after test—all others nominal mechanical stop value.

Table 5-I. (Cont)

Specimen No.	Nominal weight ratio	MgO type	Percent of theoretical density	Diameter (in.)	Height (in.)	Test height (in.)
39	57.5/42.5	F	82.7	0.610	0.708*	0.675†
40	57.5/42.5	F	82.7	0.610	0.683	0.663†
41	57.5/42.5	F	81.3	0.610	0.668	--
42	60/40	F	89.0	0.607	0.628	0.598†
43	60/40	F	88.0	0.610	0.630	0.610†
44	60/40	F	87.0	0.612	0.647	0.609†
45	63/37	F	89.2	0.606	0.691	0.600
46	63/37	F	88.1	0.607	0.690	0.600
47	63/37	F	88.5	0.607	0.692	0.600
48	33/67	C	82.4	0.608	0.648	0.600
49	33/67	C	82.1	0.610	0.648	0.600
50	33/67	C	81.4	0.609	0.649	0.642†
51	33/67	C	84.6	0.614	0.613	0.580
52	33/67	C	83.6	0.614	0.618	0.580
53	33/67	C	84.6	0.614	0.612	0.580
54	33/67	C	84.0	0.612	0.577	0.580
55	33/67	C	84.6	0.607	0.595	0.580
56	33/67	C	81.1	0.628	0.589	0.580
57	50/50	F	87.5	0.621	0.588	0.580
58	50/50	F	87.5	0.623	0.648	0.600
59	50/50	F	87.8	0.617	0.676	0.600
60	60/40	F	89.9	0.618	0.635	0.600
61	60/40	F	90.2	0.618	0.622	0.600
62	60/40	F	89.2	0.620	0.635	0.600
63	65/35	FF	84.7	0.622	0.728	0.607
64	65/35	FF	85.0	0.622	0.744	0.600
65	65/35	FF	85.1	0.625	0.718	0.602

\*Reworked before testing.

†Measured after test—all others nominal mechanical stop value.



Table 5-II.  
Conductivity specimen data.

<u>Specimen No.</u>	<u>Temperature (°K)</u>	<u>Resistance (ohms)</u>	<u>Conductivity (mho/cm)</u>	<u><math>\frac{1}{T} \times 10^3</math> (°K)<sup>-1</sup></u>
12	590	4.65	0.183	1.69
	605	4.20	0.202	1.65
	617	3.89	0.218	1.62
	622	3.77	0.225	1.60
	569	5.76	0.148	1.76
	530	10.06	0.084	1.89
	547	7.63	0.111	1.83
	515	12.22	0.069	1.94
	497	16.20	0.052	2.01
	476	30.10	0.028	2.10
13	624	5.07	0.162	1.60
	595	6.33	0.130	1.68
	556	9.44	0.087	1.80
	580	7.40	0.111	1.72
	544	11.81	0.069	1.84
	528	16.74	0.049	1.89
	503	41.00	0.020	1.99
14	625	5.11	0.160	1.60
	588	6.94	0.117	1.70
	568	8.37	0.097	1.76
	550	11.33	0.072	1.81
	522	19.63	0.041	1.92
	499	75.00	0.011	2.00
15	595	6.55	0.125	1.68
	615	5.57	0.147	1.63
	619	5.43	0.151	1.62
	566	8.67	0.094	1.77
	573	8.06	0.102	1.75
	555	10.17	0.081	1.80
	530	17.20	0.048	1.89

Table 5-II. (Cont)

Specimen No.	Temperature (°K)	Resistance (ohms)	Conductivity (mho/cm)	$\frac{1}{T} \times 10^3$ (°K) <sup>-1</sup>
16	625	6.19	0.128	1.60
	603	7.41	0.107	1.66
	576	9.62	0.082	1.74
	553	14.74	0.040	1.81
	538	24.90	0.038	1.86
17	619	6.96	0.114	1.62
	627	6.50	0.122	1.59
	598	8.25	0.096	1.67
	569	11.23	0.070	1.76
	548	18.90	0.042	1.82
	518	31.75	0.025	1.93
	536	20.54	0.038	1.87
18	626	5.70	0.144	1.60
	594	7.45	0.110	1.68
	572	9.15	0.090	1.75
	544	15.19	0.054	1.84
	519	23.94	0.034	1.93
19	629	5.08	0.157	1.59
	604	6.15	0.130	1.66
	579	7.65	0.104	1.73
	553	9.99	0.080	1.81
	515	20.54	0.039	1.94
20	629	5.10	0.159	1.59
	596	6.48	0.123	1.68
	570	8.17	0.098	1.75
	544	11.10	0.072	1.84
	520	16.87	0.047	1.92

Table 5-II. (Cont)

Specimen No.	Temperature (°K)	Resistance (ohms)	Conductivity (mho/cm)	$\frac{1}{T} \times 10^3 \text{ (°K)}^{-1}$
21	622	5.32	0.150	1.61
	596	6.52	0.122	1.68
	572	8.16	0.098	1.75
	547	10.97	0.073	1.83
	521	17.32	0.046	1.92
22	636	1.02	0.175	1.57
	609	1.25	0.143	1.64
	581	1.56	0.115	1.72
	555	2.26	0.079	1.80
	527	3.74	0.049	1.90
23	633	0.45	0.140	1.56
	598	0.55	0.114	1.67
	570	0.70	0.090	1.75
	536	1.11	0.057	1.86
	509	1.80	0.035	1.96
24	613	0.88	0.162	1.63
	595	1.00	0.143	1.68
	561	1.34	0.107	1.78
	531	2.30	0.062	1.88
	516	3.26	0.044	1.93
25	630	1.43	0.126	1.58
	609	1.70	0.106	1.64
	587	2.20	0.082	1.70
	546	5.96	0.030	1.83
26	618	0.66	0.127	1.61
	613	0.70	0.120	1.62
	585	0.90	0.093	1.70
	556	1.21	0.069	1.79
	522	2.30	0.036	1.91

Table 5-II. (Cont)

Specimen No.	Temperature (°K)	Resistance (ohms)	Conductivity (mho/cm)	$\frac{1}{T} \times 10^3 \text{ (°K)}^{-1}$
27	619	1.20	0.122	1.62
	605	1.42	0.104	1.65
	559	2.51	0.058	1.79
	524	5.55	0.026	1.91
28	635	4.60	0.195	1.57
	611	5.55	0.164	1.63
	592	6.53	0.139	1.68
	573	7.74	0.117	1.74
	551	10.36	0.091	1.81
	529	15.18	0.060	1.92
29	647	4.46	0.189	1.54
	628	5.16	0.163	1.59
	604	6.20	1.136	1.65
	568	8.67	0.097	1.74
	532	14.50	0.058	1.87
30	654	4.20	0.208	1.52
	628	5.16	0.170	1.59
	600	6.26	0.140	1.66
	573	8.04	0.109	1.79
	548	11.43	0.076	1.82
	524	17.84	0.049	1.90
31	642	4.50	0.195	1.58
	623	5.20	0.168	1.60
	591	6.84	0.128	1.69
	568	8.50	0.103	1.76
	529	15.68	0.056	1.85

Table 5-II. (Cont)

Specimen No.	Temperature (°K)	Resistance (ohms)	Conductivity (mho/cm)	$\frac{1}{T} \times 10^3$ (°K) <sup>-1</sup>
32	652	4.34	0.201	1.53
	623	5.24	0.166	1.60
	592	6.67	0.130	1.68
	565	8.67	0.100	1.76
	534	14.30	0.060	1.87
33	652	5.17	0.170	1.53
	618	6.38	0.138	1.61
	594	7.80	0.112	1.68
	563	10.44	0.084	1.77
	534	16.67	0.052	1.87
34	647	4.83	0.182	1.54
	623	5.76	0.153	1.60
	592	7.47	0.118	1.68
	560	10.65	0.083	1.78
	531	17.30	0.051	1.88
35	647	8.40	0.118	1.54
	621	10.25	0.097	1.61
	587	13.70	0.073	1.70
36	628	2.12	0.46	1.59
	595	2.70	0.36	1.68
	570	3.37	0.29	1.75
	537	4.92	0.20	1.86
37	626	2.70	0.36	1.60
	605	3.10	0.30	1.65
	577	3.86	0.25	1.73
	551	5.00	0.19	1.81

Table 5-II. (Cont)

Specimen No.	Temperature (°K)	Resistance (ohms)	Conductivity (mho/cm)	$\frac{1}{T} \times 10^3 \text{ (°K)}^{-1}$
38	635	2.04	0.47	1.57
	602	2.62	0.37	1.66
	577	3.33	0.29	1.73
	541	4.80	0.20	1.85
39	625	2.62	0.36	1.60
	610	3.00	0.32	1.64
	581	3.74	0.25	1.72
	543	5.10	0.19	1.84
40	642	2.49	0.37	1.56
	611	3.07	0.30	1.64
	580	3.97	0.24	1.72
	540	5.71	0.16	1.85
41	Broken specimen			
42	639	1.90	0.45	1.56
	616	2.25	0.38	1.62
	576	2.96	0.29	1.74
	552	3.74	0.23	1.81
43	646	1.95	0.44	1.55
	616	2.35	0.36	1.62
	592	2.75	0.31	1.69
	543	4.39	0.19	1.84
44	643	1.84	0.47	1.56
	612	2.24	0.39	1.63
	585	2.76	0.32	1.71
	547	3.89	0.22	1.83

Table 5-II. (Cont)

Specimen No.	Temperature (°K)	Resistance (ohms)†	Conductivity (mho/cm)	$\frac{1}{T} \times 10^3$ (°K) <sup>-1</sup>
45	619	0.282‡	0.231	1.62
	595	0.227	0.186	1.68
	569	0.173	0.142	1.76
	546	0.119	0.097	1.83
	522	0.027	0.022	1.92
46	599	0.2765	0.226	1.67
	626	0.3472	0.284	1.60
	603	0.2859	0.234	1.66
	564	0.1786	0.146	1.77
	548	0.1406	0.115	1.82
	527	0.0940	0.077	1.90
47	566	0.1867	0.152	1.77
	594	0.2688	0.220	1.68
	625	0.3452	0.282	1.60
	606	0.2960	0.242	1.65
	573	0.2248	0.184	1.74
	552	0.1734	0.142	1.81
	529	0.1234	0.101	1.89
48	566	0.0435	0.036	1.77
	595	0.0643	0.053	1.68
	628	0.0928	0.076	1.59
	591	0.0580	0.048	1.69
	572	0.0458	0.038	1.75
	545	0.0071	0.006	1.83
49	Contact with specimen not attained.			

Table 5-II. (Cont)

Specimen No.	Temperature (°K)	Conductance (mho)	Conductivity (mho/cm)	$\frac{1}{T} \times 10^3 \text{ (°K)}^{-1}$
50	567	0.0423	0.037	1.76
	598	0.0589	0.051	1.67
	625	0.0777	0.068	1.60
	592	0.0518	0.045	1.69
	569	0.0366	0.032	1.76
	547	0.0190	0.016	1.83
	529	0.005	0.004	1.89
51	576	0.0405	0.031	1.73
	609	0.062	0.048	1.64
	618	0.075	0.058	1.62
	628	0.078	0.060	1.59
	608	0.062	0.048	1.64
	572	0.037	0.028	1.75
	545	0.007	0.005	1.83
	524	0.0005	(0.0004)	1.91
52	569	0.027	0.021	1.76†
	601	0.055	0.042	1.66†
	621	0.078	0.060	1.61
	598	0.057	0.044	1.67
	570	0.039	0.030	1.75
	550	0.023	0.018	1.82
	518	0.002	0.002	1.93
53	574	0.041	0.032	1.74
	591	0.052	0.040	1.69
	626	0.079	0.061	1.60
	596	0.053	0.041	1.68
	572	0.038	0.029	1.75
	545	0.012	0.009	1.83
	520	0.001	0.0008	1.92



Table 5-II (Cont)

Specimen No.	Temperature (°K)	Conductance (mho)	Conductivity (mho/cm)	$\frac{1}{T} \times 10^3$ (°K) <sup>-1</sup>
54	Contact with specimen not attained.			
55	572	0.0611	0.048	1.75
	619	0.108	0.085	1.62
	592	0.080	0.063	1.69
	573	0.0616	0.049	1.74
	549	0.0388	0.031	1.82
	524	0.0118	0.009	1.91
56	574	0.0966	0.071	1.74
	601	0.1293	0.095	1.66
	653	0.1836	0.135	1.53
	622	0.1432	0.105	1.61
	598	0.1176	0.087	1.67
	573	0.0930	0.068	1.74
	548	0.0657	0.048	1.82
	524	0.0450	0.033	1.91*
57	587	0.0860	0.065	1.70†
	603	0.1170	0.088	1.66†
	628	0.1715	0.129	1.59
	603	0.1380	0.104	1.66
	578	0.1030	0.078	1.73
	553	0.0729	0.055	1.81
	529		0.023	1.89
58	598	0.1540	0.119	1.67
	620	0.2059	0.159	1.61
	589	0.1325	0.118	1.70
	571	0.1171	0.091	1.75
	547	0.0866	0.067	1.83
	514	0.0370	0.029	1.95

Table 5-II. (Cont)

Specimen No.	Temperature (°K)	Conductance (mho)	Conductivity (mho/cm)	$\frac{1}{T} \times 10^3$ (°K) <sup>-1</sup>
59	571	0.0931	0.078	1.75
	606	0.1580	0.133	1.65
	631	0.1850	0.156	1.59
	588	0.1053	0.089	1.70
	565	0.0782	0.066	1.77
	544	0.0561	0.047	1.84
	503	0.0103	0.009	1.99
60	565	0.1489	0.117	1.77
	595	0.2151	0.169	1.68
	625	0.3083	0.243	1.60
	597	0.2293	0.180	1.68
	561	0.1226	0.096	1.78
	534	0.0577	0.045	1.87
	516	0.0154	0.012	1.94
61	566	0.1487	0.117	1.77
	596	0.2218	0.174	1.68
	626	0.3056	0.240	1.60
	603	0.2474	0.195	1.66
	579	0.1722	0.136	1.73
	547	0.1058	0.083	1.83
	524	0.0605	0.048	1.91
62	568	0.1776	0.139	1.76
	600	0.2568	0.201	1.67
	629	0.332	0.260	1.59
	597	0.2532	0.198	1.68
	570	0.1645	0.129	1.75
	549	0.1165	0.091	1.82
	521	0.0830	0.065	1.92*

Table 5-II. (Cont)

Specimen No.	Temperature (°K)	Conductance (mho)	Conductivity (mho/cm)	$\frac{1}{T} \times 10^3$ (°K) <sup>-1</sup>
63	558	0.3523	0.33	1.79
	561	0.3625	0.34	1.78
	564	0.3750	0.35	1.77
	570	0.3958	0.37	1.75
	578	0.4243	0.40	1.73
	587	0.4536	0.43	1.70
	596	0.4798	0.45	1.68
	605	0.510	0.48	1.65
	614	0.5346	0.50	1.63
	578	0.4080	0.38	1.73
	561	0.3430	0.32	1.78
64	548	0.3745	0.291	1.83
	563	0.4243	0.33	1.78
	573	0.4594	0.357	1.75
	583	0.5069	0.394	1.72
	598	0.5422	0.422	1.67
65	525	0.192	0.153	1.90
	553	0.278	0.221	1.81
	596	0.407	0.325	1.68
	573	0.351	0.251	1.75
	626	0.4682	0.373	1.60
	668	0.5882	0.469	1.50
	571	0.3085	0.246	1.75
	556	0.2180	0.174	1.80
	528	0.1282	0.0922	1.89
	527	0.1175	0.0936	1.90

\*Nonequilibrium cool-down data.

†Nonequilibrium heat-up data.

‡Beginning with specimen No. 45, conductance data rather than resistance data were taken.

Figure 5-1. Conductivity of 31/69  
unconsolidated electrolyte matrices  
(type C MgO).

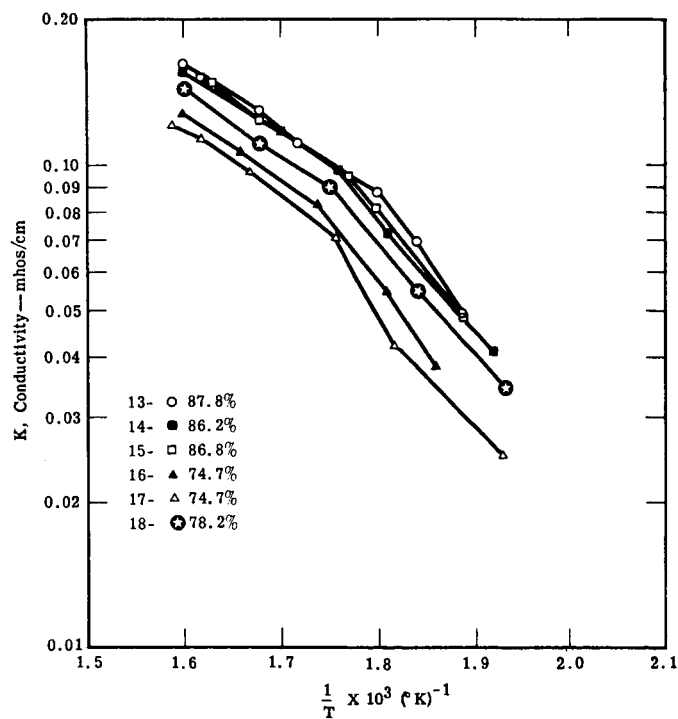
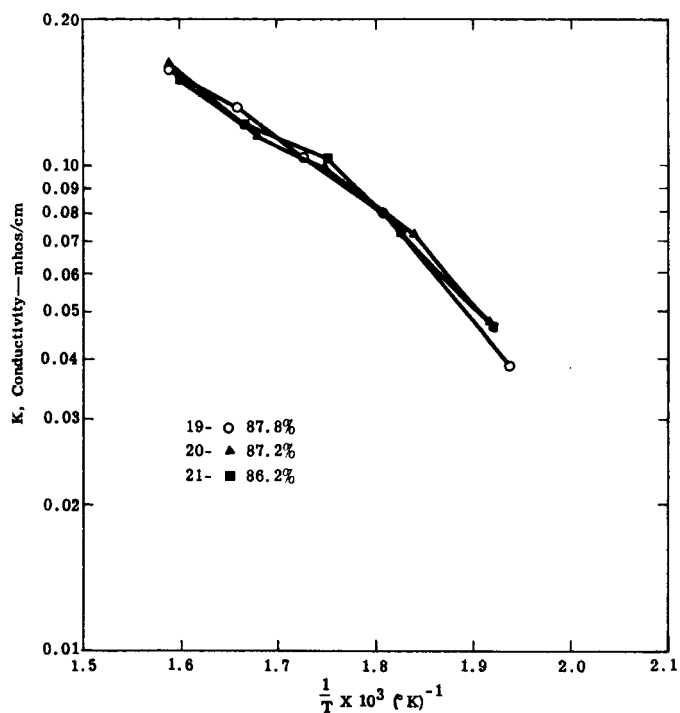


Figure 5-2. Conductivity of 33/67  
unconsolidated electrolyte matrices  
(type C MgO).

with eleven points appears to indicate two slope breaks. The break occurring at  $2.0 (10)^{-3} (^\circ\text{K})^{-1}$  is significant in that it is known to be the eutectic point of the electrolyte mixture at  $230^\circ\text{C}$ . The other break occurs at a temperature slightly higher than that for cell operation,  $310^\circ\text{C}$ .

Figure 5-4 is a replot of data to show the effect of electrolyte saturation on conductivity. Although specimen 17 has the higher electrolyte weight content, a lower density (lower saturation) causes it to be inferior to specimen 19.

The contrasting situation occurs in Figure 5-5, where identical percent theoretical densities are quite similar in conductance. It would seem logical to conclude from Figures 5-4 and 5-5 that weight ratio has no effect on conductance. This conclusion would be presumptive, however, since higher saturation may be gained by higher electrolyte content. It will be seen, however, that higher electrolyte content must be gained through the use of smaller ceramic grain size. Therefore, only within a narrow range for a given grain size material may the conclusion be drawn.

Figures 5-6 and 5-7 show the conductivity data for the 34/66, 5-micron specimens. This batch was prepared because of difficulty in correlating strength measurements between the 33/67 and 35/65 batches. A fair correlation between conductivity and density is again apparent with the tight grouping of the curves. The data of specimen 35 are questionable since testing was terminated with only three data points.

Since the program called for the use of thin specimens, an attempt was made to measure the conductivity of 1/8-in. thick specimens, and the data are shown in Figure 5-8. Difficulty in measuring the low resistance of 1/8-in. thick  $\times$  5/8-in. dia specimens is evidenced by the scattering of the data. Therefore, the conductivity measurements were continued on specimens  $5/8 \times 5/8$  in.

The first of the fine type F MgO grain electrolyte composites were prepared as a preliminary investigation of the conductivity range. Figure 5-9 contains the plots of all conductivity data for these materials. These early specimens came from the baking process with a discolored deposit on one end. This deposit came from the material on which the specimen rested in the final baking in the fabrication process. Specimens 39 and 40 were nearly identical in properties. Since specimen 39 had greater height, the end deposit was scraped off for chemical analysis. The analysis showed that minor portions of Na, Mg, and Ni along with traces of Cu, Cr, and Fe were present. Subsequent conductivity tests were performed on these two specimens.

Figure 5-3. Conductivity of 35/65 unconsolidated electrolyte matrices (type C MgO).

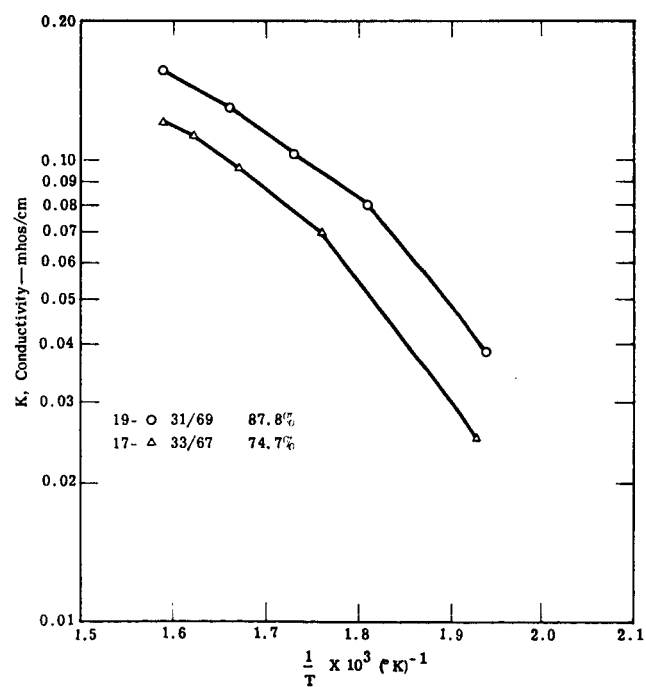
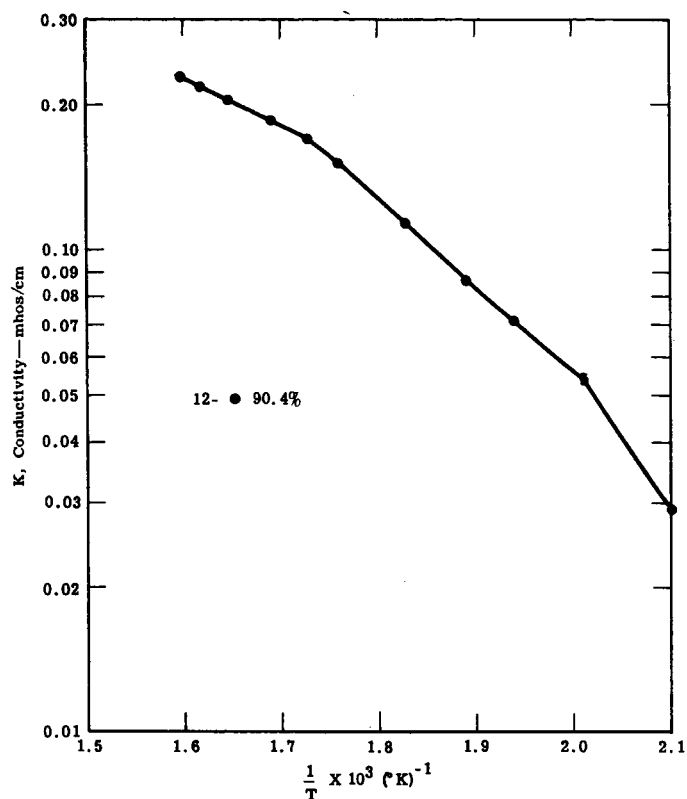


Figure 5-4. Conductivity of 33/67 and 31/69 unconsolidated electrolyte matrices to show density effect (type C MgO).

Figure 5-5. Conductivity of 31/69, 33/67, and 34/66 unconsolidated electrolyte matrices with 86.2% theoretical density (type C MgO).

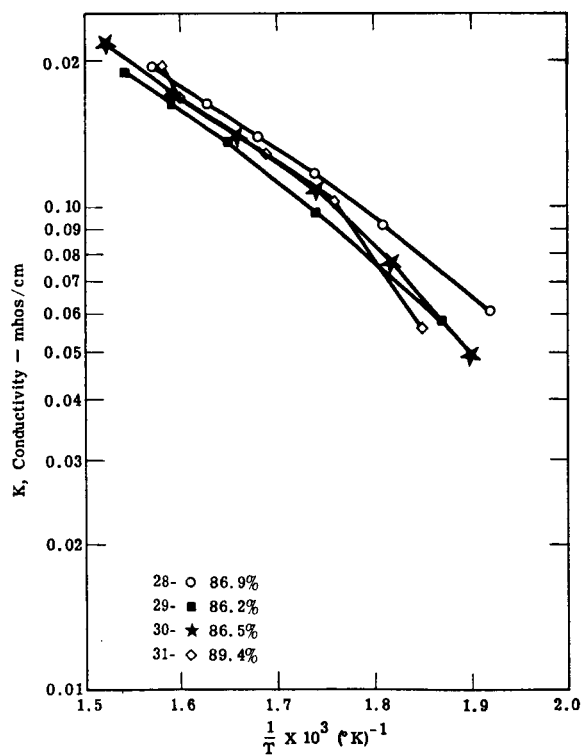
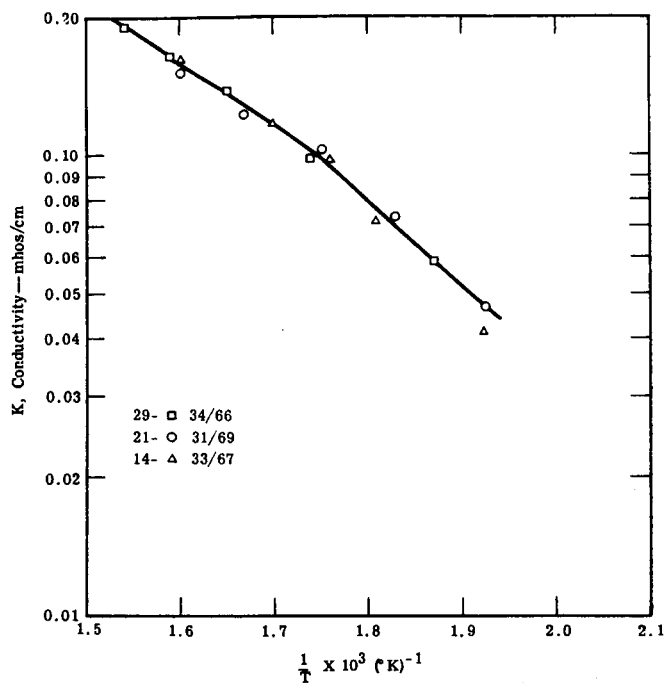


Figure 5-6. Conductivity of 34/66 unconsolidated electrolyte matrices (type C MgO).

Figure 5-7. Conductivity of 34/66 unconsolidated electrolyte matrices (type C MgO).

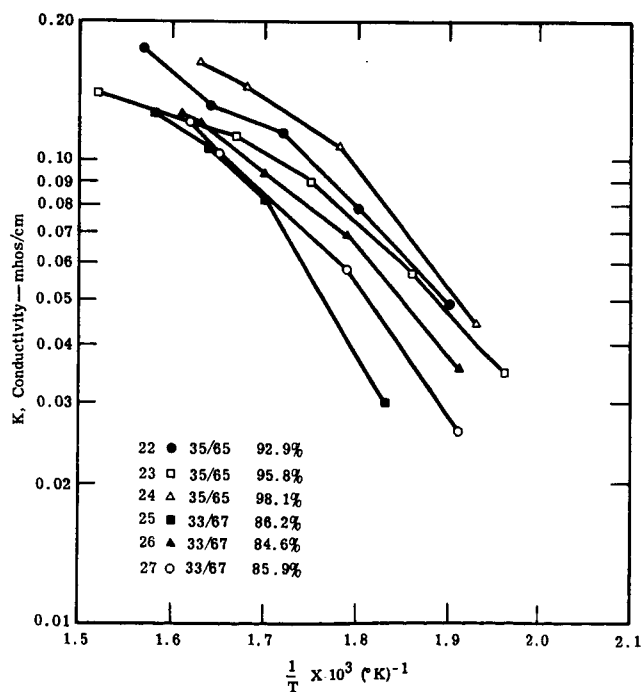
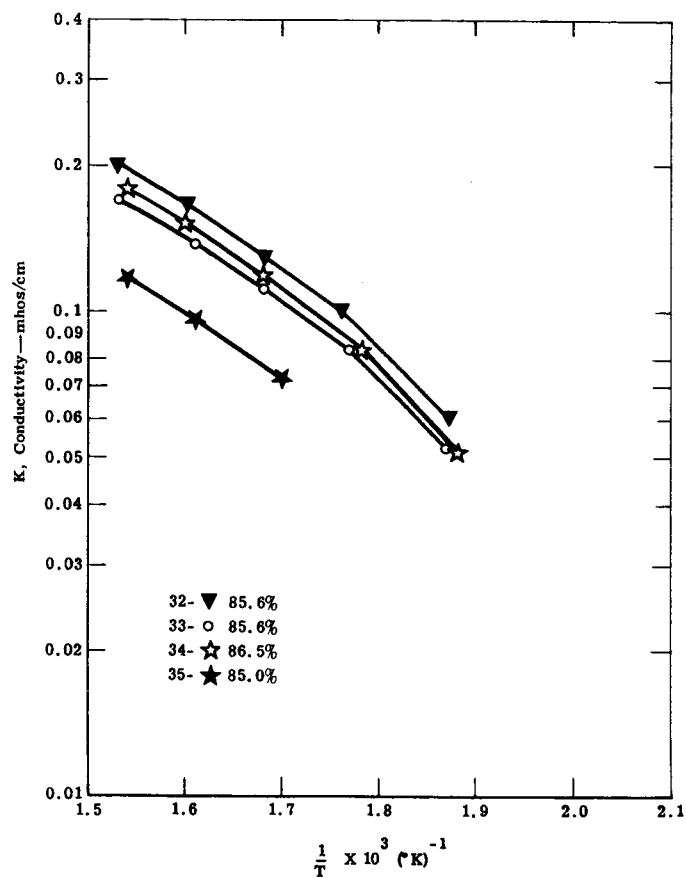
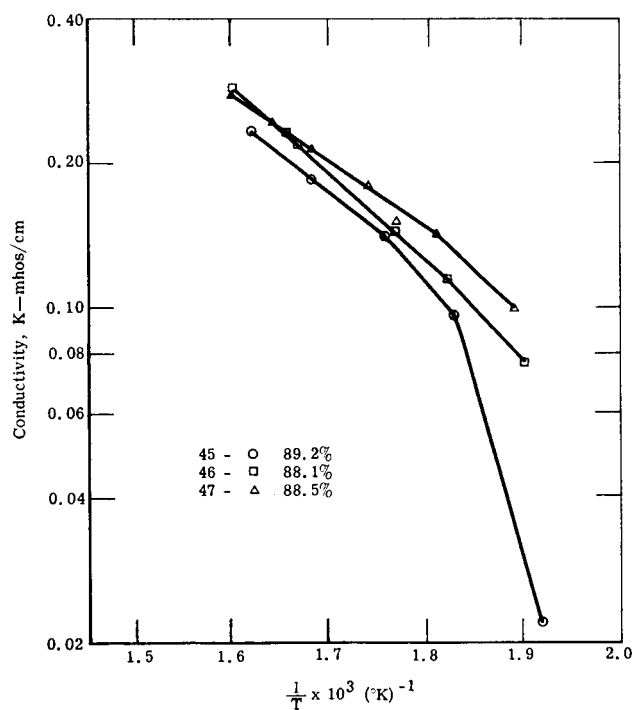
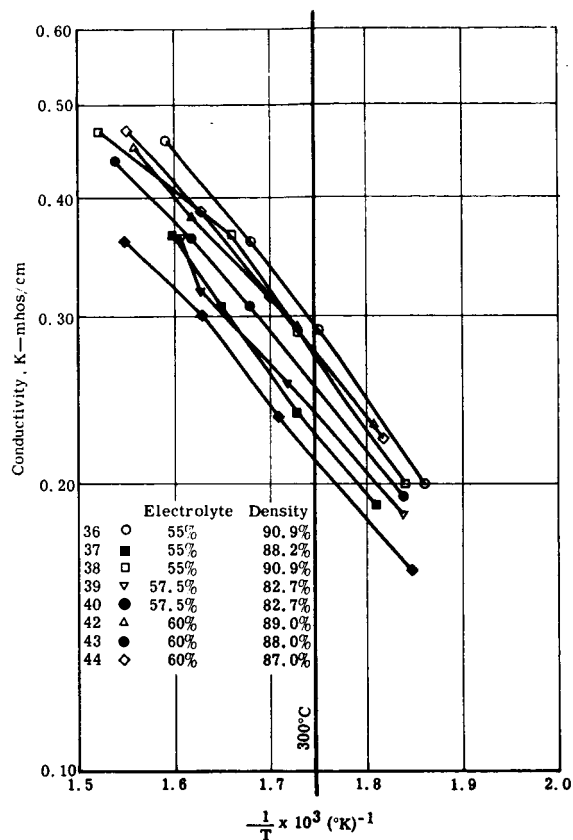


Figure 5-8. Conductivity of thin unconsolidated electrolyte matrices (type C MgO).



Figure 5-9. Conductivity of fine grain unconsolidated electrolyte matrices (type F MgO).



5-10. Conductivity of 63/37 unconsolidated electrolyte matrices (type F MgO).

During these tests, the effect of this deposit on the contact resistance was observed. It can be seen in Figure 5-9 that the conductivity for specimen 39 was slightly higher than that for specimen 40.

The conductivity measurements were made a routine project during the remainder of the program as the search for a satisfactory fabrication technique ensued. As a rule, conductivity specimens were prepared from each new batch of material prepared. However, where other consideration ruled out a batch, then conductivity measurements were not taken.

Figure 5-10 shows the typical trend of the composite electrolyte with temperature. Some discrepancy in the density effect was noted in the data, with the higher density material exhibiting the lower conductivity. The 63/37 electrolyte exhibits greater conductivity than previously reported composites, with a value of 0.15 mho/cm at cell temperature.

Figures 5-11 and 5-12 are data plots of the conductivity for these later prepared batches of coarse grain composite. In Figure 5-11, the last three specimens (51, 52, and 53) are grouped both with respect to density and conductivity. The other two, specimens 48 and 50, have higher conductivities but have lower densities. This batch was originally reported as a nominal 34/66 electrolyte content but was analyzed as 32.9% electrolyte. The data now appear questionable in view of the results shown in Figure 5-12. The results of Figure 5-12 show that the conductivity of 33% electrolyte composites is higher than that shown in Figure 5-11. Again, the conductivity is higher for the materials of lower density.

The results of the tests for a 50/50 weight ratio (type F MgO) in Figure 5-13 show considerable scattering of the data although the densities are nearly identical. This is a dry material and may not get a good contact with the electrodes. The wetter material of 60/40 ratio shown in Figure 5-14 is better grouped for density. Note that these curves and those for 63/37 (type F MgO) from earlier work shown in Figure 5-10 agree closely with the higher electrolyte content giving the higher conductivity at equal densities. This then shows that the electrolyte content affects saturation and, therefore, conductivity.

The 65/35 ratio composite data shown in Figure 5-15 are for two different batches of the type FF MgO. It becomes apparent that the light calcined type F MgO had reached a limiting factor at around 63% electrolyte. The new material shows a very pronounced increase in conductivity over that for the old.

Figure 5-11. Conductivity of 33/67 (nominal 34/66) unconsolidated electrolyte matrices (type C MgO).

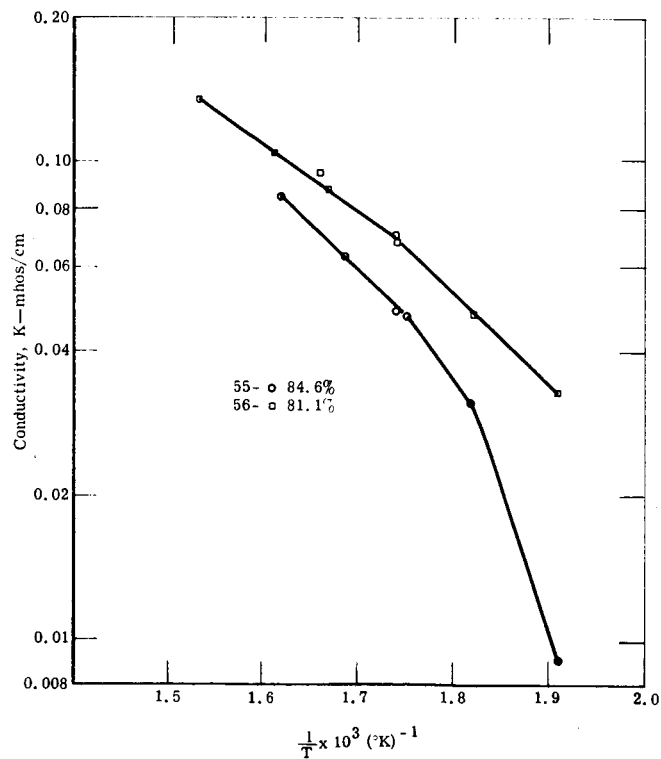
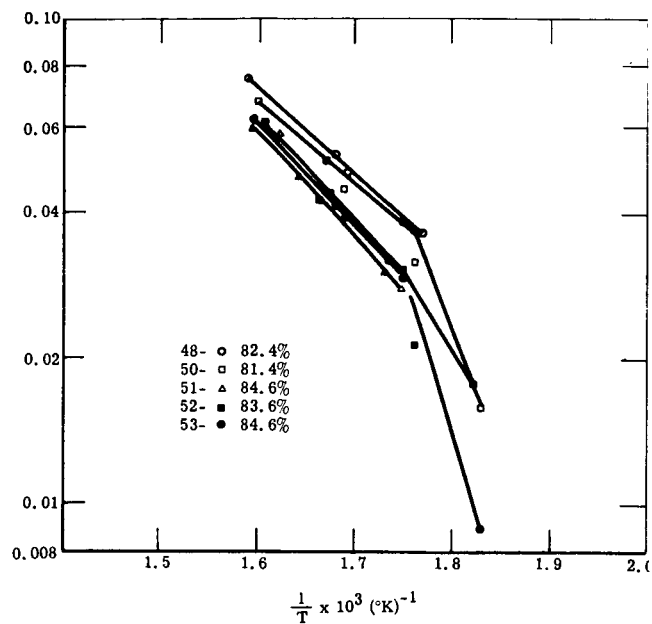


Figure 5-12. Conductivity of 33/67 unconsolidated electrolyte matrices (type C MgO).

Figure 5-13. Conductivity of 50/50 unconsolidated electrolyte matrices (type F MgO).

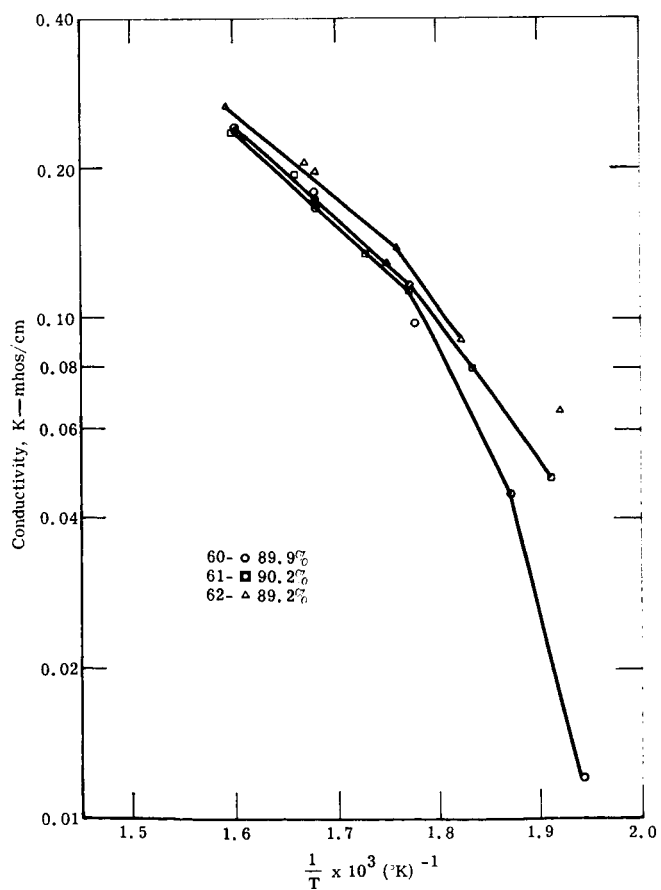
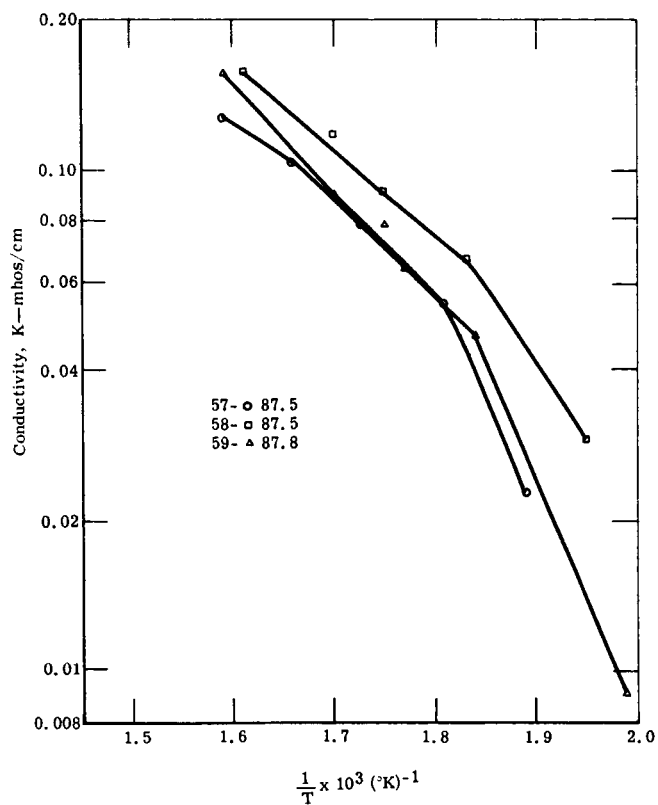


Figure 5-14. Conductivity of 60/40 unconsolidated electrolyte matrices (type F MgO).

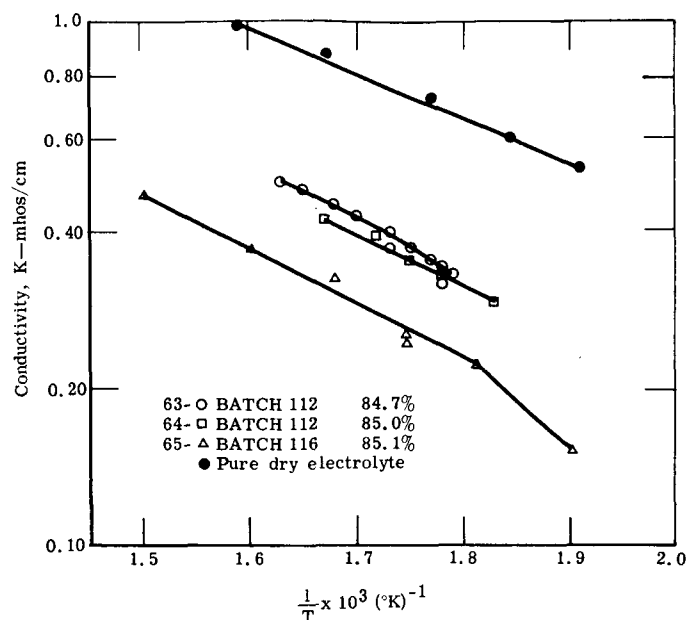


Figure 5-15. Conductivity of 65/35 unconsolidated electrolyte matrices (type FF MgO).

In subsequent paragraphs of this section, a discussion of cells which were operated from these materials shows the same trend between the two batches of materials. The only conclusion which can be made is that the two batches of material were not identical.

The results of the final tests show the resistivity of the materials to be approximately 2.8 ohm-cm and 3.9 ohm-cm.

Measurement of the pure electrolyte was accomplished during the program. First a carefully prepared electrolyte was tested in a ceramic container and found to be stable in time and quite linear on the semilog scale, as shown in Figure 5-15. A second test using a sample of the electrolyte from the composite work showed it to be inferior, probably wet, and, therefore, new processes were introduced to prepare dry electrolyte. These processes are described in in Section IV.

A significant relationship may be obtained from the values of Figure 5-15. At cell operating temperature, the pure electrolyte has a conductivity of  $K = 0.74 \text{ mho/cm}$  or a resistivity of  $\gamma = 1.35 \text{ ohm-cm}$ . The top composite curve was read as  $\gamma = 2.7 \text{ ohm-cm}$  or a ratio of 2.0. The achievement of a value of 2.0 for this ratio is nearly ideal for composite fabrication.

## SMALL CELL STUDIES

A description of the small cell is made with reference to the design sketch as shown in Figure 5-16.

This cell was designed to expose 1 in. of the 2-in. dia disk to the liquid metal. This gives an active cell area of  $5.07 \text{ cm}^2$  and a seal area of  $15.2 \text{ cm}^2$ , or a ratio of 3:1. It was intended that the liquid metal cavity wall angle be adjusted by machining to obtain other ratios of active cell area to seal area. One modification was made after cell XII.

Early work with a 0.5-in. thick composite specimen and 5 psi differential pressure using the equipment described in Section VI showed that this material is not permeable to argon gas, and that the seal region did not leak. Therefore, the same concentric serration design was adopted for this small cell.

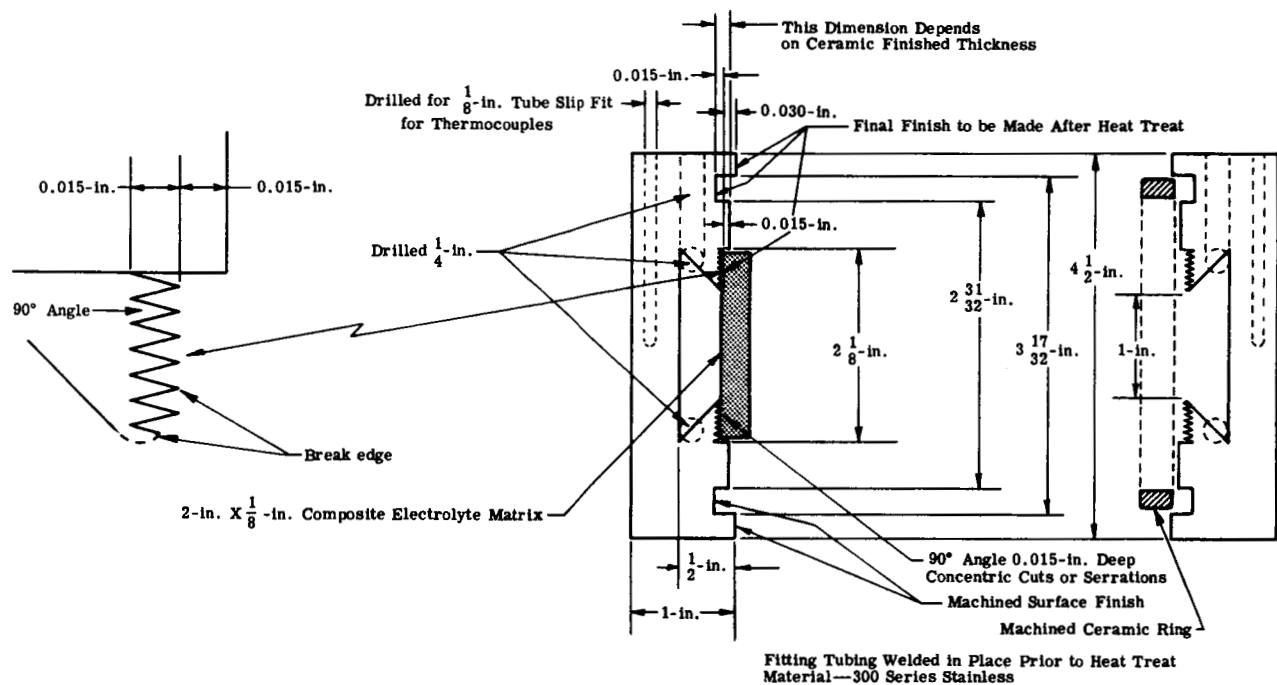


Figure 5-16. Test equipment for first small unit.

Work during the first quarter showed that some compositions (those highly saturated with electrolyte) have high flowability characteristics. This characteristic of the paste electrolyte led to the design of a mechanical stop to limit the deformation of the specimen in the cell. The stop is formed by a machined ceramic ring mounted within grooves on the two halves of the cell. This concept proved to be correct and was incorporated into the final design of large cells.

A high temperature silicon rubber is incorporated at the outside of the mating surface to protect the composite from ambient conditions. This material was tested in a number of cell configurations prior to the present program.

A special test for this program was performed to determine that the silicon rubber could be used in the form of a small O-ring in the assembly of a composite matrix cell. A 35-hr test was performed while manipulating the flange-tightening sequences in a manner simulating actual cell operation. Figure 5-17 shows the results of this test. To separate the plates after cooldown, it was necessary to pry them apart. Although the rubber was torn, it remained in contact with the metal at all points on both surfaces. This indicated very good bonding characteristics which would ensure a good seal.

The silicon rubber in the design is shown outside the ceramic ring in Figure 5-16. However, use inside this ring and in direct contact with the matrix was shown to be feasible in later cell tests, and this principle was used in the large cell design. Figures 5-18 and 5-19 show the small cell in the original test stand configuration. Modifications of this configuration were made as the program evolved.

During the development period of the final composite electrolyte material, ten small cell tests were conducted. These tests served two useful purposes. First, the engineering, fabrication, assembly, and testing techniques were studied in anticipation of the final large cell work. Second, a method for quality control of the composite matrix material preparation and processing techniques were established through actual cell testing.

Although original work statements did not specifically call for these tests, they are now seen to have made a major contribution to the success of the program. Otherwise there would have been no adequate project control to ensure that unrelated events (the development of fabrication techniques to make various size matrices, and the engineering design of hardware) would be mated and matched at the conclusion of the program.

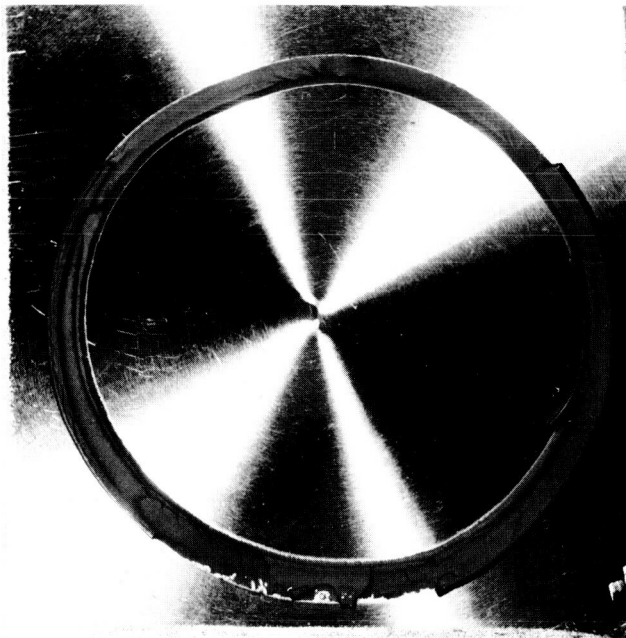
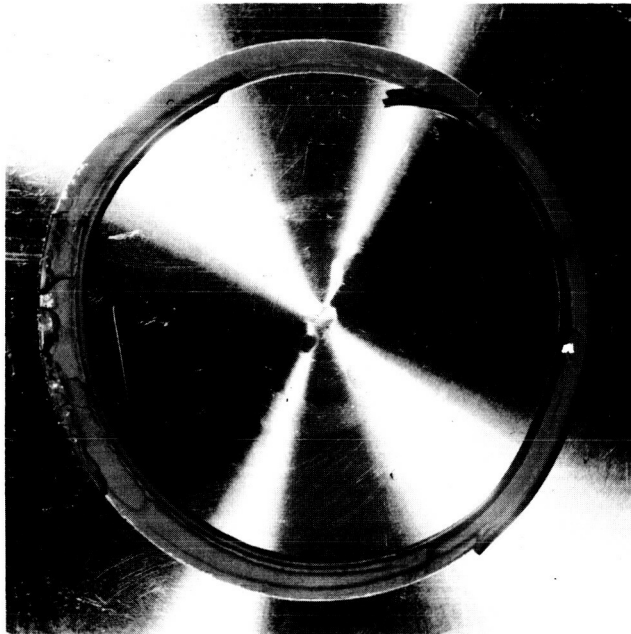


Figure 5-17. Results of test teardown on silicon rubber O-ring.



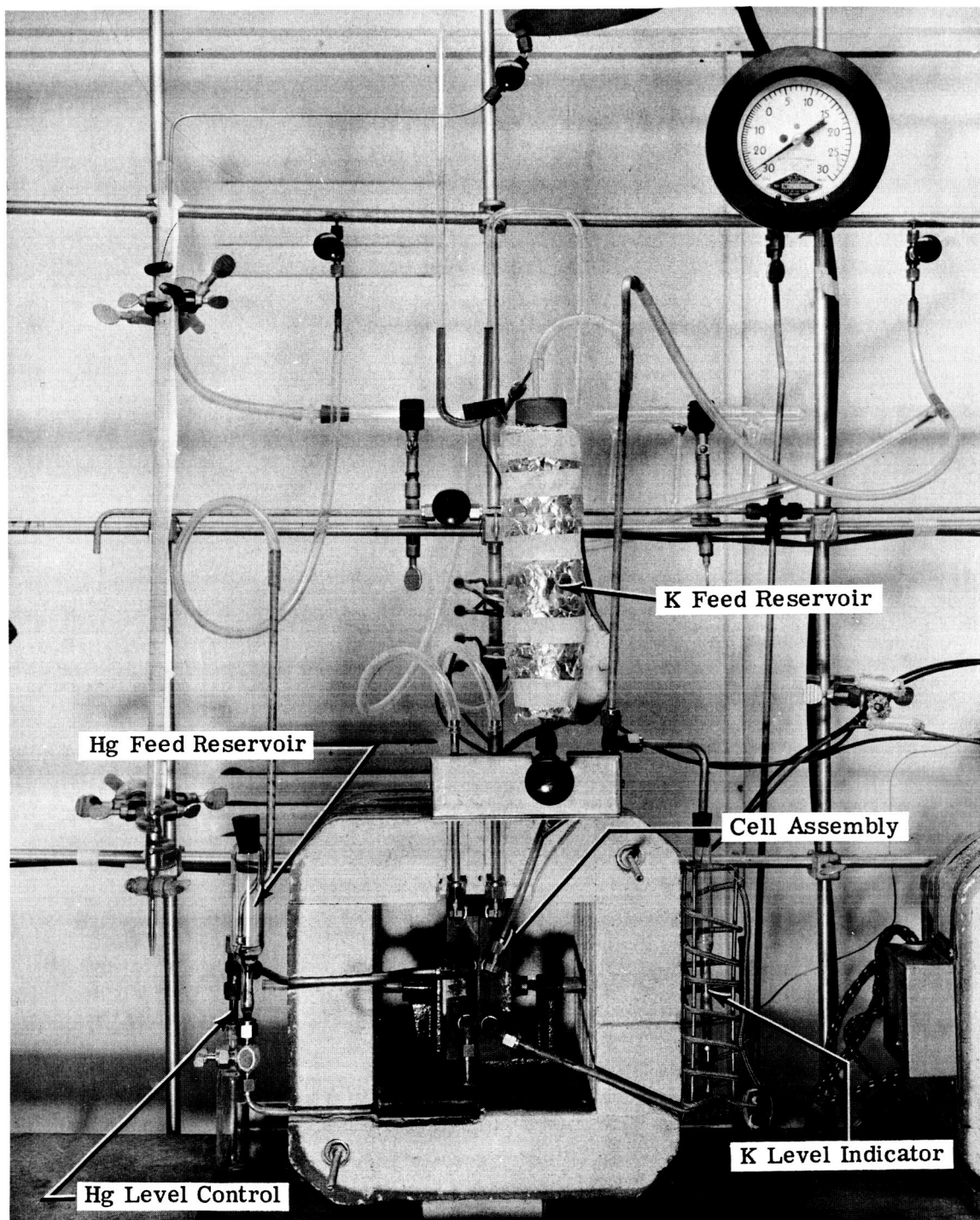


Figure 5-18. Small cell test setup.

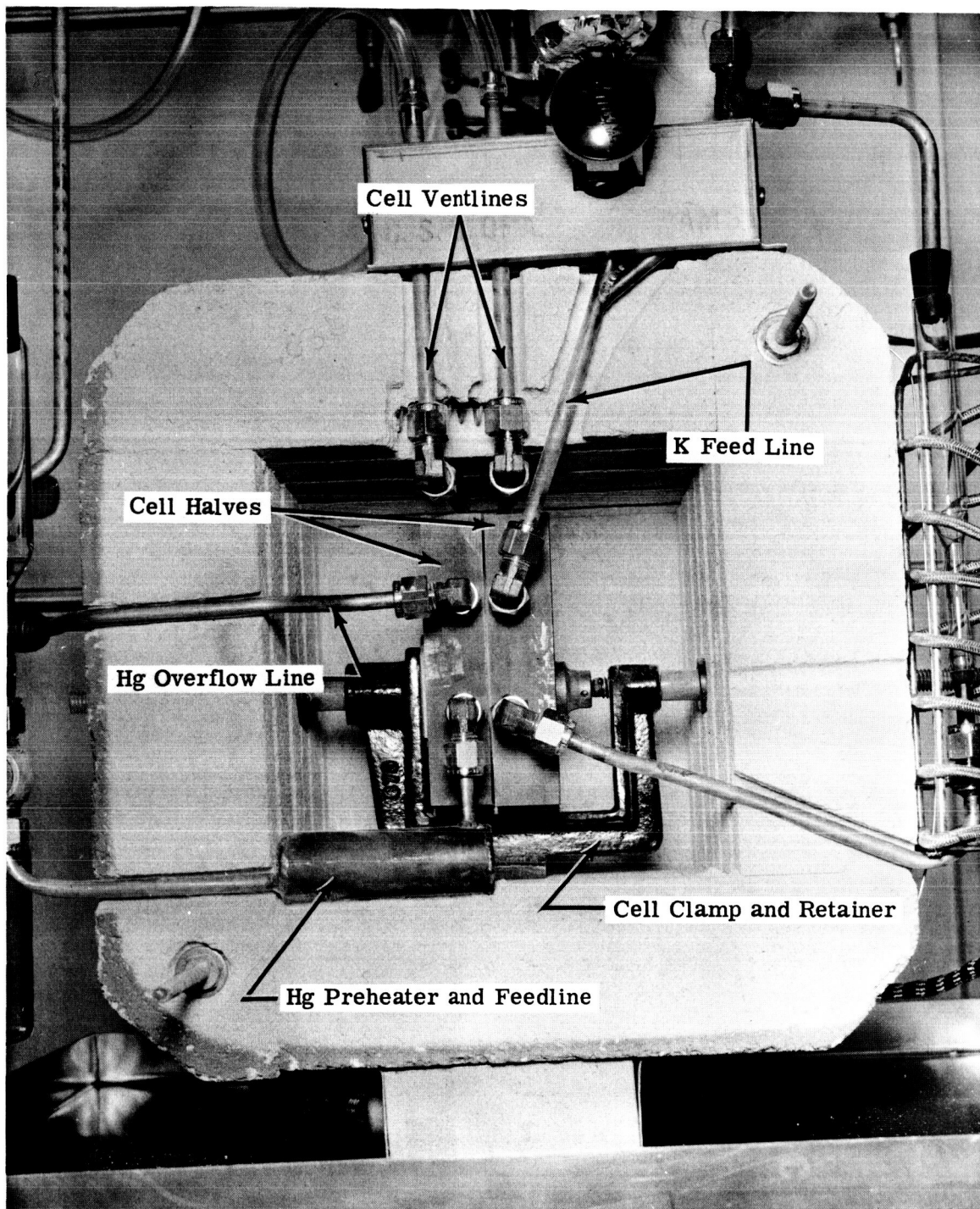


Figure 5-19. Small cell assembly.

The following paragraphs present a chronologic resume of the small testing program. All data have been compiled in Table 5-III.

Table 5-III.  
Data on composite electrolyte matrix cells.

Cell No., electrolyte percentage, and date	Time of day	Open circuit potential, $V_o$ (volts)	Operating potential, $V_o^*$ (volts)	Operating voltage, $V_c$ (volts)	Load current, I (amperes)	Computed cell resistance, R (ohms) <sup>1</sup>	Resistivity, $\gamma$ (ohm-cm)
I	3:20 PM		1.05	0.63	0.67	0.627	9.9
33%	3:30		1.02	0.66	0.59	0.610	9.6
5-14-63	4:05		1.00	0.43	1.00	0.570	9.0
Type C	4:16		0.75	0.26	0.725	0.680	10.8
MgO	4:35		0.88	0.28	0.78	0.770	12.2
II	Seal failure—no performance						
55%, Type F MgO							
III	2:17 PM	0.97					
34%	2:19	1.23					
7-5-63	2:30	1.10					
Type C		(Unstable)					
MgO	2:33		0.80	0.32	0.12	4.0	--
	2:34	0.98					
		(Unstable)					
	2:36	(Heavy internal short)					
	3:16	0.25		(Load Hg)			
	3:17	0.80					
	3:18	0.97					
		(Dead short—no recovery)					
IV	1:33 PM			0.3	~0.08		
33%	1:34			0.5	~0.08		
7-24-63	1:37		0.82	0.735	0.09	1.05	--
Type C	1:40		0.97	0.85	~0.06	~2.00	--
MgO	1:48	1.00					
	1:58	1.02					
	1:59	0.10		(Sudden short)			
	2:04	0.00					
	2:07	(Load Hg)					
	2:08	~0.25					
	2:10	0.80					

Table 5-III. (Cont)

Cell No., electrolyte percentage, and date	Time of day	Open circuit potential, $V_o$ (volts)	Operating potential, $V_o^*$ (volts)	Operating voltage, $V_c$ (volts)	Load current, I (amperes)	Computed cell resistance, R (ohms) <sup>1</sup>	Resistivity, $\gamma$ (ohm-cm)
IV	2:12	--		0.80	0.25		
continued	2:13	0.20					
	2:14	0.12					
		(Charging 0.6 to 0.9 amp)					
	4:11	0.02		(Dead)			
V (Green) 8-9-63 Type F MgO	(No performance data)						
VI	8:55 AM	(Cell in vertical position)					
53%	9:15	0.24		(Hg into preheater)			
8-15-63	1:38 PM	0.24		(Start Hg fill)			
Type FF	1:50	0.26		(Finish Hg fill)			
MgO	2:06	1.00		(K-metal load)			
	2:07	1.20					
	2:10	1.28					
	2:12	1.22		(Unstable)			
	2:13	--		1.02	0.07		
	2:14	--		1.02	0.07		
	2:15	--		0.95	--		
	2:16	0.79		(Open circuit)			
	2:17	0.24					
	2:18	0.11					
	2:19	0.04					
	2:20	0.02					
	2:21	0.02					
		(Charging)					
	3:15	0.01					
VII	8:20 AM	0.39		(Hg loaded to preheater)			
53%	8:30	0.33					
8-28-63	8:55	0.10		(Hg filled to contact matrix)			
Type FF	9:03	0.08		(Hg full)			
MgO							

Table 5-III. (Cont)

Cell No., electrolyte percentage, and date	Time of day	Open circuit potential, $V_o$ (volts)	Operating potential, $V_o^*$ (volts)	Operating voltage, $V_c$ (volts)	Load current, I (amperes)	Computed cell resistance, R (ohms) <sup>1</sup>	Resistivity, $\gamma$ (ohm-cm)
VII	9:05	0.06		(K-loading started)			
continued	9:09	0.08					
	9:10	0.14		(K contact)			
	9:10	1.20		(Step rise)			
	9:10:24	1.34					
	9:10:36	0.14					
	9:11	--		0.16	0.80	(Charging)	
	9:15	--		0.05	0.80		
	9:15+	0.00					
VIII	9:02 AM	0.6		(Without LM)			
65%	9:44		0.49	~0	~0	High	
9-12-63	9:52	0.48		(Voltage recovery)			
Type FF		(Add Hg to preheat)					
MgO	10:30	0.35					
	10:40	0.29		(Hg filled)			
	1:02 PM	0.16					
		(Add 5 grams K-metal)					
	1:09	1.20					
	1:10	1.30					
	1:13	1.34					
	1:15	1.35					
	1:32	1.35					
	1:35	1.34		(Slightly unstable)			
	1:53	1.23		(Unstable)			
		(Electrical load)					
	1:56		1.11	1.02	0.60	0.15	3.0
	1:59	1.15					
	2:05	--		0.90	0.90	--	--
	2:09		0.87	0.72	0.75	0.20	4.0
	3:31	0.87					
		(Charging)					
	3:44		1.05	1.13	0.48	0.167	3.34
	3:49	--		--	0.45	--	--
	3:57		0.74	0.68	0.37	0.162	3.24

Table 5-III. (Cont)

Cell No., electrolyte percentage, and date	Time of day	Open circuit potential $V_o$ (volts)	Operating potential, $V_o^*$ (volts)	Operating voltage, $V_c$ (volts)	Load current, I (amperes)	Completed cell resistance R (ohms) <sup>1</sup>	Resistivity $\gamma$ (ohm-cm)
VIII continued	4:17	0.80 (Charging)					
	4:40	0.935					
	6:00	0.83					
	7:00	0.83					
	8:00	0.81					
	9:00	0.78					
	10:00	0.72					
	10:30	0.69					
	11:00	0.40					
	11:30	0.09					
	12:00	0.07					
9-13-63	1:00 AM	0.16					
	2:00	0.17		(Lost recording marker)			
IX	7:30 AM					14 (measured)	
65%	10:20	0.036		(Hg added to preheater)			
9-27-63	10:52	0.060		(Hg contact with matrix)			
Type FF	11:02	0.060		(Hg full)			
MgO	11:30	--		(Amalgam loader hookup)			
	12:50 PM	0.090		(Heat up amalgam)			
	1:38	0.085		(Amalgam loading)			
	1:38	0.60		(Step rise)			
	1:38:12	0.80					
	1:38:24	0.835					
	1:39	0.87					
	1:40	0.89					
	1:41	0.91					
	1:42	0.92					
	1:44	0.935					
			(Electrically loaded)				
	1:45		0.76	0.53	0.43	0.535	10.7
	2:00	1.00					
	2:26	--		0.53	0.64		
	2:32	--		0.52	0.625		
	2:37		0.80	0.515	0.62	0.46	9.2

Table 5-III. (Cont)

Cell No., electrolyte percentage, and date	Time of day	Open circuit potential, $V_o$ (volts)	Operating potential, $V_o^*$ (volts)	Operating voltage, $V_c$ (volts)	Load current, I (amperes)	Computed cell resistance, R (ohms) <sup>1</sup>	Resistivity, $\gamma$ (ohm-cm)
IX	2:44	(Start charge-discharge cycle equipment)					
continued	3:46		0.70	0.52	0.60	0.30	6.0
	4:35		0.80	0.71	0.30	0.30	6.0
	5:20		0.83	0.97	0.50	0.28	5.6
	Cycle No. 1	0.750		0.97 (Charge)			
				0.515 (Discharge)			
	10	0.690		0.91			
				0.48			
	20	0.650		0.86			
				0.445			
	30	0.600		0.81			
				0.405			
	34	0.575		0.79 (internal load)			
				0.36			
	40	0.490		0.74			
				0.325			
	45	≈ 0.3		0.56			
				0.225			
	50	≈ 0.3		0.47			
				0.18			
	51	≈ 0.25		0.45			
9-28-63	11:34 AM			0.21	0.20		
		(Start charging)			0.62		
	11:49			0.43			
	12:04 PM			0.52			
	12:34			0.59			
	12:49			0.66			
	12:49+			0.62			
	1:04			0.50			
	1:32			0.43			
	2:02			0.415			
	2:17			0.23	0.20	(Charge rate change)	
	9:55			0.08	0.20		
				(End run)			

Table 5-III. (Cont)

Cell No., electrolyte percentage, and date	Time of day	Open circuit potential, $V_o$ (volts)	Operating potential, $V_o^*$ (volts)	Operating voltage, $V_c$ (volts)	Load current, I (amperes)	Computed cell resistance R (ohms) <sup>1</sup>	Resistivity, $\gamma$ (ohm-cm)
X	8:47 AM	0.076					
65%	9:18	0.105					
10-10-63	11:12	0.037			(Rotate into vertical position)		
Type FF	11:20	0.037			(Hg added to preheater)		
MgO	11:50	0.00			(Hg contact with matrix)		
	1:15 PM	0.30			(Charge current momentarily)		
	1:18	0.25					
	1:21	0.20					
	1:24	0.16					
	1:30	0.00			(Attach amalgam loader)		
	1:42	0.09			(Voltage recovery)		
	1:50	0.30			(Charge current momentarily)		
	2:35	0.36			(Amalgam loading)		
	2:35+	0.80					
	2:38	0.94					
	2:41	0.97					
	2:47	0.99					
	2:48	--		0.56	> 0.60	(Electrical load)	
	2:55		0.69	0.54	0.62	0.242	4.84
	2:56	0.835					
	3:00	(Charge-discharge)			0.62	(Discharge)	
	3:10		Cycle		0.40	(Charge)	
Cycle No. 1		0.815		1.00	(Charge max)		
				0.53	(Discharge min)		
	5	0.795		0.995			
			0.68	0.485	0.65	0.30	6.0
	10	0.760		0.96			
				0.57			
	15	0.745		0.93			
				0.58			
	20	0.735		0.915			
				0.58			
	25	0.730		0.905			
				0.575			
	30	0.715		0.89			
				0.57			



Table 5-III. (Cont)

Cell No., electrolyte percentage, and date	Time of day	Open circuit potential, $V_o$ (volts)	Operating potential, $V_o^*$ (volts)	Operating voltage, $V_c$ (volts)	Load current, I (amperes)	Computed cell resistance, R (ohms) <sup>1</sup>	Resistivity, $\gamma$ (ohm-cm)
Cycle No. 35		0.710		0.88			
				0.565			
	40	0.700		0.870			
				0.560			
11:13	45	0.695		0.865			
				0.150	(Shorting during cycle)		
	46	0.130		0.25			
				~0.0			

<sup>1</sup>Cell resistance is computed from an instantaneous cell potential to eliminate the effect of electrode concentration gradients. This technique is described in Figure 5-29 of this report, and is given as

$$R_c = \frac{V_o^* - V_c}{I}$$

The first test on cell I was made of a type C MgO 33% electrolyte composite of 86.2% density. Cell I gave useful electrochemical data. The primary purpose of the test was to show sealing characteristics of the composite and feasibility of the direct electrolyte-to-metal contact at the seal region. Results of the test were positive. Some concern had been shown for the electronic conduction of the electrolyte. For this cell the effect of electronic conductance was exaggerated by the use of a contact area three times that of the active cell area. The performance showed that the electronic resistivity of the electrolyte matrix must be considerably greater than the ionic resistivity since no apparent leakage current bypassed the active cell through the seal regions.

Data on this first cell test show that the seal lasted for 3 hr. Potassium was held for a period of 46 min before mercury was introduced. The cell then operated at above 1 volt, open circuit, until an intermittent internal short caused instability in the voltage trace. This instability was not severe at first but became progressively more disturbing until the cell was shut down. Near the end of the testing period, the change in the open circuit voltage approached half of the total value. Since an internal short has the same effect as an external load (except that the current cannot be measured), some insight into its nature can be determined. Half-load on a cell is accomplished by a load resistance equal to that of the cell internal resistance, by definition. Therefore, this cell was making and breaking very fine liquid metal paths having a resistance of 1 ohm or less.

Figure 5-20 shows a photo of the cell after the matrix was removed. Sections in the seal region broke away in pieces from the center region during posttest disassembly. Investigation showed that the center region had cracked in the plane of the disk. This can be seen on the center section in Figure 5-20. A general breakdown, extending into the seal region of the material, was evident. Pieces of the seal region are shown in Figure 5-21. A crack extends from the center out to the second serration mark. This is also the distance to which potassium had deposited onto the metal. This showed that the potassium did not progress in a flooding manner from one serration to the next in a radial direction, but moved through the fine cracks, spilling into the serration grooves and spreading around the circumference. These photos also show that the full 0.015-in. bite of the serrations into the composite was not accomplished. Now it is known that the composite material and silicon rubber support the clamping load. Therefore, a special silicon rubber O-ring was fabricated for later designs.

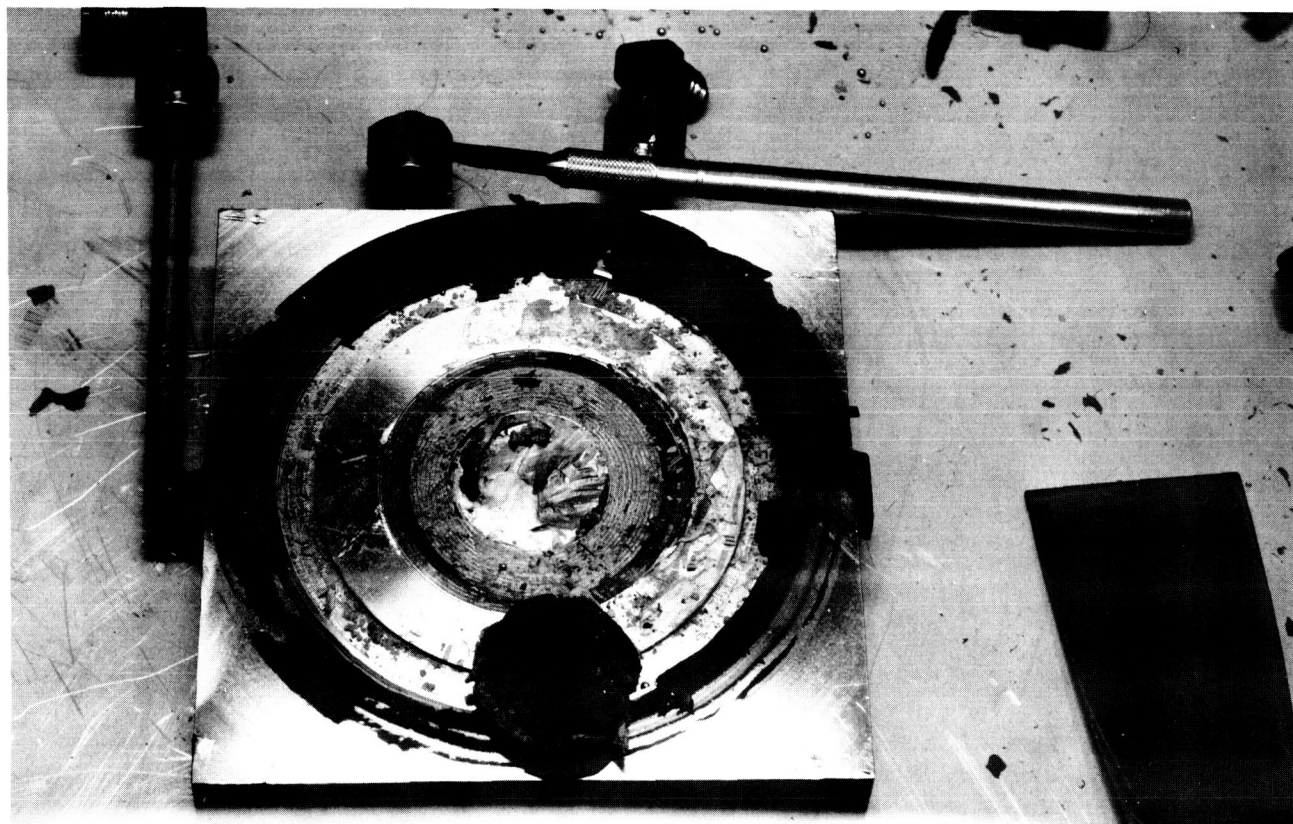


Figure 5-20. Cell after matrix removal.

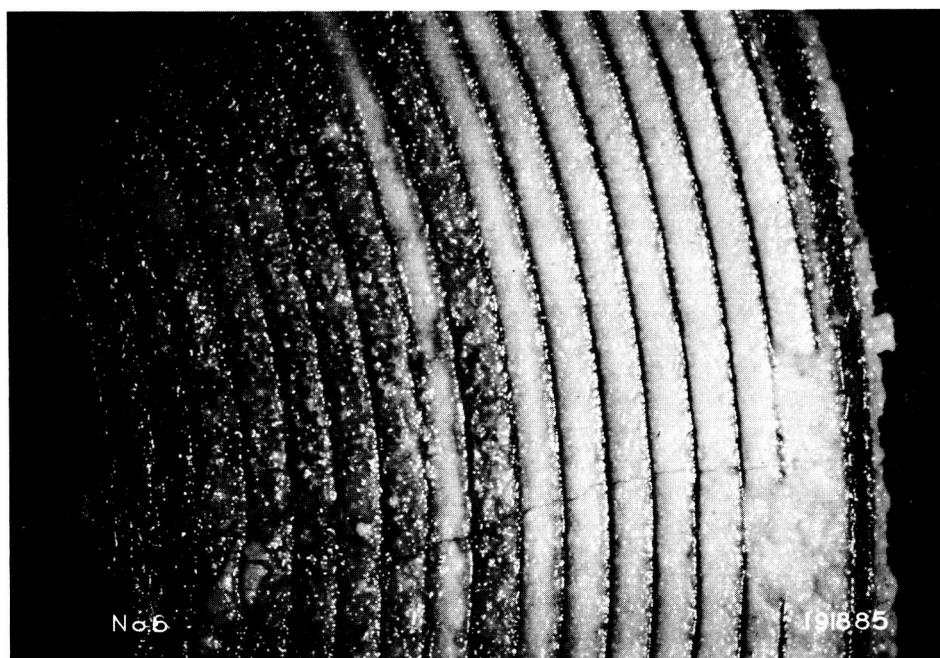
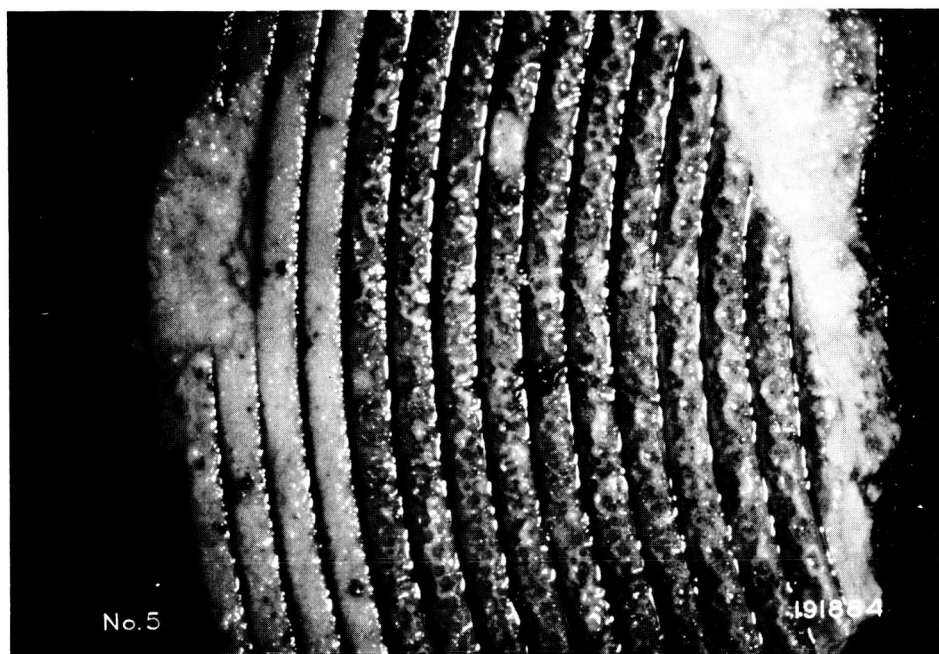


Figure 5-21. Sections of matrix from the seal region.

The second test, cell II, used an early prepared type F MgO 55% electrolyte composite. A cell potential was not attained at loading. Posttest analysis of the cell showed that the cell was not completely closed. The extra heavy silicon rubber used in this cell apparently kept it from closing on one side. Lack of a seal by the concentric serrations is evident in Figure 5-22 when compared to those in Figure 5-21. Later work showed that this material was quite hard at cell operating temperature and, therefore, would not be ideal for a seal.

Cell III was assembled with a nominal 34% electrolyte type C MgO composite matrix. The material had been estimated to be near an optimum strength value between 33 and 35%. However, the analyzed value was found to be near 35% and the strength tested out to correspond with that for 35% electrolyte composites.

Compatibility studies showed that the K-metal should be saturated with electrolyte; therefore, this cell had preloaded electrolyte. The voltage potential between the K-metal and the Hg vapor deposit from the preheater attained 1.23 volts but showed an unstable shorting from the start. An electrical load check proved the potential to be caused by a high resistance cell, greater than 4 ohms. Internal shorting eventually reduced the potential to near zero.

The test was continued by adding Hg to the cathode side. A low resistance potassium-mercury cell was formed, momentarily, with a potential of 0.97 volt. However, a dead short reduced this value to zero with a rise in temperature caused from direct reaction between the anode and cathode metals.

Posttest analysis showed that the seal region of the composite held up without leakage. The cause of failure was attributed to the rupture of the weak matrix which indicated need for a mechanical support in future testing. A rerun of the test using a nominal 33% electrolyte composite became cell IV.

Cell IV was operated to test a newly prepared composite from the type C MgO. The material was prepared by new techniques to minimize moisture. Analysis showed the electrolyte content to be near 33% and the percent of theoretical density to be 82%. This test also was accomplished without the use of mechanical support for the matrix since the strength of the material had been shown to resist deformation within cell I.

The test was started by the addition of K-metal to the anode side while Hg was in the preheater below the cathode chamber. The initial potential voltage was recorded at 0.3 volt but was

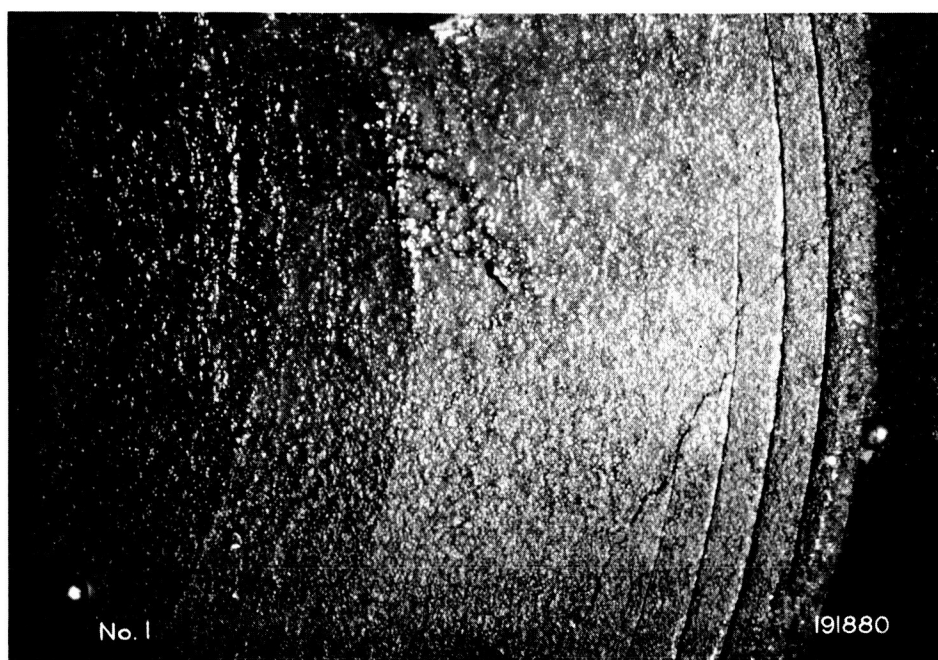


Figure 5-22. Sections of matrix from second cell seal region.

then discovered to be that of an electrically loaded cell with a current of approximately 80 ma. Instantaneous open circuit recovery to  $V_o^* = 0.82$  volt at 90 ma gave a cell resistance computed as 1.05 ohms. This was subsequently measured as 2.0 ohms and 1.4 ohms prior to shorting. The performance is indicative of a high resistance cell prior to filling with Hg on the cathode side. The early performance served as an indication of cell stability. In this case, however, a short circuit dropped the voltage to zero before the cathode chamber was completely filled with Hg.

The cell recovered with the introduction of Hg but was unstable. The open circuit potential reached 0.80 volt and 250-ma current was drawn momentarily. This cell appeared to develop an internal short circuit, which depressed the terminal voltage to nearly zero. Attempts to recharge the cell failed.

Cell testing of coarse MgO composites showed some degree of success to this point in the program. Posttest analysis showed that the concentric-serrated seal did function throughout the test. In general, the cause of failure was due to very fine cracks in the composite matrix.

Development of the fine grain MgO composites, reported in Section III, proceeded slowly. Work was hampered by the difficulty of producing sound, stress-free specimens. After one composite broke during cell assembly, a "green" specimen was used in an attempt to process the matrix within the cell housing prior to the loading of electrode metals. This configuration became cell V.

The "green" specimen was placed in cell V and care was taken not to close the cell halves before the composite baked out. During this part of the procedure, the cell was in the horizontal position. The cell was rotated to the vertical position on the following day in preparation for the test. The initial Hg loading indicated that the matrix was not sound. Further Hg filling showed that the cell chambers were electrically shorted (zero resistance). Also, Hg was detected in the anode side. Posttest analysis showed that the matrix had ripped apart at the cell opening and seal edge. This damage was caused by shrinkage of the middle of the matrix while the seal serrations held the outer perimeter material.

A new generation of fine grain composites was developed using a type FF MgO powder reported to be a high purity fused product. The grain size was measured to be from 0.04 to 0.10 micron

with the predominant sizes in the 0.07- to 0.09-micron range. The first cell to use this material was cell VI. This cell was assembled using a composite which was made up as nominal 56% electrolyte. Actual analysis showed this material to be approximately 53% electrolyte. The theoretical density was measured as 86.2%.

This cell was fabricated with a temporary stainless steel screen inserted on either side of the matrix. A change in cell operating procedure was also incorporated in the formation of this cell. Mercury was loaded into the cathode chamber through the preheater prior to K-metal loading. While in this condition, a slight potential was detected from a very high resistance cell. This potential, near 0.25 volt, was useful in indicating that the matrix was holding under a head of Hg from the cathode side. Otherwise, a zero potential from internal short would result.

Introduction of K-metal to the anode chamber caused the potential to rise to 1.28 volts; however, unstable performance began within 5 min. Electrical loading to gain specific performance values was limited by unstable operation, which dropped the open circuit voltage to zero within 10 min.

Subsequent attempts to recharge the cell proved that the cell was dead. Posttest analysis again showed that the composite possessed good strength and sealing characteristics, but very fine cracks allowed K-metal to penetrate to the cathode and short the cell.

Cell VII was assembled with another matrix prepared from the same material (type FF MgO), as that for cell VI. The theoretical density of this composite was 85.5%. The initial voltage after Hg loading was 0.39 volt but dropped off to 0.10 volt when the Hg made contact with the matrix. Although this early indicator voltage dropped, no unstable operation was apparent and K-metal was introduced into the anode.

The full cell potential of 1.34 volts was realized on this cell. This, however, occurred as a peak value for about 0.2 min and then shorted to 0.14 volt. Charging current failed to hold the cell and it was dead within 4 min. Failure analysis showed once again that fine cracks caused the electrical short through K-metal contact.

The next group of composites were made up with the type FF MgO material and also used the new vacuum-packed bake process. An effort to reduce cracks and/or repair them by a self-healing process led to the new highly saturated matrix. This specimen was prepared from a nominal 65% (analyzed as 64.8%) electrolyte composite and pressed to a high density (93%). Operation of this matrix was accomplished in cell VIII.

Prior to operating cell VIII, the cell hardware was modified. Permanent supporting stainless steel screens were used and the modification increased the cell area from  $5.1 \text{ cm}^2$  to  $6.4 \text{ cm}^2$ , thus reducing the seal area. The matrix was placed in the cell and heated to  $300^\circ\text{C}$  over a 6-hr period. The tightening sequence to close the cell and form the seal was performed over a 1-hr period.

The next morning a potential of 0.60 volt had developed across the cell halves. A check of the resistance by electrical loading proved this to be high resistance cell action. The addition of Hg to the preheater caused a reduction in this voltage.

Mercury was loaded into the cathode chamber to full capacity and allowed to set for 2.5 hr. The residual voltage (used as an indication of matrix condition) changed slowly during this time. Since 0.16 volt still remained at the end of this time, it was assumed that no shorting had occurred.

A change in procedure for K-metal loading called for loading to be accomplished in small increments over the day. The first 5 gm proved to be adequate. These 5 gm of K-metal gave a potential to the cell for over 12 hr. Only limited power operation was accomplished during this time.

The initial voltage was a typical 1.35 volts for K-Hg cells. Subsequent electrical testing gave resistance values in the range of 0.15 to 0.20 ohm. These values correspond to resistivity values of 3.0 to 4.0 ohm-cm for the matrix with an area of  $6.4 \text{ cm}^2$  and a thickness of 0.32 cm. These values are consistent with those predicted for this type of electrolyte matrix. Posttest analysis shows that there was a clear region near the bottom where the K-metal made contact and produced a cell. It appears that the limited K-metal present in the cell was sufficient to saturate the matrix and allow the full matrix area to act as an electrode. The sections shown in Figure 5-23 indicate that the K-metal completely saturated the cell area. It is also demonstrated how this saturation extends to some extent into the seal regions. The failure of the cell was found to be caused by cracks which filled with K-metal and shorted the cell.

A review of progress to this point indicated the need for increased effort in reducing and/or repairing cracks in the composite matrix. It was not determined when in the process these cracks occurred; nevertheless, it was determined that high internal stresses are set up in the specimen during thermal cycling of the bake and cooldown procedures. Subsequent heat-up within the cell may cause damage if the cell is not heated slowly. Also, sudden chilling by the intro-



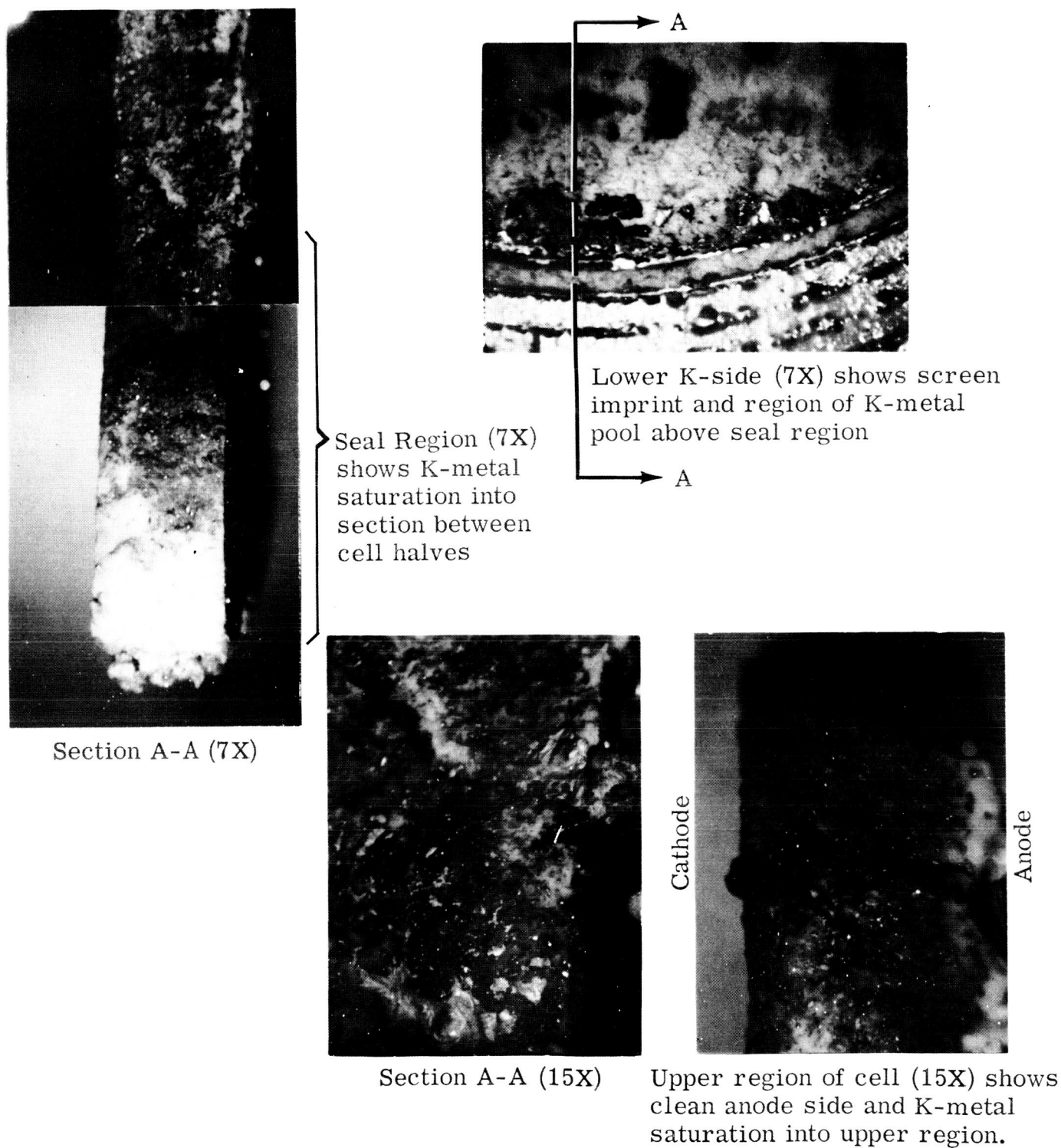


Figure 5-23. Cross section of electrolyte matrix showing failure due to K-metal penetration.

duction of liquid metal could cause failures. It was possible that the high activity of the pure potassium was too severe a condition to impose upon the nonsaturated molten salt which binds the composite through capillary forces. In consideration of these concepts, a new program emphasizing cell testing techniques followed.

The next two small cells tested were cells IX and X. Each matrix was fabricated from a 65% electrolyte composite type FF MgO using a final sift through a 200-mesh screen prior to cold press forming. X-ray examination did not reveal any flaws or suspected flaws. A change in procedure and conditions was incorporated to minimize the severity of the test on the primary specimen, the cell matrix.

Previous tests used a pure K-metal introduced to the cell above the melt point, probably 100-150°C. Two possible problems existed. First, the procedure might give a cooling depression to the matrix as the K-metal enters. Second, use of the highly active K-metal might cause a weakening of the matrix through mutual solubility between the potassium and the electrolyte. Therefore, the anode material was changed to a potassium amalgam. The new configuration approaches the conditions of the regenerative systems. Studies of the regenerative systems indicate the necessity of a low potassium amalgam in the anode of the cell.

The choice of a 32 mole percent potassium, 68 mole percent mercury amalgam was made to gain the highest melt point on the liquid-solid phase diagram. The melt point (approximately 280°C) of the selected amalgam is near the cell operating temperature and serves to automatically release the anode material to the cell at the proper condition. The high melt point also simplifies the amalgam loader design, since a valve is not required to control introduction of the metal. The cell design includes the permanent stainless steel screens used in cell VIII.

The first amalgam cell, cell IX, was assembled with a 94.2% theoretical density, 65% electrolyte content type FF MgO matrix. Data from this operation are shown in Table 5-III.

The matrix withstood the Hg head for 35 hr without apparent leakage. The first 2 hr and 45 min were prior to amalgam loading. Actual electrical performance was maintained for 32 hr and 17 min. Charge-discharge cycling was maintained for nearly 18 hr. The resistivity of the cell was computed as near 6 ohm-cm, which was higher than anticipated. Cycling data are given in Table 5-III as the maximum voltage on charge just prior to open circuit switching, and the minimum voltage on discharge just prior to open circuit switching. No continuous current recording was made; therefore, only spot-check current readings are available. The original setting of current remains fairly constant, however.

Cell IX developed a low-resistance path on the 34th cycle and dropped in performance. After 51 cycles, a continuous charge current was applied in an attempt to restore the potential. The cell terminal voltage did rise from 0.43 to 0.62 volt before the internal short circuit predominated and the voltage dropped to nearly zero.

One undesirable feature of the assembly was that of the Hg overflow. Early performance of the cell caused amalgam to be dumped away from the cathode side where it could not be recovered for recharge operation. This same opening also caused a distillation action of the Hg and, therefore, depleted the cathode material. There was no absolute measure of the effect this had on the life of the cell. This condition was corrected by placing a valve in the overflow line prior to operation of cell X.

Cell X was assembled with a matrix of 93.1% theoretical density and 65% electrolyte content. Data from this test are shown in Table 5-III. This cell performed much like cell IX, except for period of operation.

A problem with assembly caused the cell halves to close unevenly. The gap at the top of the cell was slightly larger than the gap at the bottom. This did not appear to hinder cell operation, since the Hg head was maintained for 2 hr and 45 min prior to amalgam loading. Posttest analysis (see Figure 5-24) revealed only a possible failure of the seal in the top region. Serration marks are not evident in this region on the anode side.

A study of Table 5-III shows that the cell performed for 8 hr and 40 min before a sudden internal short dropped the potential to zero. The resistivity was again near 6 ohm-cm with one reading close to 5 ohm-cm.

## COMPATIBILITY STUDIES

Tests were carried out to determine the mechanical compatibility of composite matrices to potassium and mercury at the cell operating temperature (300°C). Compatibility tests were conducted in a large pyrex test tube, positioned in a furnace, and instrumented as shown in Figure 5-25. The composite was held by a wire harness and submerged into liquid potassium or mercury. The liquid is not shown, but the K-metal loader is shown on top with heaters in place. A thermocouple was used to measure the liquid metal temperature.

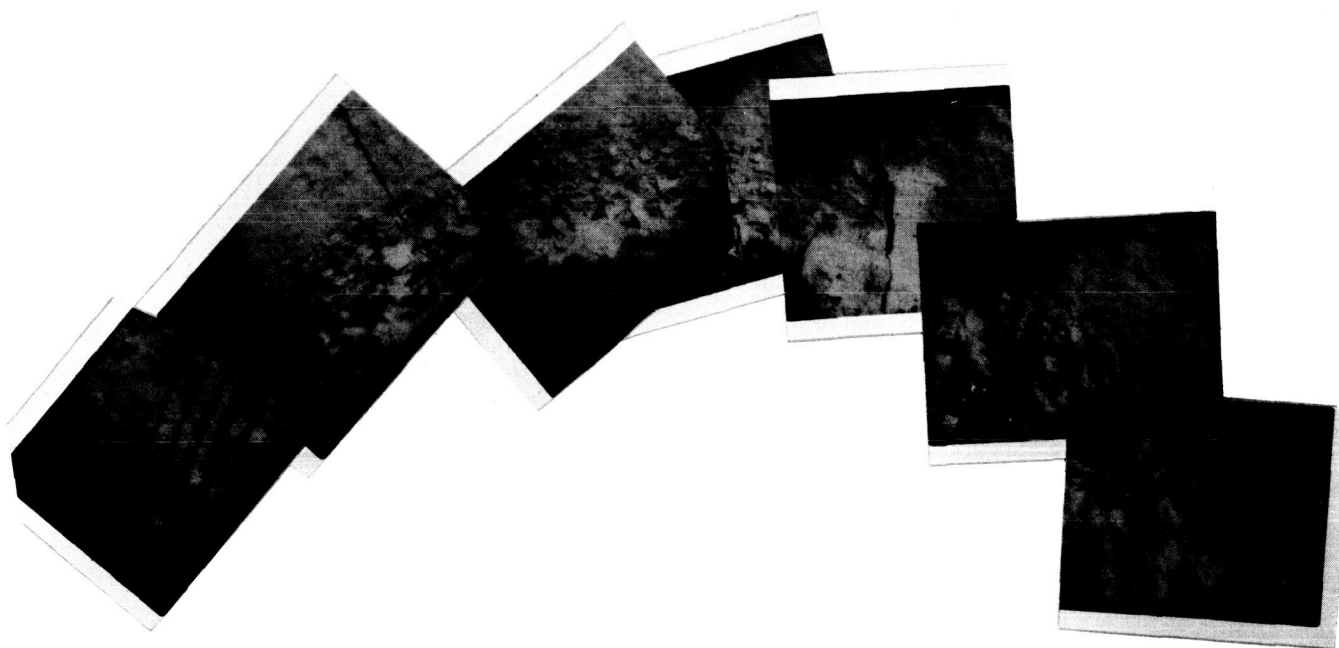


Figure 5-24. A series of photos showing serration marks near the top of the anode side, which indicate improper sealing. The fractures resulted from teardown stresses.

The first compatibility test was run using  $1 \times 1/8$ -in. specimens of 33% electrolyte composite. For this test, a specimen was submerged in mercury. The specimen was held below the surface for 24 hr at  $300^{\circ}\text{C}$ . Gassing from the specimen was observed early in the test run. Postrun analysis showed that no penetration of metal into the composite occurred. The composite also showed good strength characteristics—no deformation was observed. It was concluded that hot mercury, alone, will not destroy a composite.

The second compatibility test was performed to check the gassing observed from the first composite. This was done by breaking a 33% electrolyte composite, as received, under mineral oil. Microscopic examination showed that this specimen contained gas pockets. Gas was observed coming from various pockets and cracks as it was displaced by the mineral oil. Therefore, a new effort in the preparation of the composite was begun to eliminate cracks, large voids, and, in general, the nonhomogeneous mixture.

A third test was carried out to check the compatibility of the composite in pure potassium. This was done with 30 gm of K-metal at  $300^{\circ}\text{C}$  using 33% composite. This test only served to verify previous conclusions—the electrolyte is slightly soluble in the potassium metal. As a result of 24 hr operation, the composite was partially dissolved into the K-metal. The MgO particles and undissolved salts settled to the bottom.

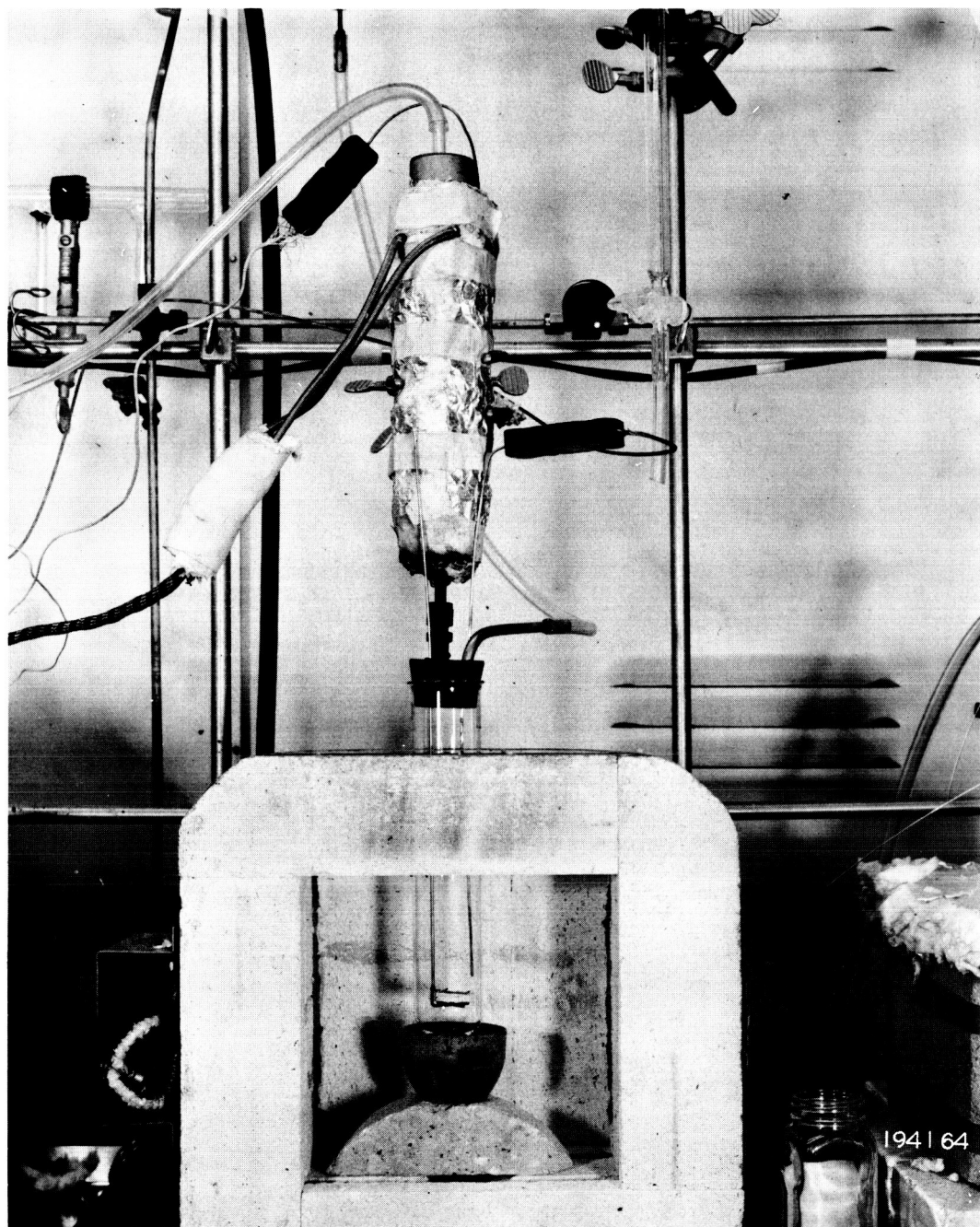


Figure 5-25. Test rig for compatibility studies.

Another test of this type, using a 50-50% molar K-Hg amalgam and a 35% electrolyte composite, was run for 42 min. This test was discontinued when the specimen disintegrated. It was shown by the next test that the 35% composite was highly saturated and fluid. The next test, incorporating a 35% electrolyte composite to be immersed in an electrolyte-saturated K-metal, was terminated prior to immersion in the liquid metal pool when the composite lost strength and fell from the wire harness. It was concluded that the 35% electrolyte composite, which had shown as high as 50% deformation under flowability test, did not have sufficient strength for this work without other support.

For the sixth test a newly-prepared 33% electrolyte composite measuring  $1 \times 1/8$  in. was used. Care was taken to exclude air from the composition. This specimen was carefully preheated in the region above the electrolyte-saturated K-metal prior to immersion. After a 24-hr test at  $300^{\circ}\text{C}$ , the composite was removed, cooled in an inert atmosphere, and placed in dry mineral oil. The results are shown in Figures 5-26 and 5-27. Probing of the surface to remove K-metal while under mineral oil revealed a large fissure of approximately 0.8-in. length. Some smaller grooves were also visible as seen in Figure 5-26, which shows the specimen after it was deliberately broken along the large crack. Figure 5-27 shows the edge view. Only about 10% of the material was serving as a strong bond between the two halves. Potassium completely penetrated the cracked surface. The darker regions were deposits of K-metal which arrived through the normal solubility of the liquid metal into the salts.

A seventh test was performed during this period. A  $1 \times 1/8$ -in. specimen was fabricated from the newly prepared 34% electrolyte composite. Since this material had been under considerable development, and since refinements had been made in the technique, it was anticipated to have different properties than the older batches of composites. Compatibility tests were performed after an X-ray check indicated no cracks to be present. The results of this test were encouraging. This specimen was tested in an electrolyte-saturated K-metal pool at  $300^{\circ}\text{C}$  for a period of 18 hr. From an outward appearance, no attack on the specimen had occurred. Figure 5-28 is a micrograph of a section that was broken for examination. The lower photo (7X) shows that the material had many holes. The upper photo (15X) shows the interconnection of two dark cavities near the center.

The compatibility studies were ended because properly prepared composites exhibited mechanical compatibility. It was shown that extensive development was necessary in the fabrication of the composites to eliminate gas pockets and cracks and, in general, to develop a homogeneous product.



Figure 5-26. Electrolyte matrix after test number 6—note cracks.

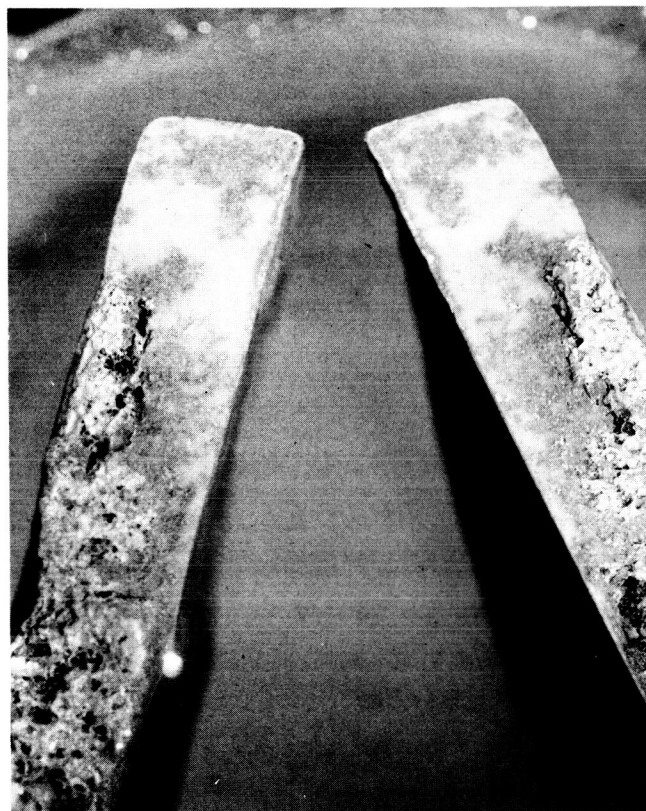


Figure 5-27. Broken edges of sixth test matrix—about 10% bonded through cracked area.



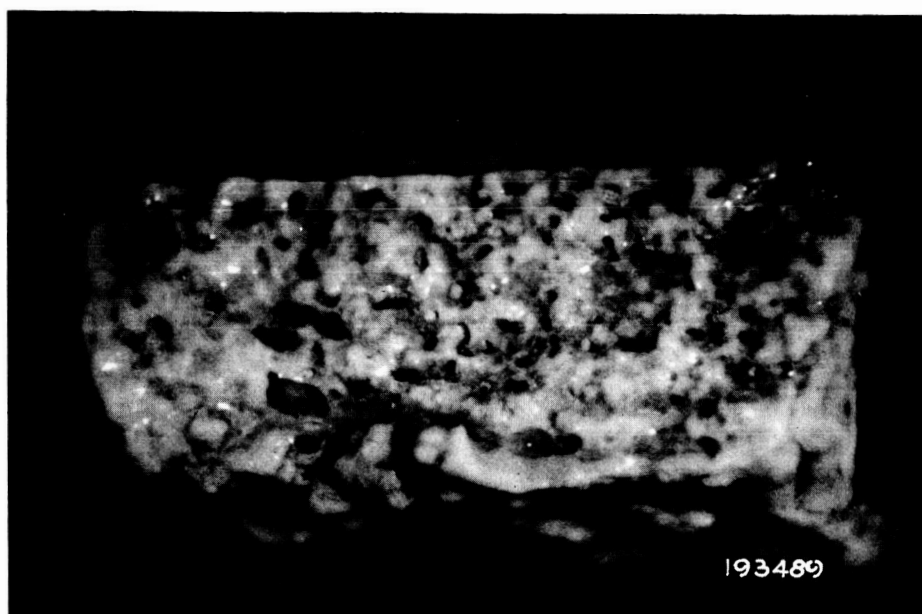
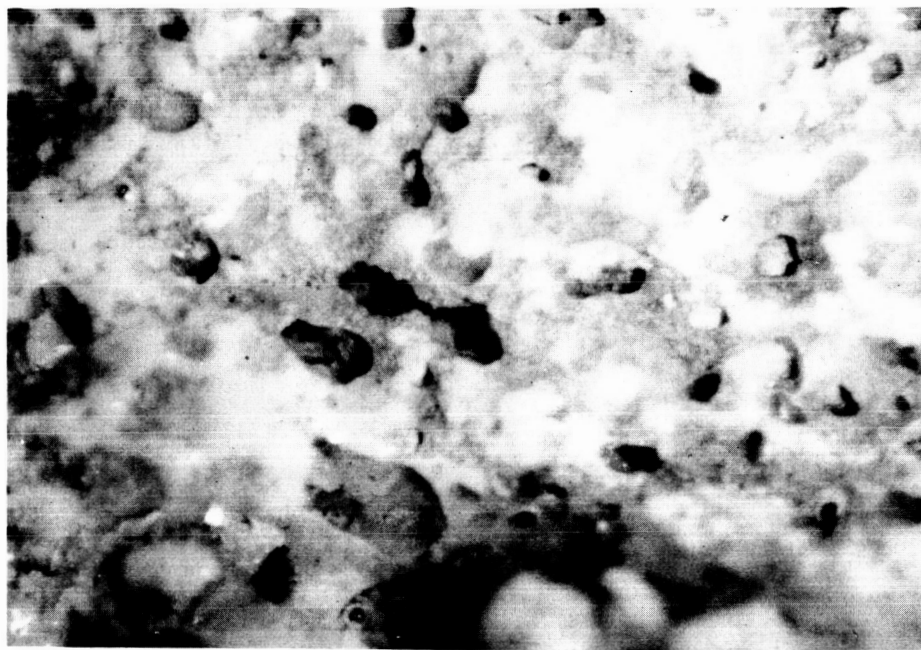


Figure 5-28. Cross section of matrix showing holes.



## SMALL DIFFERENTIAL DENSITY CELL RESISTIVITY STUDIES

Performance characteristics of potassium-mercury electrochemical devices are shown in Figure 5-29. The potential,  $V_0$  (bulk), is caused by the concentration levels of the liquid metal on each side of the electrolyte. The dashed line represents the ideal performance from no-load condition out to a short circuit current,  $I_{sc}$ . The internal resistance of this device is given by the first equation,  $R_c = V_0/I_{sc}$ . Actual data, however, will show a deviation from this condition due to a concentration gradient in either or both of the electrode pools. A cell resistance which is calculated from the difference between terminal voltage and the potential based on the true bulk concentration,  $V_0$  (bulk), will show an increase with higher current loads. If, on the other hand, care is taken to read the cell potential,  $V_0^*$ , at the instant of open circuit switching, the effect of flow dynamics of diffusion and ion exchange are eliminated. The internal resistances therefore remain constant (designated by the slope of dashed lines) and are not a function of current. The technique described and illustrated in Figure 5-29 is that used to obtain resistivity values for comparison with those obtained from a-c bridge conductivity measurements. It was found that this technique did not produce results which agreed with values obtained from conductivity work. Therefore, the following study ensued.

### Cell resistance

$$\text{Ideal } R_c = \frac{V_0}{I_{sc}}$$

$$\text{Data } R_c = \frac{V_0^* - V_c}{I} \neq f(I)$$

### Resistivity

$$\gamma = \frac{R_c A}{t}$$

$$\gamma = \frac{V_0^* - V_c}{I} \left( \frac{A}{t} \right) \quad \text{Constant geometry}$$

$$\text{or } \gamma = \frac{V_0^* - V_c}{t} \left( \frac{1}{I/A} \right) \quad \text{Specific performance}$$

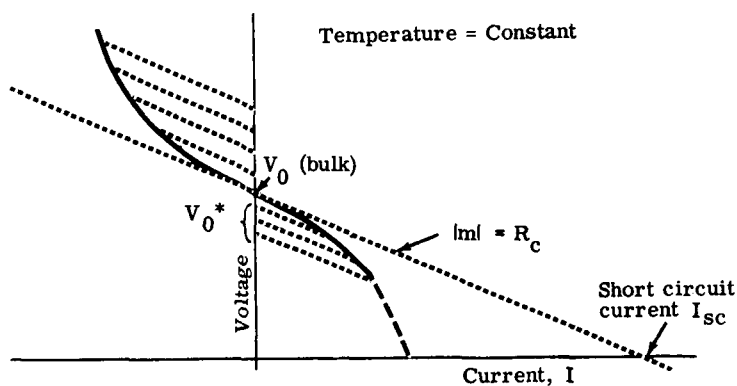


Figure 5-29. Liquid metal cell performance characteristics.

Consider the relationship

$$R_c A = \gamma_c t_e = \gamma_e t_e + \gamma'$$

where

$\gamma_c$  is the resistivity of the cell

$\gamma_e$  is the resistivity of the electrolyte

This equation states that the cell resistance area product is a function of the electrolyte resistance,  $\gamma_e t_e$ , plus a term,  $\gamma'$ , which is associated with the interfaces. Interfacial resistance ( $\gamma'$ ) would place a limit upon the development of the liquid metal cell. Studies were made using various thickness of electrolyte to check this linear equation.

Figure 5-30 is a schematic of the small cells used for this study. The first five cells did not incorporate separate voltage leads and therefore included lead resistance.

Figure 5-31 is a plot of the data from the eight cells which were tested. Cells 1, 2, 3, 4, and 5 show the effect of an extra resistance in the cell, not associated with the electrolyte. Cells 1A, 3A, and 4A were operated with voltage leads and, therefore, although data are not conclusive, indicate no interfacial resistance. However, the value of the electrolyte resistivity is seen to be greater than 2 ohm-cm.

During later studies, the conductivity of the pure electrolyte was measured to determine whether the slope given by these three cells was correct. The data from this study revealed that electrolytes containing traces of moisture, when placed in an alumina cup, increased in resistivity with time to  $\gamma > 2.0$

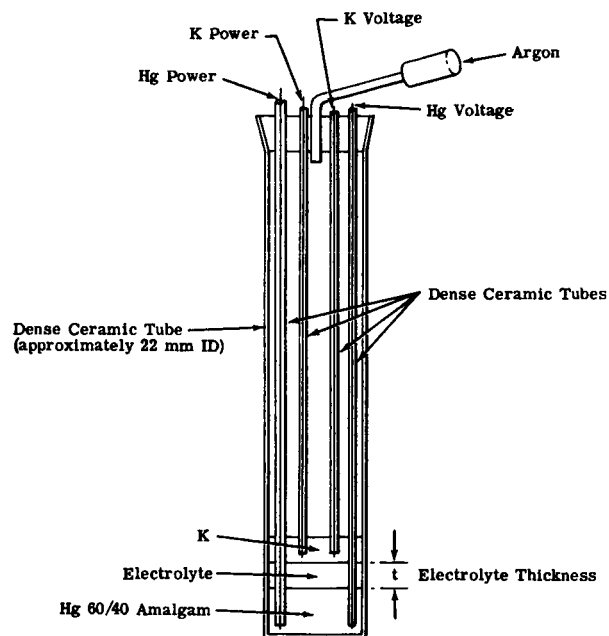


Figure 5-30. Schematic diagram of differential density cell used in resistivity studies.

ohm-cm. Tests performed with very carefully dried electrolyte showed a resistivity of  $\gamma = 1.35$  ohm-cm. Therefore, traces of moisture in the electrolyte used in cells 1A, 3A, and 4A may explain the higher resistivity results shown in Figure 5-31.

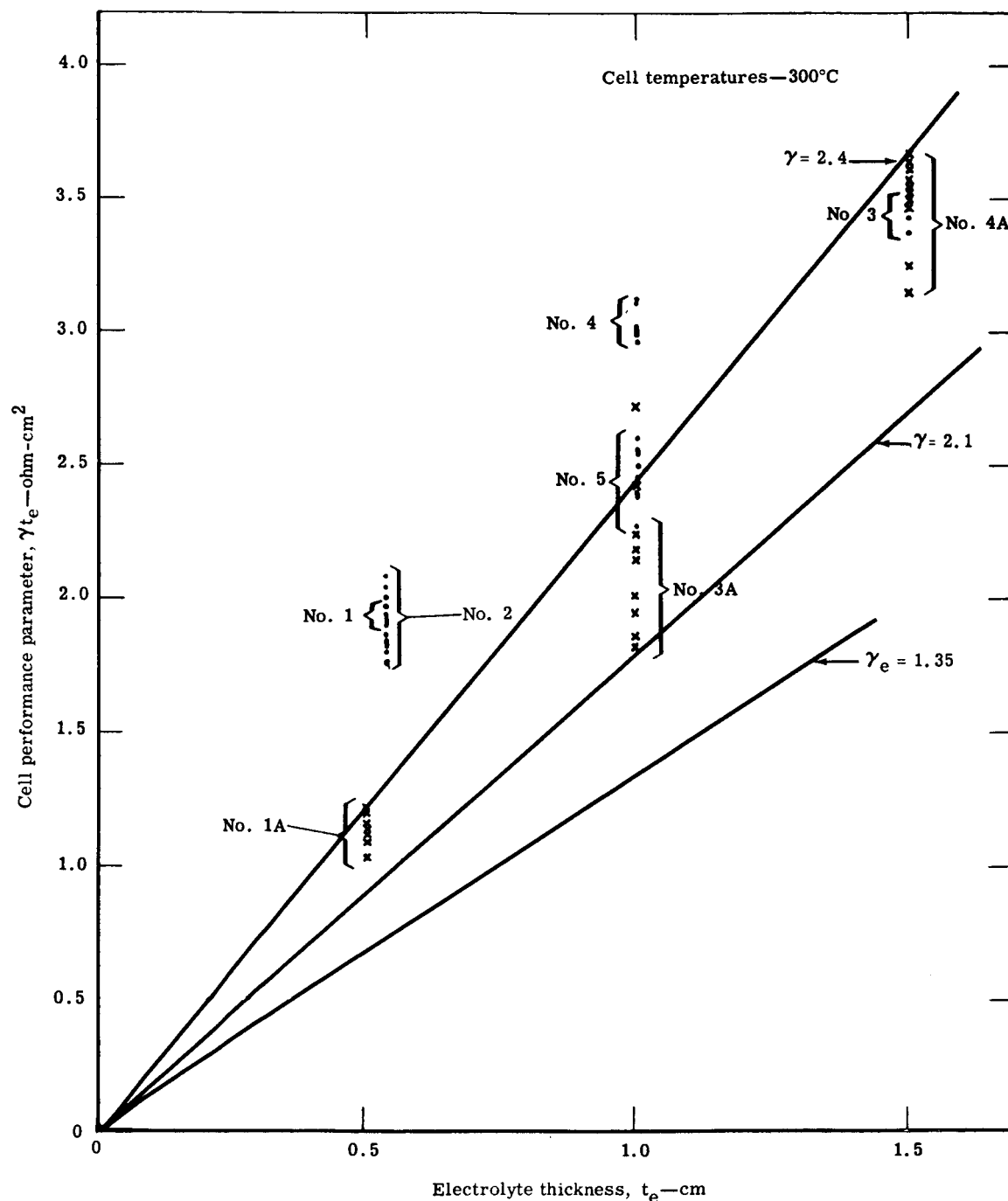


Figure 5-31. Plot of data obtained from cell resistivity studies for the pure electrolyte.

## VI. APPARATUS AND TECHNIQUES

### MECHANICAL TESTING

The strength of a paste or plastic material is difficult to measure. Yield strength is generally a function of time and, although useful as a limiting factor, is not used as a specific design parameter. The approach to strength measurement in this program makes use of relative or comparative strengths. In this technique, specimens may be compared on the basis of relative strength, but the ultimate test of strength for usability must be derived from final configuration testing. The following paragraphs describe the procedures, techniques, and apparatus used in preliminary strength analysis.

#### Ball Penetration Test

A test procedure for approximating material strength at cell temperature was established in which a steel ball was permitted to sink under a given weight into the flat face of a 1-in. diameter cylinder of the composite electrolyte. A relative strength was calculated from the resulting impression diameter. A fixture (see Figure 6-1) was built whereby several 1/2-in. diameter steel balls were stacked within a suspended steel tube and the cumulative weight was allowed to bear on a composite electrolyte specimen. This arrangement was heated in a furnace under argon. The stress imposed through the steel ball in contact with the specimen diminished as penetration occurred until a state of equilibrium existed, giving a value closely associated with the yield strength of the material.

The area of the impression made by the loaded steel ball in the composite electrolyte at temperature was used to calculate the effective strength. This test was in effect a hot indentation hardness test. The test specimens were 1 in. dia  $\times$  1/2 in. high or 1 in. dia  $\times$  1/8 in. high.

#### Flowability Test

Strength tests at operating temperatures were conducted using apparatus designed and built for compressive creep studies on this material. This equipment is shown in Figure 6-2. All tests on this material were conducted under an argon atmosphere to restrict material contamination, especially absorption of carbon dioxide. The 1-in. diameter specimens were cumulatively loaded and the deflection was observed on a dial indicator to establish the load level at which principal yielding of the material occurred.

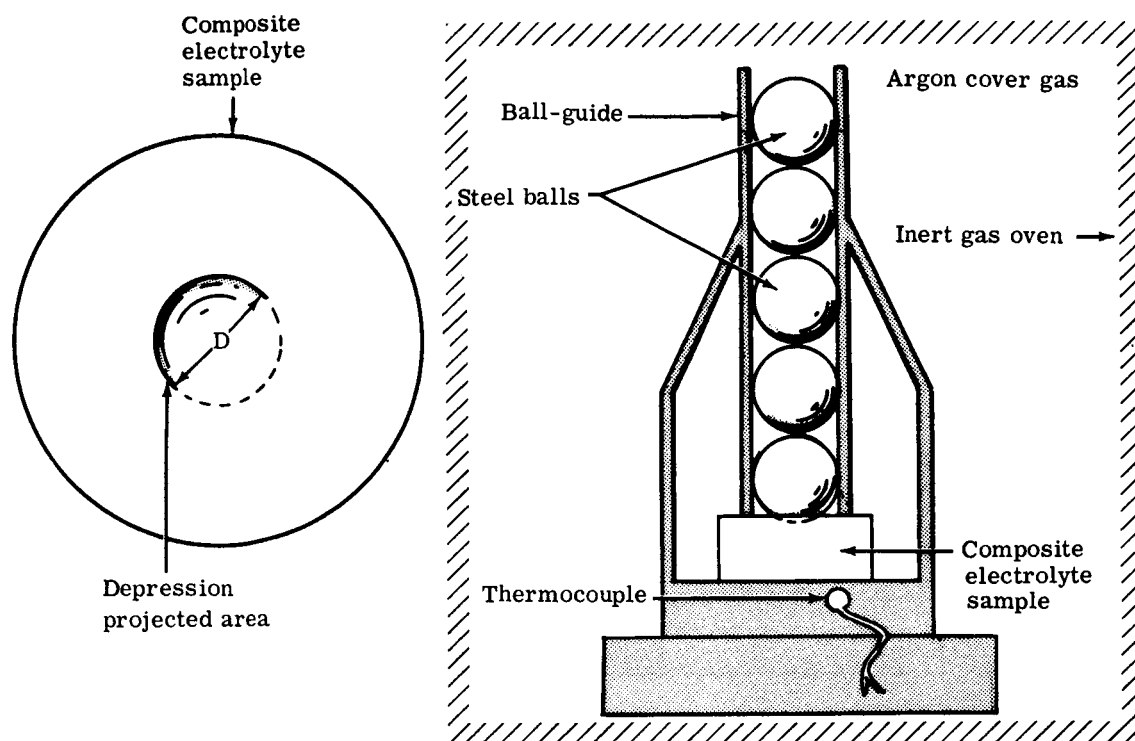


Figure 6-1. Compressive strength test apparatus.

Flowability testing was done on an adaptation of the low compressive creep machine. The composite electrolyte specimen, which was 1 in. dia  $\times$  1/2 in. high, was placed between two thin nickel sheets and compressed between two steel plates at temperature as shown in Figure 6-3. Movement of the upper plate was controlled by a screw mechanism outside the chamber and measured by a dial indicator as seen in Figure 6-2. The specimen was then deformed a certain percentage of its thickness and examined for evidence of cracking. Figure 6-4 shows a typical group of specimens after testing.

## ELECTRICAL TESTING

Electrical measurements were made to determine the electrolyte matrix resistance. In the case of the past composite, a quality control test was set up to measure conductivity by means of a-c bridges.

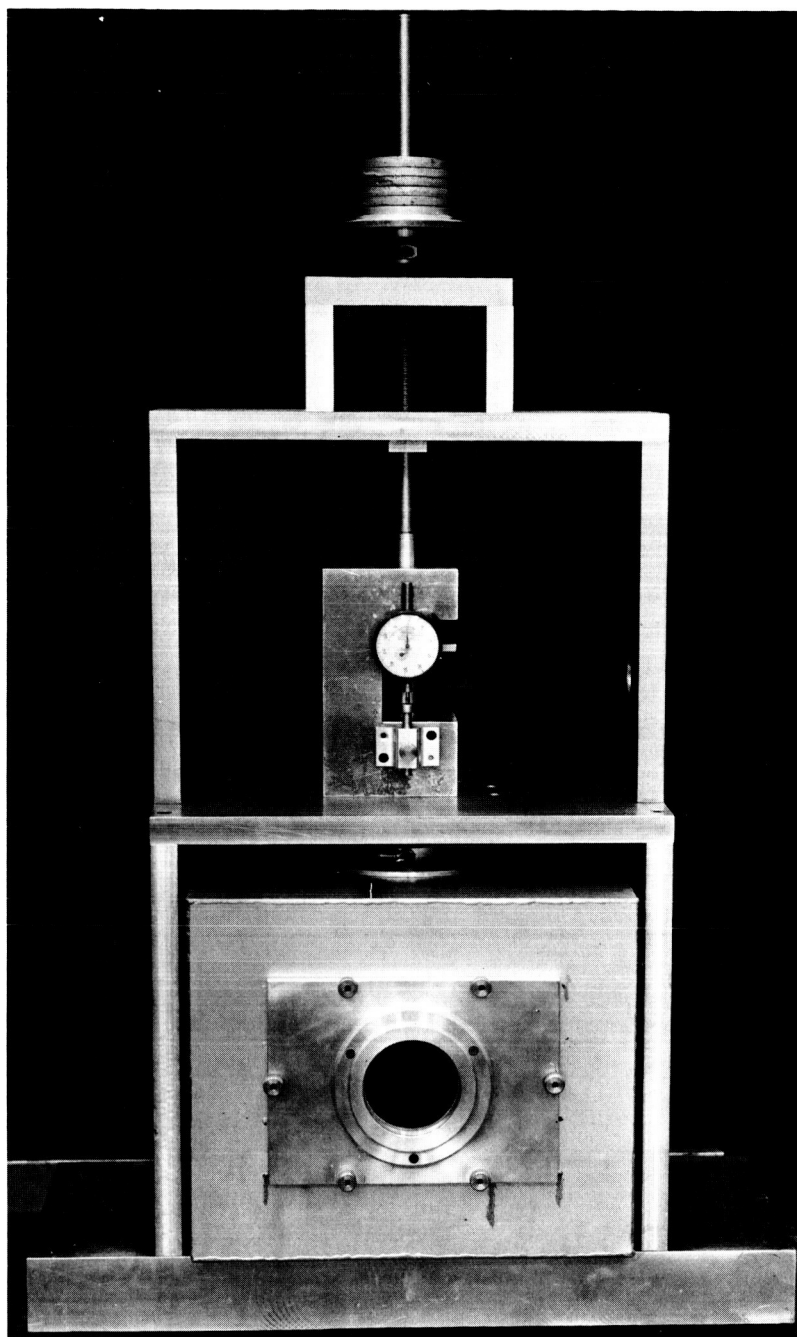


Figure 6-2. Low-stress compressive creep machine.

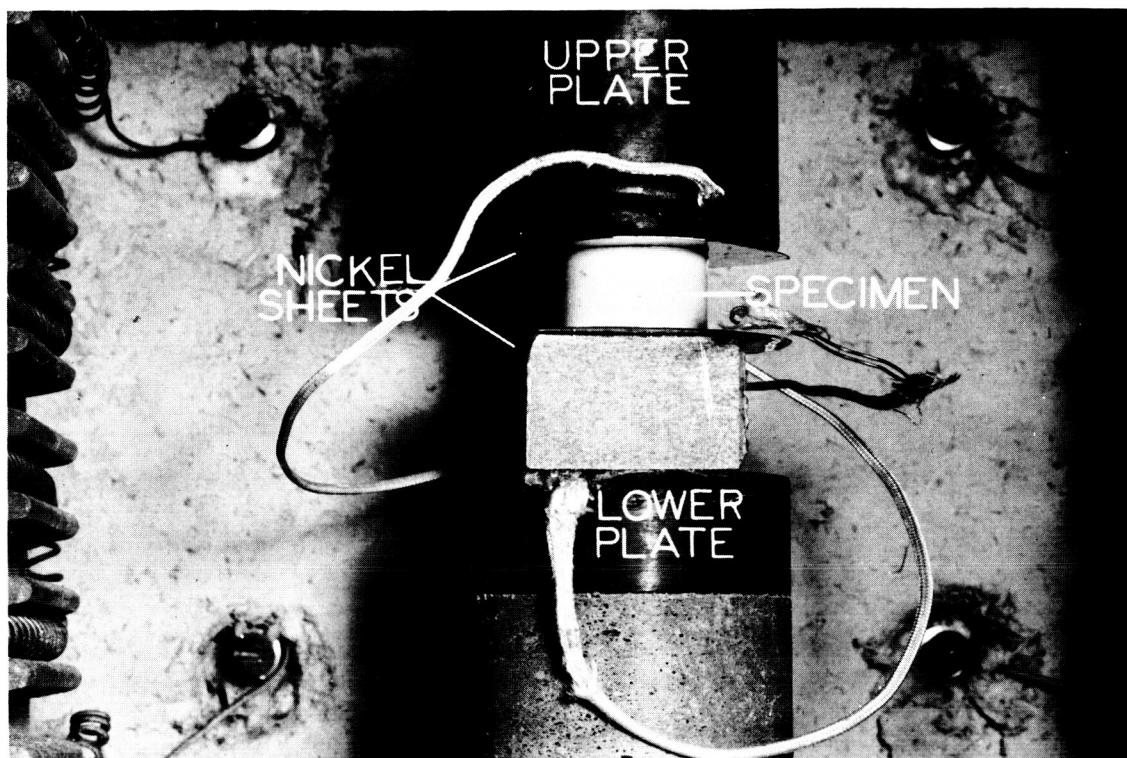


Figure 6-3. Flowability test apparatus.

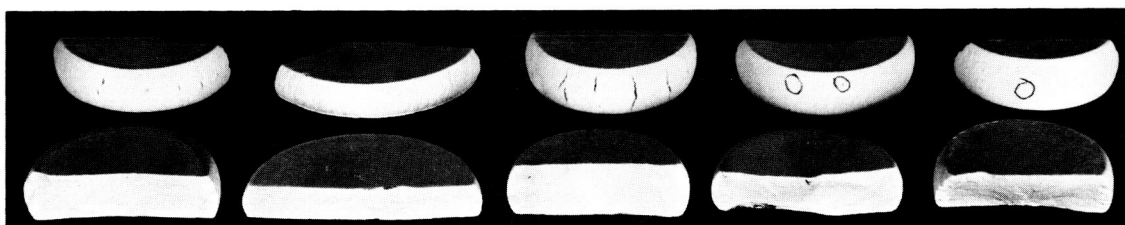


Figure 6-4. Flowability specimens after compression.

The conductance measurement of composites was obtained by observing the ohmic impedance of a conductance cell. The resistance measurement was made with an alternating current Wheatstone bridge operating at 10 kc. Polarization at the electrodes of the conductance cell was inversely proportional to the square root of the bridge frequency. Operating the bridge at 10 kc negates the polarization effect, allowing direct measurement of the true ohmic drop of the conductance cell. This ohmic drop includes lead and contact resistances as well as the desired electrolytic resistance.

The conductance cell for the unconsolidated electrolyte specimens is shown in Figure 6-5. The cylindrical specimen, which was 1.6 cm in diameter  $\times$  1.6 cm high, was compressed between two gold electrodes to a new height of 1.55 cm, determined by a ceramic ( $\text{Al}_2\text{O}_3$ ) bushing containing the specimen. The furnace was necessary because of the temperature requirement for an operational fused salt electrolyte. The conductance cell was continuously flooded with argon during the test.

The cell constant was calculated from the geometry of the conductance cell, and is  $K = \frac{L}{A}$

where

$L$  = compressed height of the specimen

$A$  = electrode contact area (identical electrodes assumed)

The specific conductance at a given temperature was obtained by dividing the cell constant by the electrolytic resistance.

For some time, measurements of conductivity of the fused salt electrolytes were performed with an a-c excited version of the Wheatstone bridge. In certain conductivity cells where the cell constant is low, and especially in the unconsolidated matrix (paste electrolyte) cells, the cell resistance may approach 1 ohm. Under these conditions, the resolution of the Wheatstone bridge is poor. Therefore, a design incorporating a modified Kelvin bridge is indicated.

The general schematic of the Kelvin bridge, modified for a-c use, is given in Figure 6-6. With this circuit, if the resistance of link S is kept low and  $P_1$  and  $r_1$  are kept approximately equal to  $P_2$  and  $r_2$ , then at balance:

$$R = \frac{P_1 Q}{r_1} \quad \text{and} \quad X = \frac{P_1 C}{r_1}$$



Figure 6-5. Electrolyte matrices conductivity apparatus.

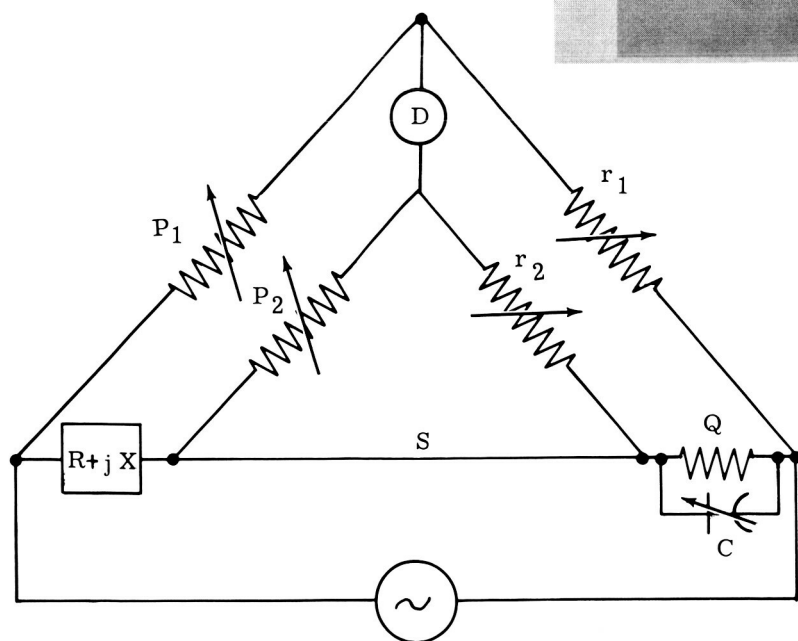
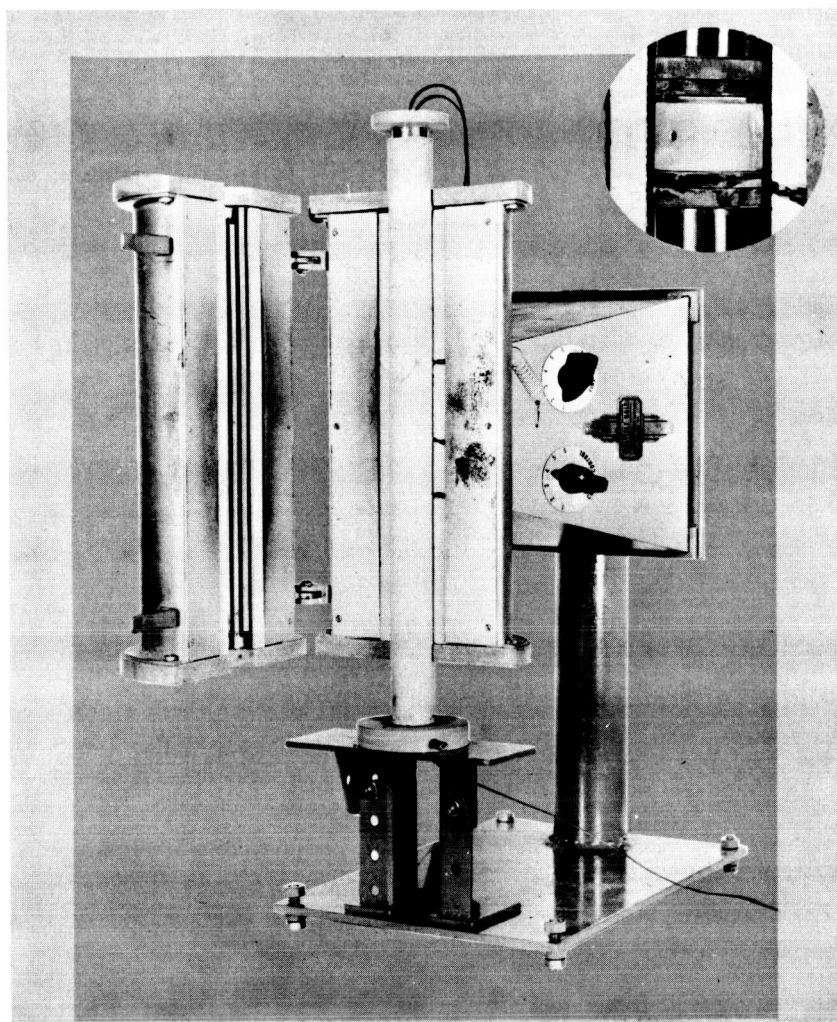


Figure 6-6. Modified Kelvin bridge.

If the conductivity cell under test is assumed to be the  $R + jX$  factor and known values of  $P$ ,  $r$ , and  $Q$  are used, then the resistance,  $R$ , of the cell may be computed.

In selecting the bridge components, it was decided to choose values which would cause the bridge to read out in meaningful numbers.

Since conductance  $G = 1/R = r_1/P_1Q$ ,  $P_1$  was chosen as 10,000 ohms and  $Q$  was a 1-ohm precision resistor. By choosing for  $r_1$  a nominally 10,000 ohm Dekastat, the outer ring reads directly in 1/10-mho units of conductivity. In addition to this, a second value of  $P_1$  (1000 ohm) was made available on an X10 range selector switch. When reading in this position, the decimal point is moved one place to the right. When this unit was first built, attempts were made to drive it with standard a-c powered oscillators of different types. All attempts were unsuccessful, apparently due to coupling with the a-c line. However, successful operation has been achieved with a battery-powered oscillator. The null detector used is a General Radio Model 1232-A.

In use, this bridge is best applied to the measurement of cells with resistances between 0.1 ohm and 100 ohms. The cell should be of the four-terminal type—i. e., two potential leads and two current leads. After the cell is connected, the oscillator is turned on, and the detector is peaked, the procedure is as follows:

1. Select the appropriate range switch setting.
2. Adjust  $P_1$  for the best null, starting with the outer ring of the Dekastat and working into the center.
3. Match the setting of  $P_2$  to  $P_1$ .
4. Repeat Steps 2 and 3.
5. Adjust the capacity balance for a better null, turning up the detector sensitivity as required.
6. Repeat Steps 2 and 3.

Read the dial setting of  $P_1$  on the selected scale as previously described. This is the cell conductance. The electrolyte conductivity may be obtained by multiplying this number by the cell constant.